



A MULTINUCLEAR NMR STUDY OF  
INCLUSION PROCESSES

A THESIS

PRESENTED FOR THE DEGREE OF  
DOCTOR OF PHILOSOPHY

in the

UNIVERSITY OF ADELAIDE

by

IAN MALCOLM BRERETON, B.Sc. (Hons.)

Department of Organic Chemistry

June, 1985

*Awarded 4-12-85*

"There is something fascinating about science. One gets such wholesale returns of conjecture out of such a trifling investment of fact."

Mark Twain, *Life on the Mississippi*, 1874.

CONTENTS

	<u>Page</u>
SUMMARY	(iv)
STATEMENT	(vi)
ACKNOWLEDGEMENTS	(vii)
FOREWORD	(viii)
 <b>PART 1. A Study of <math>\alpha</math>-Cyclodextrin Inclusion Complexes by <math>^{19}\text{F}</math> NMR Spectroscopy</b>	
<u>CHAPTER 1</u> INTRODUCTION	1
1.1 Structural Properties of Cyclodextrins	1
1.2 Cyclodextrin Inclusion Complexes	5
1.3 Biomimetic Chemistry	6
1.4 Driving Force for Inclusion Complex Formation	8
1.5 Application of NMR Spectroscopy	10
1.6 Objectives	13
 <u>CHAPTER 2</u> RESULTS AND DISCUSSION	 15
2.1 Preparation of Fluorocinnamic Acids	15
2.2 Inclusion of Fluoro- and Difluorocinnamates by $\alpha$ -Cyclodextrin	17
(i) Results	17
(ii) Equilibrium Aspects	28
(iii) $^{19}\text{F}$ Chemical Shifts	31
(iv) Stereochemistry of complexation	32
2.3 Inclusion of Trifluoromethyl Substituted Cinnamates	36
2.4 Conclusion	43

## CONTENTS (continued)

	<u>Page</u>
<u>CHAPTER 3</u> EXPERIMENTAL	45
3.1 General	45
3.2 Solution Preparation	45
3.3 NMR Spectra	46
3.4 Materials	47
3.5 Preparation of Fluorocinnamic Acids	48
<u>REFERENCES</u> - Foreword and Part 1	52
Part 2. A $^{23}\text{Na}$ NMR Study of Sodium Cryptates	
<u>CHAPTER 4</u> STRUCTURAL ASPECTS OF CRYPTATES	56
4.1 Cryptates: General Introduction	56
4.2 Structural Aspects: Introduction	60
4.3 Results and Discussion	63
(i) Synthesis of Cryptand $\text{C}_{21}\text{C}_5$	63
(ii) X-ray Crystallography	64
(iii) Cryptate Structure in Solution - $^{13}\text{C}$ NMR	72
4.4 Experimental	80
(i) Materials	80
(ii) Preparation of $\text{C}_{21}\text{C}_5$	80
(iii) X-ray Diffraction	82
a) X-ray Crystallography of $[\text{Na}.\text{C}_{21}\text{H}_{11}.\text{NCS}]$	82
b) X-ray Crystallography of $[\text{Na}.\text{C}_{21}\text{C}_5.\text{NCS}]$	84
(iv) NMR Spectroscopy	86

## CONTENTS (continued)

	<u>Page</u>
<u>CHAPTER 5</u> CRYPTATE STABILITY	89
5.1 Introduction	89
(i) Stability Constant Determination	90
5.2 Results and Discussion	93
<u>CHAPTER 6</u> KINETIC AND MECHANISTIC ASPECTS OF THE CRYPTATES OF C <sub>211</sub> AND C <sub>21C<sub>5</sub></sub>	99
6.1 Introduction	99
(i) Experimental Methods	100
a) <sup>23</sup> Na NMR Spectroscopy	100
b) Lineshape Analysis	101
6.2 Results and Discussion	104
(i) General Mechanistic Aspects	104
(ii) Dynamics of C <sub>211</sub> Cryptates	106
(iii) Kinetics of [Na.C <sub>21C<sub>5</sub></sub> ] <sup>+</sup>	117
(iv) Mechanistic Conclusions	127
6.3 Experimental	132
(i) Materials	132
(ii) Stability Constant Measurements	132
(iii) NMR Spectroscopy	133
<u>REFERENCES</u>	135
<u>PUBLICATIONS</u>	140
<u>APPENDIX 1</u> <sup>19</sup> F Chemical Shifts of Fluorocinnamates	141
<u>APPENDIX 2</u> Supplementary Crystallographic Data	146

### SUMMARY

Multinuclear NMR techniques have been used to investigate molecular and ionic inclusion processes. In the first part of this work, molecular complexes formed by the inclusion of fluorocinnamates by the cyclic oligosaccharide  $\alpha$ -cyclodextrin were studied by  $^{19}\text{F}$  NMR spectroscopy. The complex association constants were obtained from analysis of chemical shift data for a range of selectively fluorinated cinnamates, and the variation of chemical shifts of the complexed species provided information pertaining to the stereochemistry of the complexes.

The results indicated that 1:1 (binary) and 1:2 (ternary) complexes are formed in  $\text{D}_2\text{O}$  solution, generally with the binary complexes dominant in the case of mono- and difluorocinnamates and a highly stable ternary complex in the case of *p*-trifluoromethyl cinnamates. The chemical shift data indicated that the predominant binary complex is that in which the carboxylate side chain of the fluorocinnamate enters the wide end of the cyclodextrin cavity first. The ternary complex probably has a structure in which the cinnamate is encapsulated by two cyclodextrin molecules with the wide ends of their cavities in close proximity.

In the second part of this work,  $^{23}\text{Na}$  and  $^{13}\text{C}$  NMR spectroscopy were employed in a structural, kinetic and mechanistic investigation of the complexes formed by the macrobicyclic ligands, cryptands. The sodium cryptates of the cryptand C211, and a structurally modified cryptand, C21C<sub>5</sub>, were found to exist in the solid state, as determined by X-ray crystallography, in an 'exclusive' form in which the sodium

ion resides on one of the fifteen membered cryptand rings, rather than in the centre of the cryptand cavity as in the 'inclusive' form.  $^{13}\text{C}$  NMR studies indicated that this conformation is retained in solution, whereas the analogous lithium cryptates possess inclusive structures.

Variable temperature NMR studies and subsequent lineshape analysis of the spectra of these cryptates in various solvents, together with the determination of the stability of the  $\text{C}_{21}\text{C}_5$  cryptate, allowed a detailed mechanistic discussion of the processes involved in cryptate formation and dissociation. In general, the rate determining step for sodium exchange on cryptates is the dissociation of the cryptate, and the solvent variation of the formation and dissociation rate constants indicated a correlation between the solvent donor strength and the structure of the transition state for the exchange process.

STATEMENT

This thesis contains no material which has been accepted for the award of any other degree or diploma in any University, and to the best of my knowledge and belief, contains no material previously published or written by another person except where due reference is made in the text.

I consent to the thesis being made available for photocopying and loan, provided due acknowledgement to this work is made.

I. M. Brereton



ACKNOWLEDGEMENTS

I extend sincere thanks to my supervisors, Drs. T. M. Spotswood and S. F. Lincoln for their guidance and encouragement during the course of this work.

I wish to thank my colleagues in the Chemistry Departments for their helpful discussion and suggestions. I am indebted to Dr. E. H. Williams for his expert tuition and advice on spectrometer operation and for his general interest in the progress of this work. I especially wish to thank Andrea Hounslow for her help and encouragement, particularly during recent years.

I gratefully acknowledge the financial support of a Commonwealth Postgraduate Research Award for the period of my candidature. I also wish to thank my parents for their interest and concern throughout my University studies.

Finally, I wish to dedicate this thesis to Kathy, without whose support, encouragement and understanding this work may never have been finished.

## FOREWORD

Molecular and ionic inclusion phenomena are known to play a vital role in a number of biochemical processes which sustain life, from enzyme catalysis and drug receptor systems to the ionophoric activity of antibiotics. Physical organic chemists have made important contributions to the understanding of many biochemical systems, particularly to those processes which involve specific complexation of one species by another. The strategy usually adopted in such research is either to probe the actual biological system *per se*, or to develop and study practical models which emphasize the particular features of the system which are of interest so that subsequent comparisons with the real biological system can be made.

Such 'biomimetic' models have been very successfully applied to various aspects of biochemistry involving inclusion complexes, including enzymic catalysis and ion transport processes. This has led to an enormous amount of research activity in the field of inclusion complexation chemistry which has now evolved into an important branch of chemistry in its own right. The transport of a metal cation across a membrane, or the specific reaction catalysis of a substrate bound to an enzyme are clearly of interest. However, the physiochemical basis of complexation of molecules and ions in solution is fundamental to a complete understanding of these biochemical processes.

The process of enzyme catalysis involves the formation of a molecular inclusion complex where the substrate is bound within the active site of the enzyme. This binding has been

successfully mimicked by the use of the cyclic oligomeric saccharides, cyclodextrins.<sup>1,2</sup> Antibiotics such as valinomycin which facilitate the transport of metal ions across membranes, function as ionophoric ligands and complex the metal ion within a cavity formed by the arrangement of coordinating atoms around the ion as depicted in the figure below.

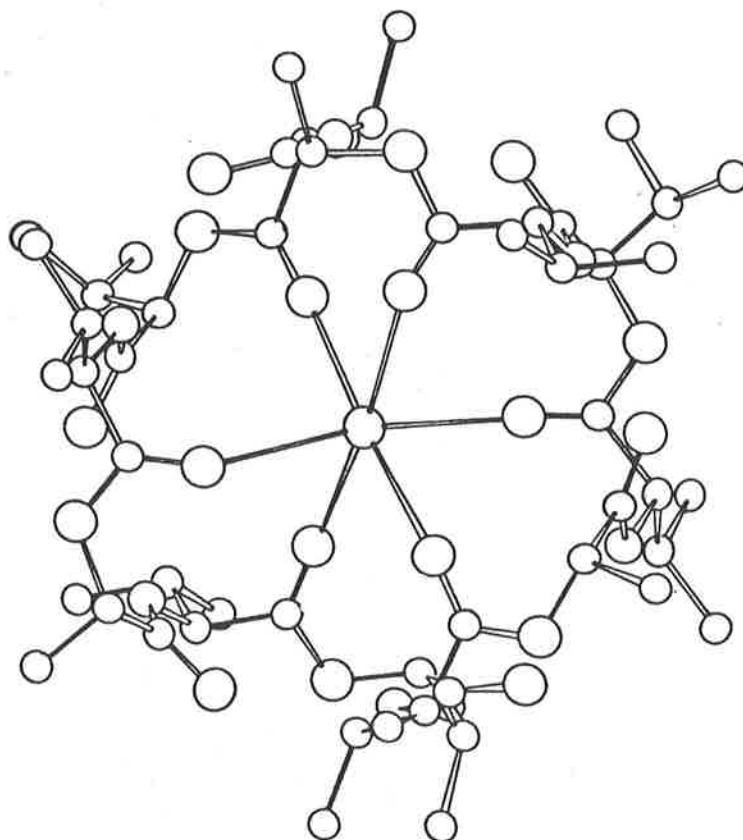


*Figure. Structure of the potassium - valinomycin complex. Potassium is the approximately octahedral coordinated central atom. The eighteen oxygen atoms are represented by the larger spheres, six nitrogen atoms by medium sized spheres, and the carbon by small spheres. Hydrogen atoms are not shown.*

The synthetic crown ethers<sup>3</sup> and cryptands<sup>4-6</sup> have been proposed as models for the action of antibiotics and much insight into complexation and binding phenomena has been gained from the extensive studies of the chemistry of these systems. A technique which has proven very powerful and productive is nuclear magnetic resonance (NMR) spectroscopy. NMR spectroscopy is particularly well suited to the study of inclusion complexation chemistry since the spectra of species involved are generally quite sensitive to any changes in environment which occur due to complexation. In this work, NMR spectroscopy has been utilized in the study of two forms of complexation, molecular inclusion complexes of cyclodextrins and the complexation of sodium ions by cryptands.

PART 1

A STUDY OF  $\alpha$ -CYCLODEXTRIN INCLUSION COMPLEXES

BY  $^{19}\text{F}$  NMR SPECTROSCOPY



Cyclodextrins are formed during the degradation of starch by the glucosyltransferase of *Bacillus macerans* which was first discovered by Villiers in 1891,<sup>7</sup> and were subsequently recognized to be cyclic oligosaccharides by Schardinger in 1904.<sup>8</sup> Freudenberg determined that cyclodextrins consisted of  $\alpha(1-4)$ -linked glucopyranose units<sup>9</sup> and with Cramer, realized their ability to form inclusion complexes in solution,<sup>10</sup> thus pioneering an extremely prolific field of chemistry.

1.1 Structural Properties of Cyclodextrins

Cyclodextrins are named according to the number of D(+)-glucopyranose units present. Of the most commonly studied members,  $\alpha$ -cyclodextrin (cyclohexaamylose, Figure 1.1),  $\beta$ -cyclodextrin (cycloheptaamylose) and  $\gamma$ -cyclodextrin (cyclo-octaamylose) are comprised of 6, 7 and 8 glucose residues respectively, while species containing up to 12 units per ring have been reported.<sup>11</sup>

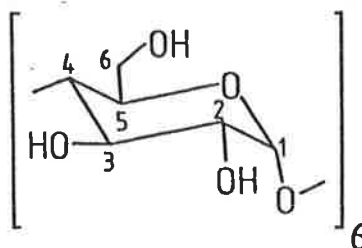


Figure 1.1. Schematic representation of the structure of  $\alpha$ -cyclodextrin.

The gross structure of the cyclodextrin molecule defines a cavity with the shape of a truncated cone, which in the case

of  $\alpha$ -cyclodextrin, is  $6.7\text{\AA}$  in depth and has a diameter of about  $4.5\text{\AA}$  at the narrow end.<sup>12</sup> Other physical properties of the cyclodextrins are included in Table 1.1.

**Table 1.1** Physical properties of the cyclodextrins.<sup>14</sup>

Cyclodextrin	No. of glucose units	Mol. Wt.	Water solubility (g/100 ml) <sup>a</sup>	Cavity Diameter ( $\text{\AA}$ ) <sup>b</sup>
$\alpha$	6	972	14.5	4.7 - 5.2
$\beta$	7	1135	1.85	6.0 - 6.4
$\gamma$	8	1297	23.2	7.5 - 8.3

a) Room Temperature b) Smaller value for ring of H atoms bonded to C(5) and larger value for ring of H atoms bonded to C(3) as measured from CPK models.

As depicted in Figure 1.2, the wider rim of the  $\alpha$ -cyclodextrin torus consists of the 12 secondary hydroxyl groups of the glucose residues and the narrow rim is defined by the 6 primary hydroxyl groups. The internal cavity thus formed is lined by the ring of glycosidic oxygens and the hydrogen atoms bonded to carbons 3 and 5, and is therefore thought to be apolar in nature relative to the water environment in solution. An x-ray crystallographic study of  $\alpha$ -cyclodextrin hexahydrate revealed that in the solid state the glucose units are in the D1 chair conformation<sup>12</sup> and as confirmed by other studies, including NMR spectroscopy,<sup>13</sup> this conformation persists in both  $D_2O$  and dimethylsulphoxide solution.

Two water molecules were found to be included within the cavity of crystalline  $\alpha$ -cyclodextrin and one of the glucose residues is tilted with respect to the other five residues, lying almost normal to the axis of the cavity. This allows hydrogen bonding to occur between the water molecules and two

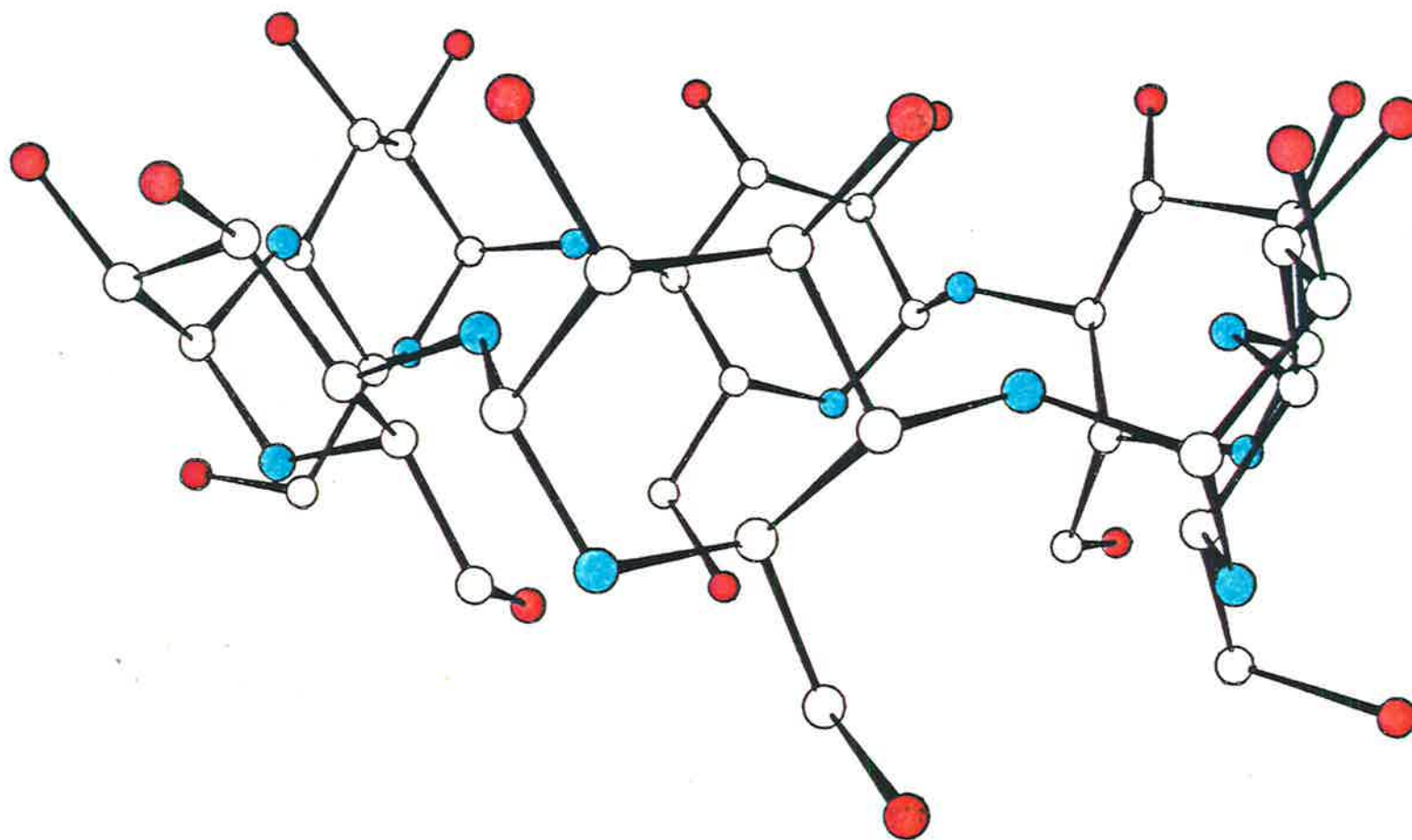


*Figure 1.2 a) Perspective view of the  $\alpha$ -cyclodextrin (H<sub>2</sub>O)<sub>6</sub> molecule. The red shaded spheres represent the oxygen atoms of the primary and secondary hydroxyl groups, and the blue spheres represent the glycosidic ether oxygen atoms.*



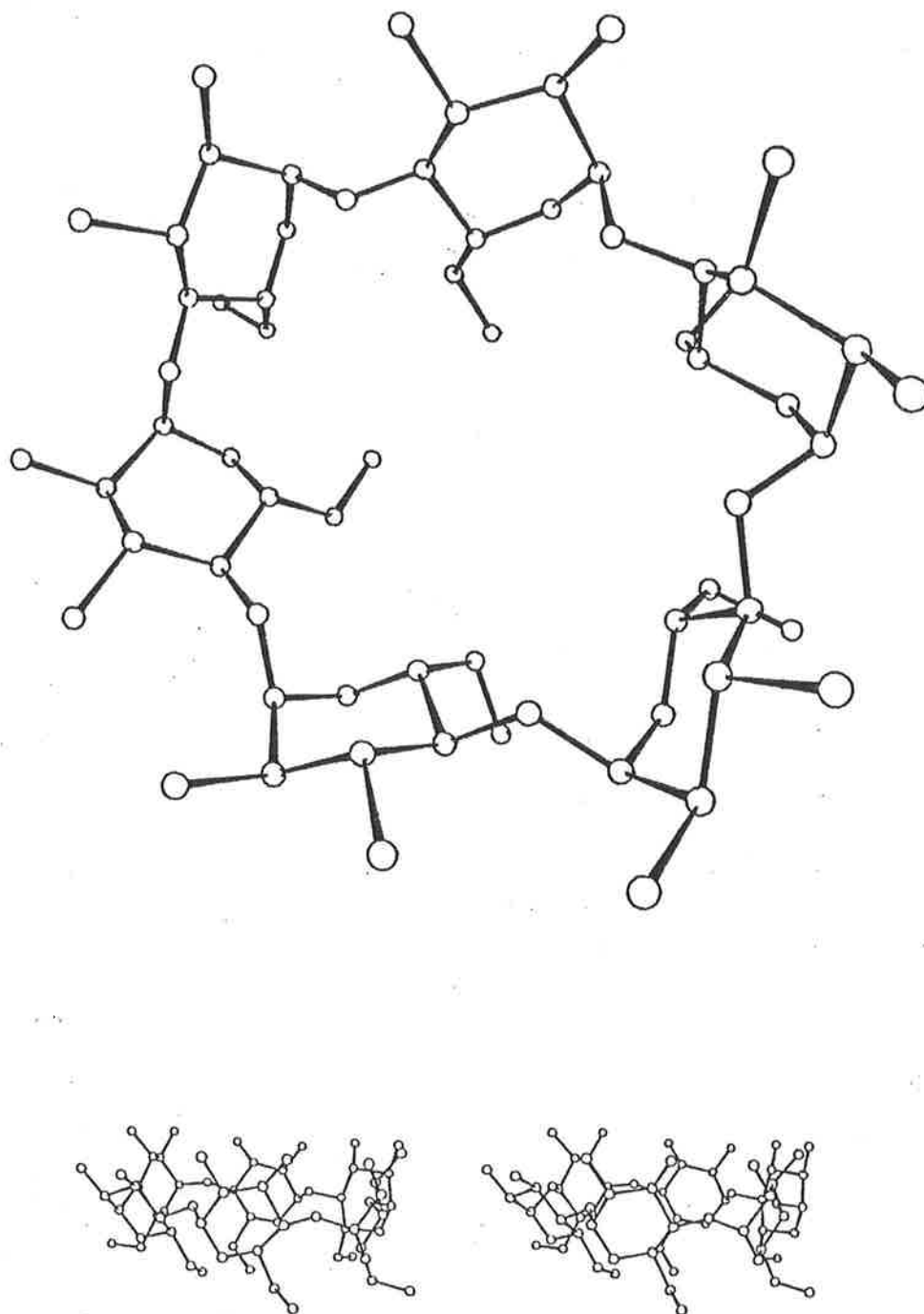


Figure 1.2 b) View of the  $\alpha$ -cyclodextrin ( $H_2O$ )<sub>6</sub> molecule from above the wider rim (top), and a stereoscopic view (bottom).

of the primary hydroxyl groups.

## 1.2 Cyclodextrin Inclusion Complexes

It is the relative rigidity of the cyclodextrin molecule allowing the maintenance of the cavity in solution which gives rise to its most interesting and useful property - the formation of inclusion compounds with molecular 'guests' of appropriate sizes. This ability to act as a 'host' molecule and the considerable specificity or selectivity toward the geometry and size of the guest has been successfully exploited in many applications, including biomimetic chemistry and in the food, pharmaceutical and chemical industries. The cyclodextrins are toxologically harmless and are finding increasingly important uses in the latter industries, including the stabilization of drugs and active ingredients towards oxidation, decomposition or hydrolysis; the reduction in volatility of drugs, food flavours and cosmetic fragrances; the suppression of unpleasant tastes and odours; the enhancement of bioavailability of drugs via increased solubility or the formulation of small amounts of liquid drugs as their solid cyclodextrin complexes; and the stabilisation of explosives and agricultural poisons.

The major drawback to industrial utilization of cyclodextrins appears to be their prohibitive cost. However, with the rapidly increasing number of patents and publications appearing describing such potentially important applications, the industrial and commercial use of the cyclodextrins is likely to increase. The above facets of cyclodextrin research are both interesting and important and will be responsible for

increased support for research by industry. Many examples of the above applications of cyclodextrin complexation may be found in the literature<sup>1,2,14,15</sup> and a detailed review will not be attempted here.

### 1.3 Biomimetic Chemistry - Cyclodextrins as Enzyme Models

The inclusion of molecular substrates in the hydrophobic cavity of cyclodextrins has led to their extensive use in biomimetic chemistry as enzyme models. This complexation process is analogous to the formation of the Michaelis-Menten complex between catalyst and substrate in enzymic catalysis. To act as an enzyme analogue, a catalytic species must stabilize the transition state of a reaction relative to the starting materials and the cyclodextrins exhibit the following number of features which allow such comparisons to enzymes. They contain structural features such as the hydrogen bonding hydroxyl groups which can be used as handles for stabilizing interactions and promoting reactions. The molecule is quite rigid in solution so that the binding is generally specific and the host-guest relationship is usually readily defined. The source or region of binding (the cavity) is removed from the reaction site (the secondary or primary hydroxyl groups) so that it is the transition state of the catalytic reaction centre which is preferentially stabilized.

Apart from these important requirements of complex formation, other features of cyclodextrin inclusion chemistry which are analogous to enzymic reactions include selectivity and specificity toward the substrate structure. The reactions may show enantiomeric specificity and are usually carried out in aqueous solution.

Indeed, cyclodextrins have been shown to catalyse a number of biochemically significant reactions, usually involving the participation of the hydroxyl groups in hydrolysis of substrates. In most examples of catalytic hydrolysis, such as phenyl ester cleavage which is analogous to the action of the enzyme  $\alpha$ -chymotrypsin<sup>16,17</sup>, the complexed substrate undergoes nucleophilic attack by a secondary hydroxyl group resulting in the release of the leaving group and either reversible or irreversible modification of the cyclodextrin. Examples of other reactions accelerated by cyclodextrins include hydrolysis of amides, cleavage of organophosphates, carbonates and sulphates, decarboxylation of cyanoacetates, oxidation of  $\alpha$ -hydroxyketones and intramolecular acyl migrations.<sup>18,19</sup>

However, while the acceleration factor (the ratio of the pseudo first order rate constant of the complexed substrate to the rate constant of the uncomplexed species under identical conditions) for some of these reactions is high (e.g. 300 for phenyl ester hydrolysis), the catalytic activity of cyclodextrins is often lower than for natural enzymes. Consequently, there has been much effort to prepare chemically modified cyclodextrins in which strategically designed functional groups for specific reactions are introduced to simulate residues within the catalytic sites of enzymes, while the cavity serves as the substrate binding site.<sup>18,19</sup> For example, replacement of a secondary hydroxyl group of  $\alpha$ -cyclodextrin with a histamine group leads to an 80 fold increase in the rate of hydrolysis of *p*-nitrophenyl acetate relative to  $\alpha$ -cyclodextrin itself.<sup>20</sup>

Another approach to host design has been to modify the

cyclodextrin with a view to improving its binding characteristics instead of the catalytic reaction site. Association constants may be increased by enhancing hydrophobic effects which are considered to be important in complex formation.<sup>21</sup> The hydrophobicity of the cavity can be increased by the capping of one end with bifunctionalized aromatic moieties. Capping of  $\beta$ -cyclodextrin across the primary hydroxyl end with diphenylmethane-*p,p*-disulphonate (actually forming a mixture of two possible regioisomers) increases the catalytic effect for hydrolysis of nitrophenyl acetates by a factor of 200 and also increases the para/meta selectivity of the reaction.<sup>22</sup> A large number of such chemical modifications have been reported,<sup>23</sup> many of which demonstrate the effective use of host design in the preparation of enzyme analogues.

#### 1.4 Driving Force for Inclusion Complex Formation

Various processes are considered to contribute to the thermodynamic stability of cyclodextrin inclusion complexes, the predominance of particular factors depending on the system under investigation. The inclusion process is usually associated with a favourable enthalpy change and, in the case of the binding of apolar substrates, a positive entropy change. These free energy changes have been explained in terms of the following interactions:

a) van der Waals forces between the host and guest molecules as evidenced by the dependence of the complex stabilities on guest polarizability;<sup>24</sup>

b) hydrogen bond formation between the hydroxyl groups

of the cyclodextrin and the substrate;<sup>25</sup>

c) the release of strain energy of the cyclodextrin via conformational changes upon substrate inclusion (applying mainly in the case of  $\alpha$ -cyclodextrin where the tilted glucose residue causes considerable bond angle strain);<sup>12,26</sup>

d) polar guest - host interactions;<sup>27</sup>

e) and possibly most importantly, particularly for binding of apolar guests in aqueous solution, hydrophobic interactions between the apolar cavity environment and the guest.<sup>18,21,24,28</sup> These forces are derived from the solvational changes which occur during the inclusion process and their significance is due to the structure of water itself. Water molecules in the solvation shell of an apolar substrate are more tightly bound to each other, since hydrogen bonding in the direction of the solute is reduced, and the degree of molecular order in the region is greater. So the removal of this solvation assembly on inclusion should result in an increase in both entropy and enthalpy. Also accompanying the inclusion of the substrate is the expulsion of the water molecules initially included in the cyclodextrin cavity. The liberated water molecules form hydrogen bonds and van der Waals interactions with the bulk water and gain motional degrees of freedom.<sup>16,29</sup>

While the overall free energy change on complexation probably consists of contributions from all of the above interactions, the relative importance of each depends on the nature of the substrate involved. However, the most essential requirement for inclusion complex formation is an appropriate spatial 'fit' between the substrate and the cyclo-

dextrin cavity. A knowledge of the stoichiometry and spatial geometry of the complex is obviously important when considering the relative predominance of the various factors influencing the driving force for inclusion.

### 1.5 Application of NMR Spectroscopy to the Study of Complexation

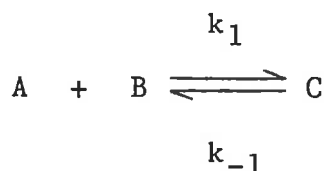
The biochemist's understanding of many biological phenomena has been greatly enhanced since the development of NMR spectroscopy and its use in the elucidation of problems of biological interest. Many of the problems associated with the measurement of  $^1\text{H}$  NMR spectra of complex biological systems have recently been overcome with the advent of sophisticated multi-pulse two-dimensional NMR techniques and spectral editing techniques. However, the  $^1\text{H}$  NMR study of the association of macromolecules with small molecules may remain difficult due to spectral overlap. In these cases, much success has been achieved by selectively labelling the species of interest with other nuclei which are observable by NMR spectroscopy, such as  $^{13}\text{C}$ ,  $^2\text{H}$  or  $^{19}\text{F}$ .

The use of  $^{19}\text{F}$  NMR spectroscopy in the biological field was first reported by Spotswood et al.<sup>31</sup> in 1967 and has since become particularly important in studies of enzyme - substrate interactions.<sup>32</sup> Observation of the  $^{19}\text{F}$  nucleus has a number of advantages over  $^1\text{H}$  NMR spectroscopy. The spectra are usually simple, consisting of only a few sharp resonances, thus eliminating the problem of the broad macromolecule spectrum envelope masking the small molecule resonances.  $^1\text{H}$  coupled  $^{19}\text{F}$

resonances may be broad band decoupled, further simplifying the spectrum. The small size of the fluorine atom allows its incorporation into a molecule without significantly affecting its molecular structure, since fluorine is approximately isosteric with hydrogen.  $^{19}\text{F}$  chemical shifts extend over a much larger range (ca. 150 ppm) than protons (ca. 15 ppm) so assignment difficulties due to overlapping resonances rarely occur. More importantly however, the  $^{19}\text{F}$  chemical shifts (and to a lesser extent, the relaxation times) are extremely sensitive to changes in environment and are therefore a very useful probe in providing spatial orientation and binding strength information in complexation processes.

The majority of  $^{19}\text{F}$  NMR studies of biological processes involve examination of a small molecule undergoing exchange between free solution and a macromolecular bound state, such as in enzyme - substrate or drug - receptor systems. Information obtained from such investigations include complex association constants and molecular orientations from chemical shifts and exchange kinetics from linewidth and relaxation rate data.<sup>33</sup> The association constant and chemical shift on binding for complexation between a particular host molecule (A) and guest (B) may be obtained as follows:

For the equilibrium



the association constant K is given by

$$K = k_1/k_{-1} = \text{C}/\text{A}.\text{B}$$



$$\text{i.e. } K = C/(A_0 - C)(B_0 - C) \quad (1.1)$$

where  $A_0$  = initial concentration of A

$B_0$  = initial concentration of B

Under conditions of rapid exchange, the observed chemical shift,  $\delta$ , is given by the weighted average of the free solution shift,  $\delta_0$ , and the shift in the complex,  $\Delta$ .

$$\text{i.e. } \delta = p.\Delta + \delta_0 \quad (1.2)$$

where  $p$  is the mole fraction of the complex and  $\Delta$  is measured relative to  $\delta_0$  as 0.

The concentration of the complex,  $C$ , may be obtained by rearranging and expanding (1.1),

$$C = (A_0 + B_0 + 1/K) \pm \sqrt{[(A_0 + B_0 + 1/K)^2 - 4A_0B_0]}^{1/2} \quad (1.3)$$

2

Thus,  $K$  may be obtained by iterative adjustment in (1.3) and minimization of the least squares error in (1.2) for the experimental values of  $\delta$ ,  $A_0$  and  $B_0$  as described by Sykes.<sup>34</sup>

By varying the position of the fluorine probe within the structure of the guest, and comparing the magnitudes of the shifts on complexation and the association constants, direct information about the geometry of binding sites and molecular motion of the guest in the complex is available. This approach has proved successful in the study of the binding of various fluorinated substrates, including derivatives of phenylalanine and <sup>35-37</sup> tryptophan<sup>38</sup> to the serine protease  $\alpha$ -chymotrypsin. The results of these investigations allowed the formulation of a detailed model for the enzyme-substrate complex formation.

The elucidation of the mechanism of the  $\alpha$ -chymotrypsin catalysed hydrolysis of cinnamoyl esters and amides by Bender<sup>39</sup> led to a number of studies of the complexes formed by the enzyme and the competitive inhibitor *trans*-cinnamic acid<sup>40</sup> and some fluorinated derivatives<sup>41,42</sup> to gain information about the structure of intermediates in the hydrolysis process. As the cyclodextrins had been proposed as models for the catalytic binding site of enzymes, it seemed a logical progression to apply the techniques developed in the above mentioned work to the study of inclusion complexation of *trans*-cinnamic acids by cyclodextrins.

#### 1.6 Objectives

A series of substituted *trans*- and *cis*- cinnamic acids were shown to form inclusion complexes with both  $\alpha$ -cyclodextrin ( $\alpha$ CD) and  $\beta$ -cyclodextrin ( $\beta$ CD) in a study by Uekama et al<sup>43</sup> in an attempt to investigate the spatial and steric dependency of inclusion. Ultra-violet and circular dichroism data were interpreted in terms of the formation of 1:1 complexes only and the authors speculated from <sup>1</sup>H NMR data for the *trans*-cinnamic acid -  $\beta$ CD complex which was not given in detail, that the conformation of the complex was that with the aromatic ring of the cinnamic acid included in the cavity, leaving the carboxylic acid side chain substantially solvated. However, in a more detailed investigation by Connors and Rosanske<sup>44</sup>, it was found that analysis of solubility, potentiometric and UV spectral data for complexation of *trans*-cinnamic acid by  $\alpha$ CD required the formation of a subsequent 1:2 complex where the substrate molecule is encapsulated by

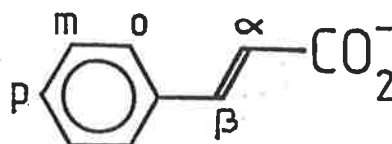
two cyclodextrin molecules.

The aim of this work was to examine the inclusion of a series of selectively fluorinated *trans*-cinnamic acids by  $\alpha$ CD employing  $^{19}\text{F}$  NMR spectroscopy with a view to determining the stoichiometry of the complexes formed and to assess the environmental changes experienced by the substrates, thereby gaining insight into the stereochemistry of the inclusion complex. This would allow a comparison to be made with the mode of complexation of the cinnamic acids by the enzyme  $\alpha$ -chymotrypsin.

CHAPTER 2.RESULTS AND DISCUSSION2.1 Preparation of Fluorocinnamic Acids

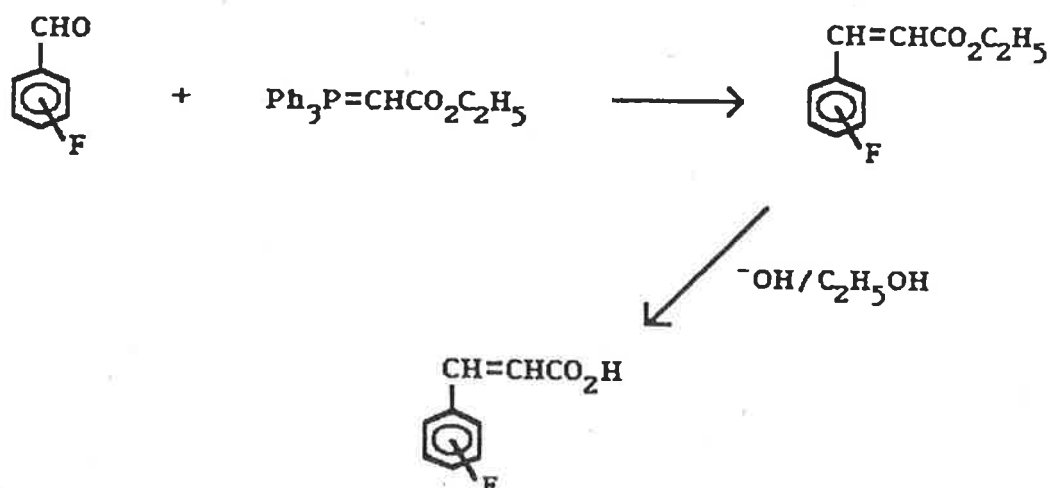
A comprehensive investigation of the inclusion of *trans*-cinnamic acid by  $\alpha$ CD requires information from a range of sites on the substrate molecule (for convenience, the *trans*-prefix will not be used hereafter, since all cinnamic acids studied were the *trans*-isomer). Thus a series of fluorocinnamic acids were prepared, both mono-labelled and di-labelled with fluorine in positions around the aromatic ring and in the  $\alpha$ -position of the carboxylic acid side chain (Figure 2.1).

Figure 2.1

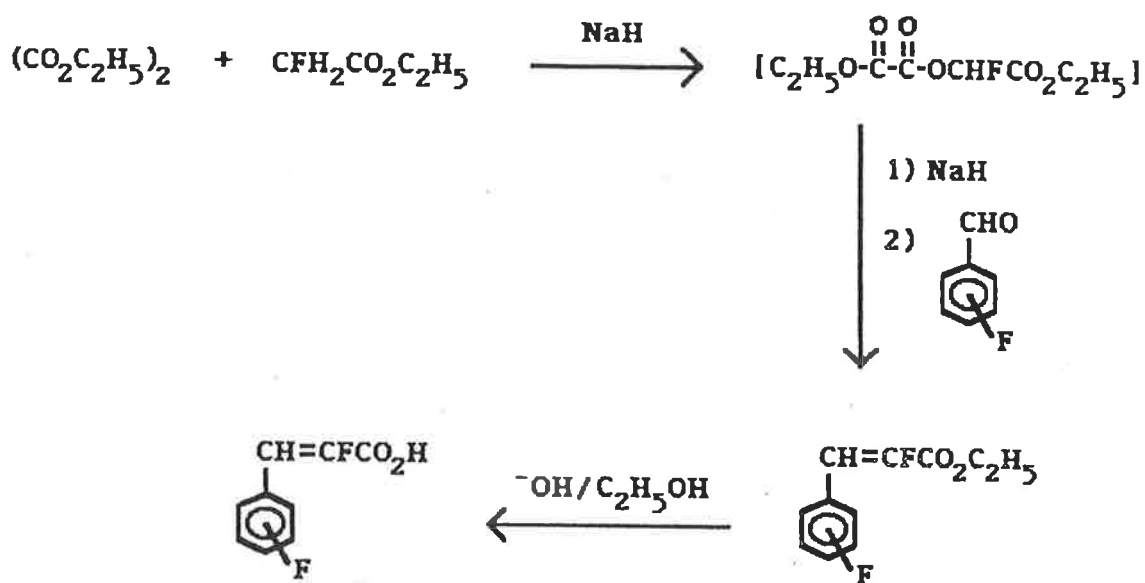


The ring fluorinated cinnamic acids can be conveniently prepared by saponification of the corresponding ethyl esters obtained via a Wittig condensation of the appropriate fluoro-benzaldehyde and carboethoxymethylidetriphenylphosphorane<sup>45</sup> as depicted in Scheme 2.1.

Scheme 2.1



The  $\alpha$ -fluorinated cinnamic acids were also obtained from the corresponding ethyl esters which were best prepared by the Claisen reaction of ethyl fluoroacetate, ethyl oxalate and the appropriate benzaldehyde<sup>46</sup> (Scheme 2.2).



Scheme 2.2

To gain some insight into the steric effect on inclusion of cinnamates, derivatives with trifluoromethyl substituents in the *m*- and *p*- positions were also synthesized by the above methods. The yields of the preparations are summarized in Table 2.1.

As a consequence of the poor solubility of the cinnamic acids in water, this study is of the soluble sodium or lithium cinnamates. Samples of *p*-fluoro,  $\alpha$ -fluoro, *o,p*-difluoro- and *m*-trifluoromethyl cinnamic acids were available from previous work in this laboratory.<sup>47</sup>

**TABLE 2.1**

R	YIELD (%)	
	Cinnamate Ester	Cinnamic Acid
<i>o</i> -fluoro	87	83
<i>m</i> -fluoro	92	86
<i>p</i> -trifluoromethyl	92	92
$\alpha$ , <i>p</i> -difluoro	41	87
$\alpha$ -fluoro- <i>p</i> -trifluoromethyl	52	93

## 2.2 Inclusion of Fluoro- and Difluorocinnamates by $\alpha$ -Cyclodextrin

### (i) Results

The  $^{19}\text{F}$  NMR resonances of the ring substituent fluorines (multiplets with  $J_{\text{F-H}} = 7-9$  Hz for *o*-, *p*- and *m*-F and  $J_{\text{F-F}} = 15.7$  for *o,p*-difluorocinnamate) and the  $\alpha$ -fluorines (doublets with  $J_{\text{F-H}} = 36.2$  and  $37.6$  Hz for  $\alpha$ -fluoro- and  $\alpha,p$ -difluorocinnamate respectively) are characterised by chemical shifts upfield from the  $^{19}\text{F}$  resonance of  $\text{CF}_3\text{COO}^-$  (Table 2.2). The hyperfine splitting of these resonances is lost as  $[\alpha\text{CD}]$  is increased and a systematic variation of the chemical shift occurs. The magnitude and direction of the chemical shift variation depends on the site of the fluorine atom in the fluorocinnamate as does the systematic broadening of the  $^{19}\text{F}$  resonances as exemplified by  $\alpha,p$ -difluorocinnamate (Fig. 2.2). Over the total  $[\alpha\text{CD}]$  range examined for all six fluorocinnamates only one resonance was observed for each fluorine consistent with site exchange of the fluorocinnamate occurring rapidly on the NMR timescale. With the possible exception of

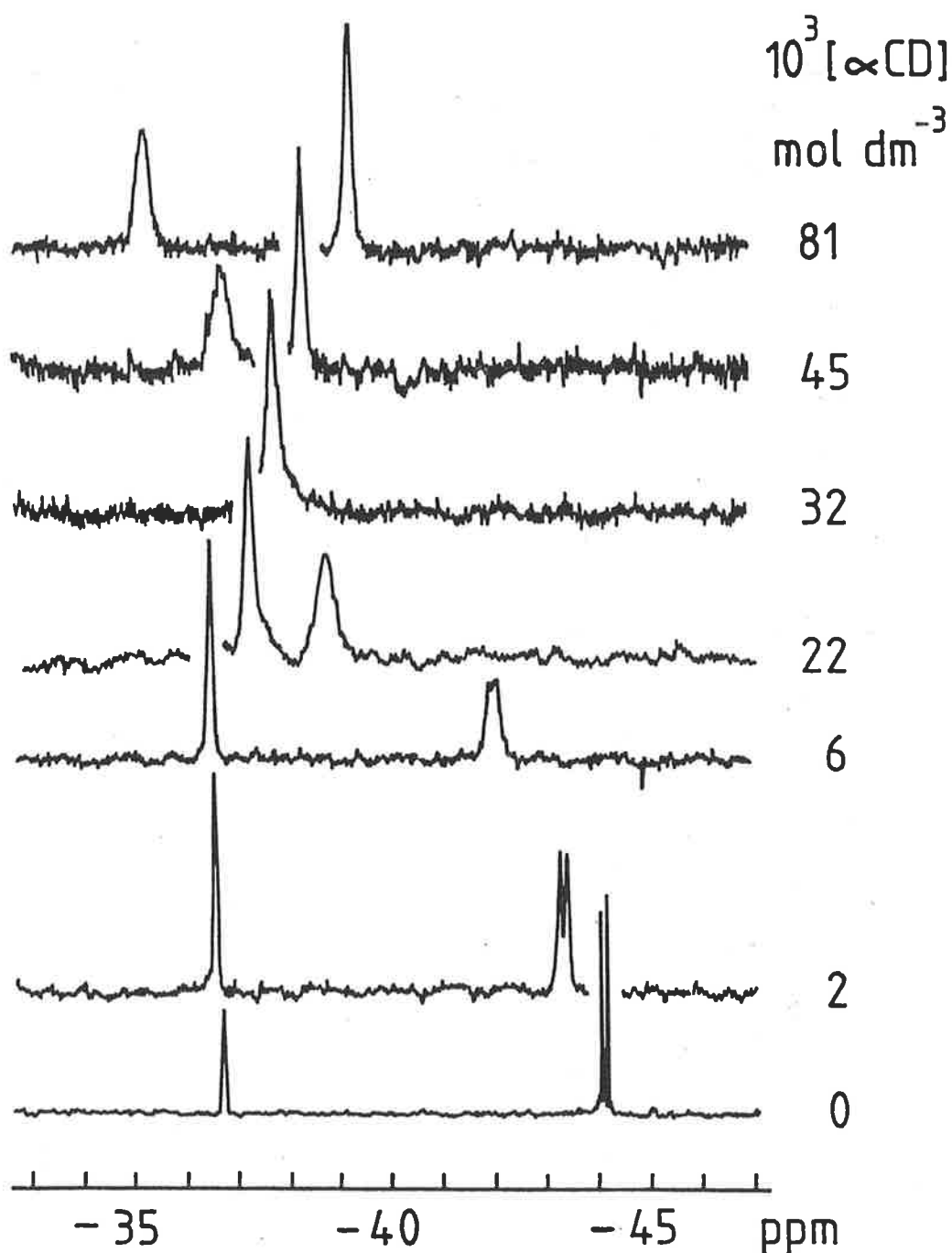
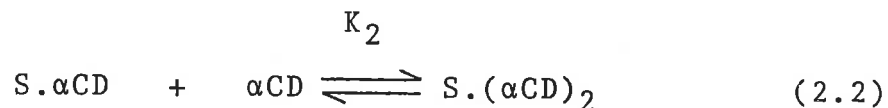
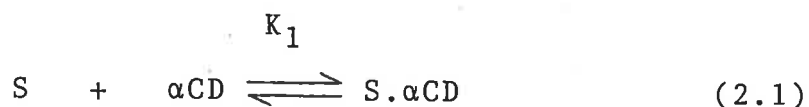


Figure 2.2. Variation of the  $282.35 \text{ MHz } ^{19}\text{F}$  NMR spectrum of  $\alpha,p$ -difluorocinnamate in the presence of  $0.1 \text{ mol dm}^{-3}$  NaCl at  $294.0 \text{ K}$ . In the bottom spectrum the doublet ( $-44.11 \text{ ppm}$ ) arises from  $\alpha\text{-F}$  and the unresolved multiplet ( $-36.80 \text{ ppm}$ ) arises from  $p\text{-F}$ . [ $\alpha,p$ -difluorocinnamate] was  $10^{-3} \text{ mol dm}^{-3}$ .

*m*-fluorocinnamate the  $^{19}\text{F}$  chemical shift variations are biphasic (Figs. 2.3 and 2.4) consistent with consecutive formation of binary (1:1) and ternary (1:2) inclusion complexes:



Under such fast exchange conditions the observed chemical shift,  $\delta$ , is given by

$$\delta = \frac{\delta_0[\text{S}] + \delta_1[\text{S} \cdot \alpha\text{CD}] + \delta_2[\text{S} \cdot (\alpha\text{CD})_2]}{[\text{S}] + [\text{S} \cdot \alpha\text{CD}] + [\text{S} \cdot (\alpha\text{CD})_2]} \quad (2.3)$$

where  $\delta_0$ ,  $\delta_1$  and  $\delta_2$  are the chemical shifts of S, S. $\alpha$ CD and S. $(\alpha$ CD) $_2$ , respectively. The equilibrium concentration of the species in solution may be determined in the following manner:

Let	[S]	=	S	(free substrate)
	[ $\alpha$ CD]	=	C	(free cyclodextrin)
	[S. $\alpha$ CD]	=	C1	(1:1 complex)
	[S. $(\alpha$ CD) $_2$ ]	=	C2	(1:2 complex)

then from (1)  $C1 = K_1 \cdot S \cdot C$  (i)

and from (2)  $C2 = K_2 \cdot C1 \cdot C = K_1 \cdot K_2 \cdot S \cdot C^2$  (ii)

and  $S_0 = S + C1 + C2$  (iii)

$C_0 = C + C1 + 2C2$  (iv)

Substituting for C1 and C2 in (iii):

$$S_0 = S + K_1 \cdot S \cdot C + K_1 \cdot K_2 \cdot S \cdot C^2$$



Rearranging:

$$S = S_0 / (1 + K_1.C + K_1.K_2.C^2) \quad (v)$$

Similarly from (iv):

$$C_0 = C + K_1.S.C + 2.K_1.K_2.S.C^2 \quad (vi)$$

Substituting for S from (v) in (vi) and rearranging gives

$$(C_0 - C) = S_0(K_1.C + 2.K_1.K_2.C^2) / (1 + K_1.C + K_1.K_2.C^2)$$

This is then expanded and solved for C using the Newton-Raphson method of evaluating the roots of equations. Thus S follows from (v) and C1 and C2 from (i) and (ii). Using a weighted non-linear least squares computer program, DATAFIT, the parameters  $K_1$ ,  $K_2$ ,  $\delta_1$  and  $\delta_2$  were obtained by fitting the experimental values of  $S_0$ ,  $C_0$ ,  $\delta_0$  and  $\delta$  to equation (2.3). The free solution shift,  $\delta_0$ , was measured in the absence of  $\alpha$ CD.

DATAFIT minimizes the residuals between the experimental and calculated surfaces defined by the experimental variables keeping the fractional change of any of the parameters to within 0.001 at convergence. The standard deviations for the calculated shifts and association constants produced by the program serve as true measures of the statistical uncertainties since account is taken of the experimental errors in the individual input variables. In the case of the cinnamates with two fluorinated positions, both chemical shift variations were fitted simultaneously to equation (2.3).

The  $^{19}\text{F}$  chemical shift data for all systems studied are presented in Appendix 1. The curves in Fig. 2.3 and 2.4 represent the best fits of the data to equation (2.3) and the best-fit values of  $K_1$ ,  $K_2$ ,  $\delta_1$  and  $\delta_2$  are given in Table 2.2. Qualitatively, the variation of  $\delta$  with  $[\alpha\text{CD}]$  for the two o-, three p- and two  $\alpha$ -  $^{19}\text{F}$  resonances are seen to represent three

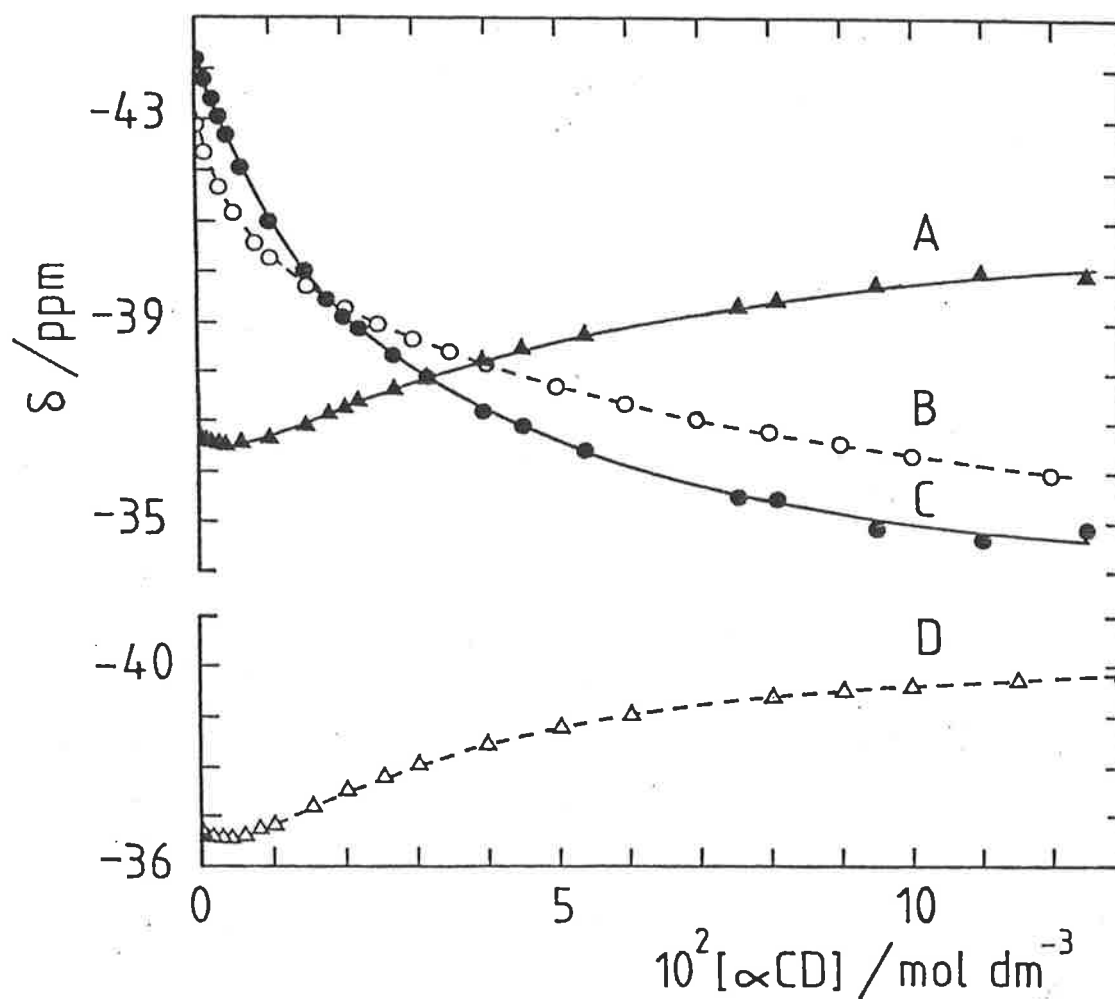


Figure 2.3. Variation of the  $^{19}\text{F}$  chemical shifts ( $\delta$ ) of fluoro- and difluorocinnamates with  $[\alpha\text{CD}]$ . The experimental data are shown as individual points and the best fits of these data to equation 2.3 are shown as curves. Curves A and C pertain to *p*- and  $\alpha$ -F, respectively, of  $\alpha$ ,*p*-difluorocinnamate and curves B and D pertain to  $\alpha$ - and *p*-fluorocinnamate respectively. The chemical shifts are referenced to  $\text{CF}_3\text{COO}^-$  and are corrected for bulk susceptibility variations.

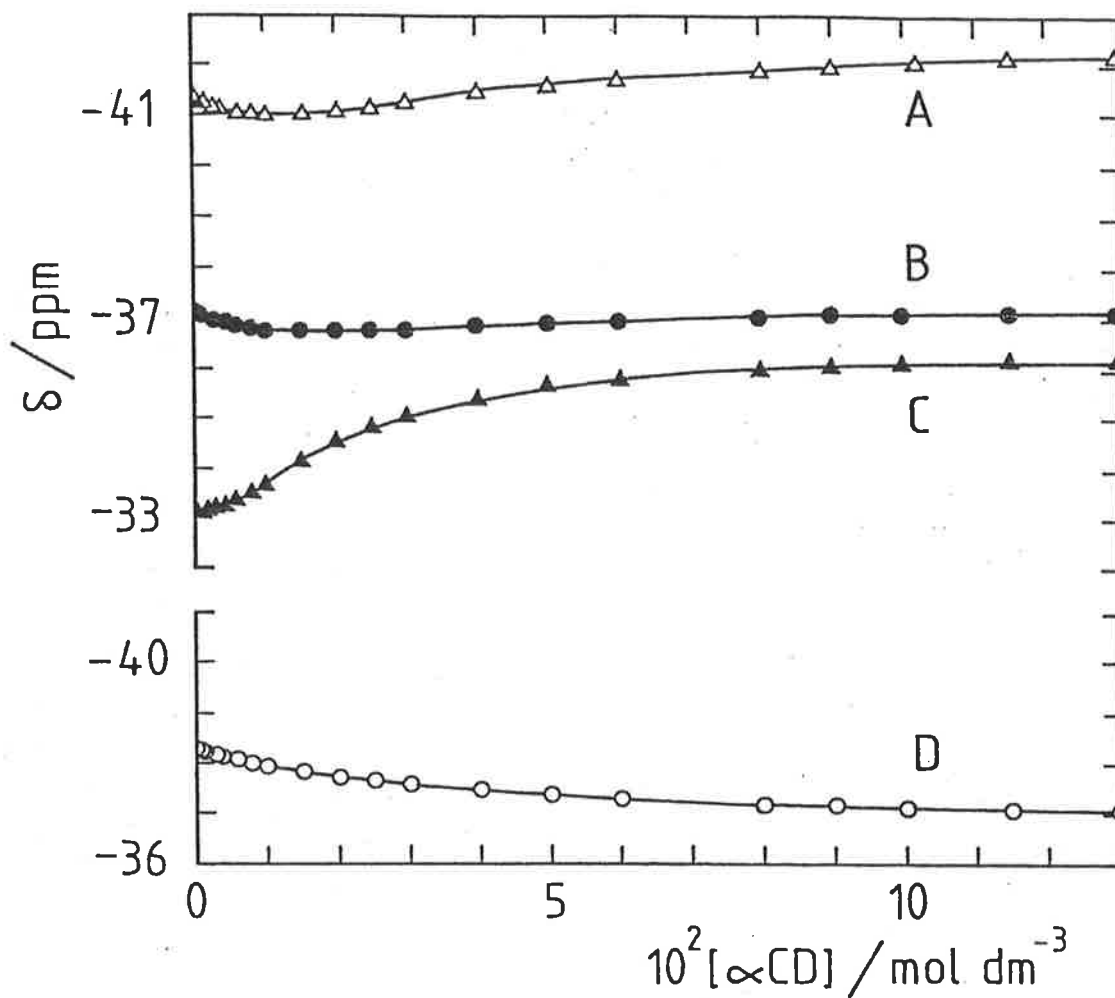


Figure 2.4. Variation of the  $^{19}\text{F}$  chemical shifts of fluoro- and difluorocinnamate with  $[\alpha\text{CD}]$ . The experimental data are shown as individual points and the best fits of these data to equation 2.3 are shown as curves A-C. Curves B and C pertain to *o*- and *p*-F, respectively, of *o,p*-difluorocinnamate and curve A pertains to *o*-fluorocinnamate. Curve D for *m*-fluorocinnamate represents the best fit of the data to equation 1.2. The chemical shifts are referenced to  $\text{CF}_3\text{COO}^-$  and are corrected for bulk susceptibility variations.

Table 2.2. Equilibrium constants and  $^{19}\text{F}$  chemical shifts for Fluoro- and Difluoro-cinnamates.<sup>a</sup>

<u>trans</u> -cinnamate	$K_1$ $\text{dm}^3 \text{ mol}^{-1}$	$K_2$ $\text{dm}^3 \text{ mol}^{-1}$	$\delta_0^b$ ppm	$\delta_1$ ppm	$\delta_2$ ppm	$\delta_1 - \delta_0$ ppm	$\delta_2 - \delta_0$ ppm	$\delta_2 - \delta_1$ ppm
$\alpha$ -fluoro-	$184 \pm 16$	$7.8 \pm 1.0$	-42.82	$-39.44 \pm 0.17$	$-32.0 \pm 0.01$	3.38	10.81	7.43
$p$ -fluoro-	$109 \pm 10$	$35 \pm 1$	-36.72	$-35.66 \pm 0.05$	$-40.78 \pm 0.03$	1.06	-4.06	-5.1
$\alpha, p$ -difluoro-	$111 \pm 13$	$23 \pm 2$	( $\alpha$ ) -44.11	$-39.75 \pm 0.39$	$-32.54 \pm 0.15$	4.36	11.57	7.21
			( $p$ ) -36.80	$-35.54 \pm 0.10$	$-41.68 \pm 0.13$	1.26	-4.89	-6.15
$o$ -fluoro-	$49 \pm 2$	$39 \pm 2$	-41.43	$-39.51 \pm 0.08$	$-42.75 \pm 0.01$	1.92	-1.33	-3.25
$o, p$ -difluoro-	$32 \pm 3$	$94 \pm 5$	( $o$ ) -37.13	$-35.03 \pm 0.14$	$-37.32 \pm 0.01$	2.10	-0.19	-2.29
			( $p$ ) -33.14	$-33.09 \pm 0.09$	$-36.55 \pm 0.02$	0.06	-3.41	-3.47
<sup>c</sup> cinnamate	110	15						
<sup>c</sup> cinnamic acid	2260	60						

a Shifts are relative to  $\text{CF}_3\text{COO}^-$  and are corrected for bulk susceptibility variations. A negative sign signifies an upfield shift.

b Error is 0.01 ppm.

c Ref. 44.

distinct families of curves, which implies a correlation between the stereochemistry of the inclusion complexes and the  $^{19}\text{F}$  chemical shift variation. Similar trends are observed in the  $\delta_1$  and  $\delta_2$  data of Table 2.2. In the case of the *m*-fluorocinnamate the  $^{19}\text{F}$  chemical shift variation is relatively small and does not exhibit a noticeable biphasic variation. By analogy with the other fluorocinnamates it is reasonable to assume that both  $\text{S.}\alpha\text{CD}$  and  $\text{S.}(\alpha\text{CD})_2$  are also formed in this case. Nevertheless, a unique fit of the *m*-fluorocinnamate data to equation (2.3) could not be obtained. A possible explanation for this may be that a fortuitous combination of  $\delta_1$ ,  $\delta_2$ ,  $K_1$  and  $K_2$  values eliminates the biphasic chemical shift variation observed in the other data sets. A fit of the *m*-fluorocinnamate data to the appropriate equation for the equilibrium shown in equation (2.1) as described in the introduction yields  $K_1 = 31.0 \pm 0.4 \text{ dm}^3 \text{ mol}^{-1}$  and  $\delta_1 - \delta_0$  (apparent) =  $1.50 \pm 0.01 \text{ ppm}$ ; the best fit is shown in Figure 2.4.

The variation of the  $^1\text{H}$  decoupled fluorocinnamate  $^{19}\text{F}$  linewidth with  $[\alpha\text{CD}]$  is also markedly biphasic with the exception of the *m*-fluorocinnamate system which exhibits no significant broadening. In the absence of  $\alpha\text{CD}$  the  $^{19}\text{F}$  linewidths are 3-5 Hz (1.6 Hz digital resolution) and the maximum broadenings observed for the  $\alpha$ ,*p*-difluorocinnamate system are 120 and 45 Hz for the  $\alpha$ - and *p*-  $^{19}\text{F}$  resonances, respectively. As  $[\alpha\text{CD}]$  increases the line broadening increases systematically to a maximum coincident with the maximum  $[\text{S.}\alpha\text{CD}]$  as calculated from  $K_1$  and  $K_2$  (Table 2.2) and thereafter decreases as shown in Figure 2.5. Similar but smaller systematic line broadenings were observed for the other fluorocinnamates as shown in Figure 2.6 for *o*,*p*-difluorocinnamate.

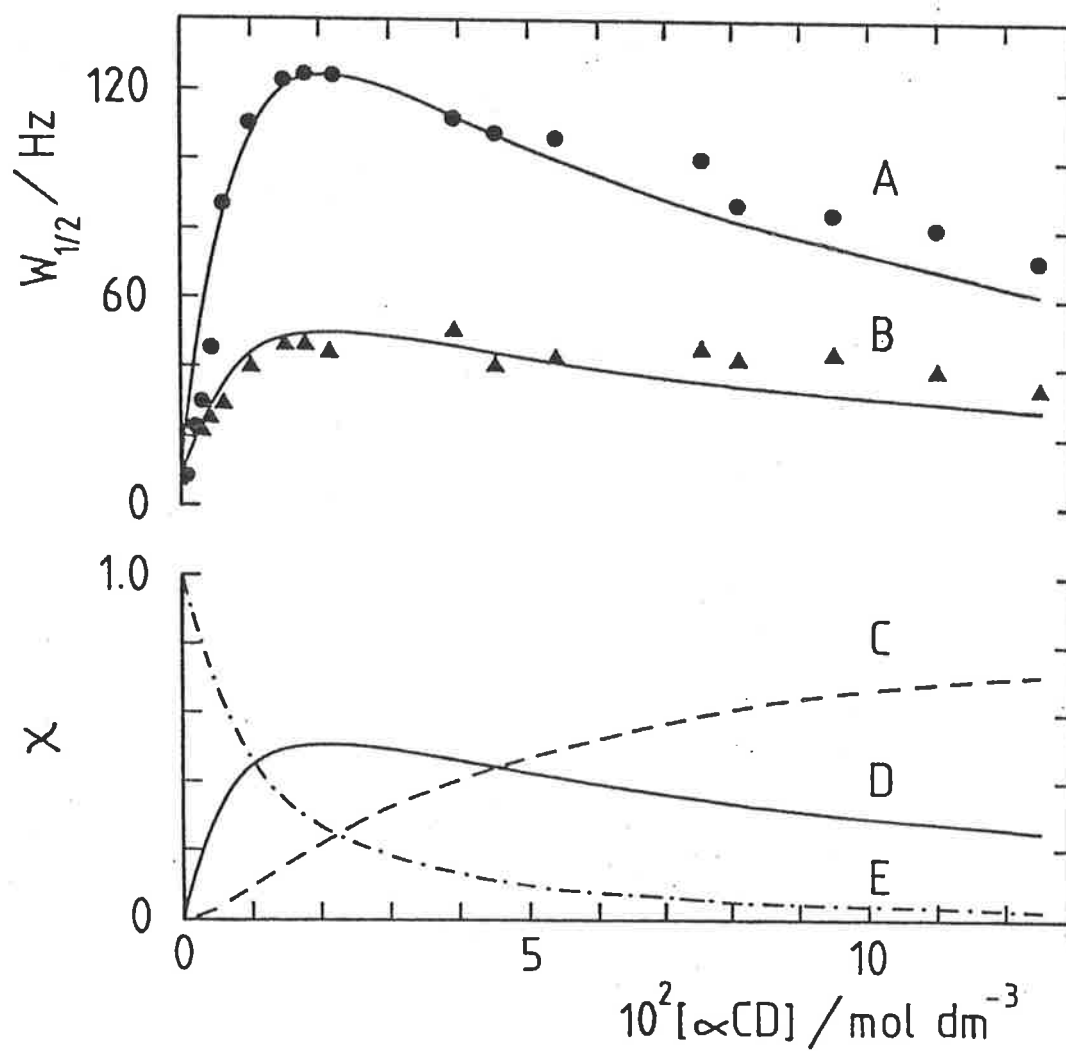


Figure 2.5. The variation of the width at half height,  $W_{1/2}$ , of the  $^1\text{H}$  decoupled  $^{19}\text{F}$  resonances of the  $\alpha$ -F (A) and  $p$ -F (B) of  $\alpha,p$ -difluorocinnamate with  $[\alpha\text{CD}]$ . In the lower part of the figure, the variations of the mole fractions,  $\chi$ , of S, S. $\alpha\text{CD}$  and S. $(\alpha\text{CD})_2$  with  $[\alpha\text{CD}]$  calculated from  $K_1$  and  $K_2$  in Table 2.2 are represented by curves E, D and C respectively.

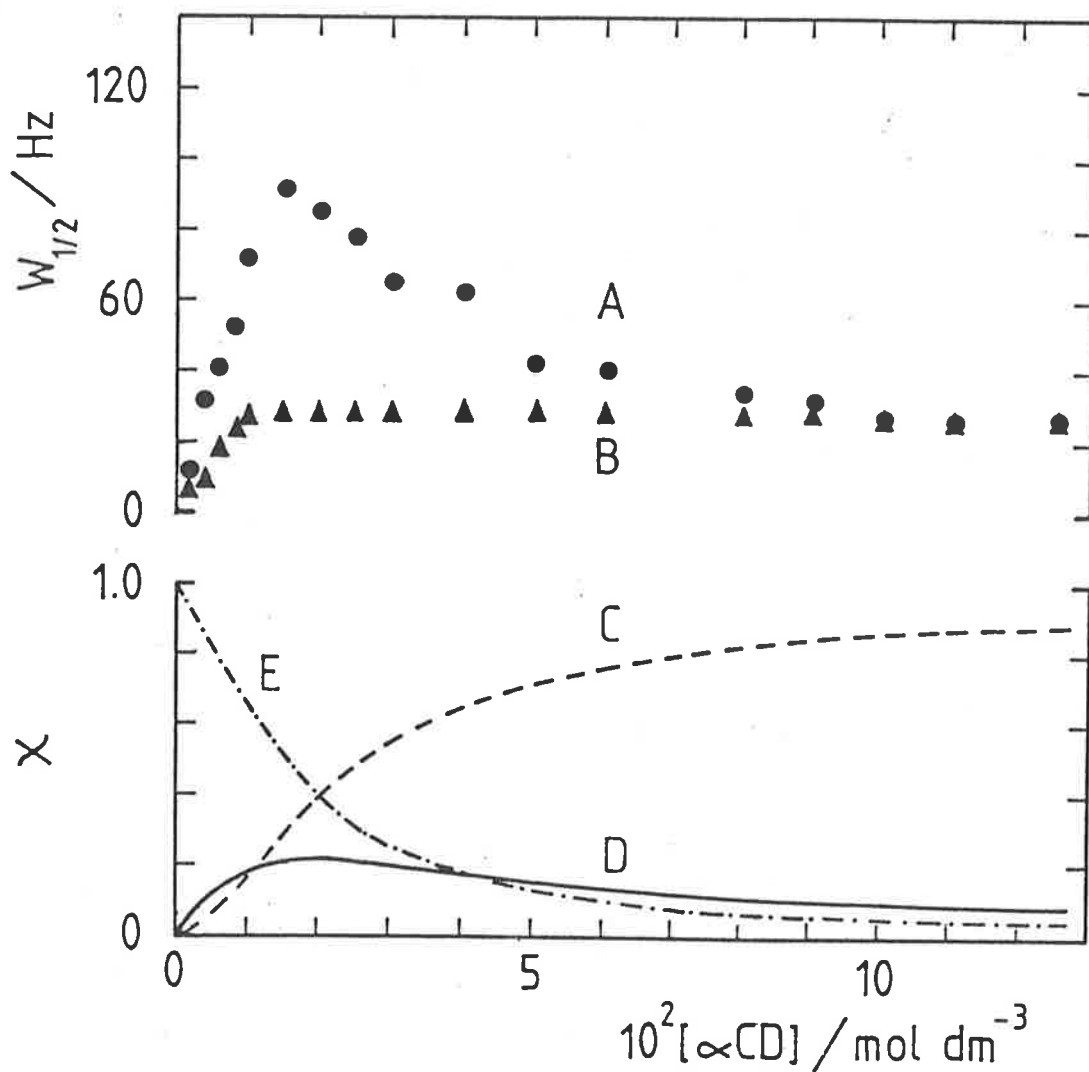


Figure 2.6. The variation of the width at half height,  $W_{1/2}$ , of the  $^1\text{H}$  decoupled  $^{19}\text{F}$  resonances of the *p*-F (A) and *o*-F (B) of *o,p*-difluorocinnamate with  $[\alpha\text{CD}]$ . In the lower part of the figure, the variations of the mole fractions,  $\chi$ , of *S*, *S*. $\alpha\text{CD}$  and *S*.( $\alpha\text{CD}$ )<sub>2</sub> with  $[\alpha\text{CD}]$  calculated from  $K_1$  and  $K_2$  in Table 2.2 are represented by curves E, D and C respectively.

NMR studies<sup>48,49</sup> show that the tumbling or correlation time,  $\tau_c$ , of the complex  $S.(\alpha\text{CD})_2$  as an entity (where  $S = p$ -methylcinnamate) is  $6 \times 10^{-10}$  s at 306 K in water and it may be assumed that similar and smaller  $\tau_c$  values apply for  $S.(\alpha\text{CD})_2$  and  $S.\alpha\text{CD}$  when  $S =$  fluorocinnamate. Such  $\tau_c$  values appear to be too small to produce significant longitudinal  $^{19}\text{F}$  relaxation through dipole-dipole, chemical shift anisotropy or related relaxation processes,<sup>50,51</sup> and hence it is likely that the observed  $^{19}\text{F}$  line broadening occurs predominantly through transverse relaxation. This transverse relaxation is probably a consequence of fluorocinnamate exchange occurring between the  $S$ ,  $S.\alpha\text{CD}$  and  $S.(\alpha\text{CD})_2$  environments. These three species co-exist in significant temperature dependent concentrations over the  $[\alpha\text{CD}]$  range studied and as only a single  $^{19}\text{F}$  resonance is observed even down to 273 K it is clear that the chemical exchange between these species is occurring sufficiently rapidly to coalesce the three resonances to a broad singlet.

Computer simulation of chemical exchange (see chapter 6) between two sites characterised by two singlets of equal intensity of 3 Hz width at half height,  $W_{1/2}$ , and separated by 3.45 ppm shows that single Lorentzian resonances of  $W_{1/2} = 560$  and 50 Hz are observed when the site exchange rate constants are  $5 \times 10^3$  and  $5 \times 10^4 \text{ s}^{-1}$ , respectively. Qualitatively, this indicates that the observed  $\alpha$ -F line broadening is consistent with transverse relaxation being induced by chemical exchange occurring at rates within the range reported for a temperature-jump spectrophotometric study<sup>52</sup> in which amongst other included species, the dissoc-

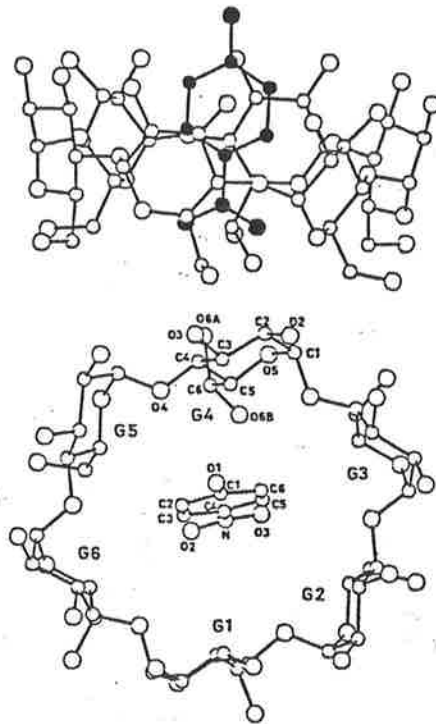


iation of *p*-nitrophenolate from S.αCD was characterised by a dissociation rate constant  $k_d$  (287 K) =  $3.1 \times 10^4 \text{ s}^{-1}$ . However, as for all of the fluorocinnamate systems studied, only a single chemical exchange averaged signal was observed for each fluorine substituent at 273 K it proved impossible to make a quantitative analysis of the exchange kinetics.

(ii) Equilibrium Aspects

The  $^{19}\text{F}$  chemical shift data (Table 2.2) show that S.αCD and S.(αCD)<sub>2</sub> are readily formed when S = fluorocinnamate. However, four different structures potentially exist for S.αCD if the possibilities of either end of S entering either the narrow end or the wide end of the αCD cavity are considered. An examination of space-filling models indicates that entry of the fluorocinnamate through the wider end is favoured on steric grounds over entry through the narrow end. Consistent with this, a  $^{13}\text{C}$  NMR solution study<sup>48</sup> indicates that *p*-methylcinnamate enters through the wider end of the αCD cavity and X-ray diffraction studies<sup>53,54</sup> of crystalline S.αCD, where S = *p*- and *m*-nitrophenol and *p*-hydroxybenzoic acid, reveal molecular structures in which the nitro and carboxylic acid substituent ends of S are inserted into the wider end of the cavity as shown in Figure 2.7. It appears therefore, that the two S.αCD species most likely to be produced in this study are those in which either end of fluorocinnamate is inserted into the wide end of the αCD cavity. This steric restriction requires that S.(αCD)<sub>2</sub> consist of the fluorocinnamate encapsulated by two αCD with the wide ends of their cavities in close proximity, consistent with deductions made from the  $^{13}\text{C}$  NMR spectroscopic studies of

(a)



(b)

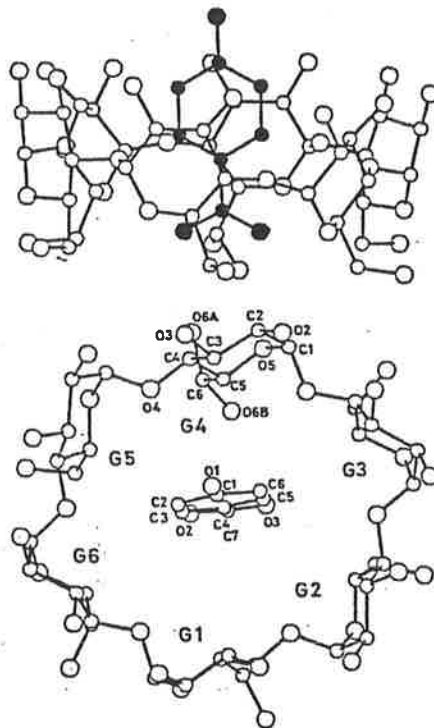


Figure 2.7. X-ray crystallographic structures<sup>53</sup> of the  $\alpha$ CD-p-nitrophenol (a) and  $\alpha$ CD-p-hydroxybenzoic acid (b) complexes.

the inclusion of *p*-methylcinnamate.<sup>48</sup> In consequence of these considerations the four possible environments for a given fluorocinnamate are encompassed by the four equilibria characterised by the constants  $K'_1$ ,  $K''_1$ ,  $K'_2$  and  $K''_2$ , as shown in Figure 2.8. The ratio of the concentration of the two S.αCD species is constant but the  $^{19}\text{F}$  data do not permit a determination of these concentrations separately. It is readily shown, however, that the equilibrium constants in Table 2.2

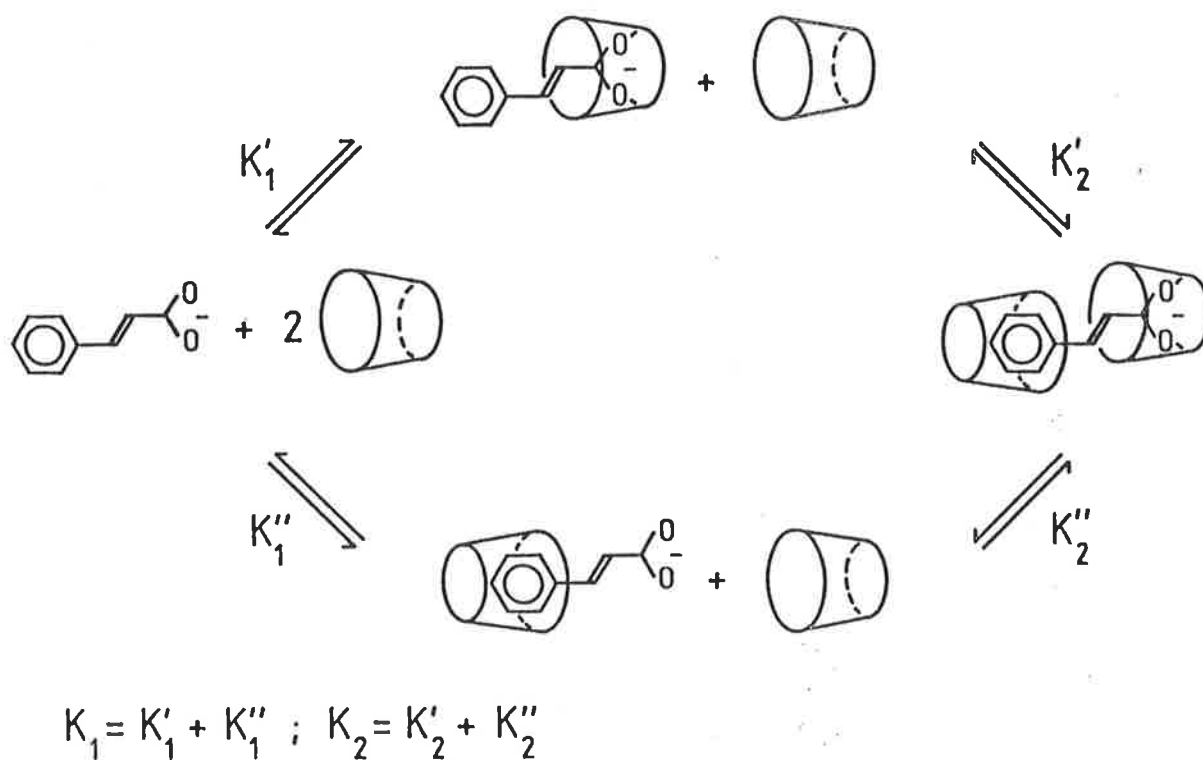


Figure 2.8. Representation of the inclusion equilibria possible in the fluoro- and difluorocinnamate / αCD systems. The truncated cone represents the αCD cavity.

and Figure 2.8 are related through the equalities:

$$K_1 = K'_1 + K''_1$$

and

$$K_2 = K'_2 + K''_2.$$

It is seen from Table 2.2 that the magnitudes of  $K_1$  and  $K_2$  vary with the fluorocinnamate, which probably reflects a combination of the electronic, solvational and stereochemical changes caused by fluorination of cinnamate in the *o*-, *p*- and  $\alpha$  positions. However, the variation of  $K_1$  and  $K_2$  with the fluorocinnamate is modest and encompasses the  $K_1$  and  $K_2$  values reported for cinnamate,<sup>44</sup> which indicates that fluorination of cinnamate does not have a major effect on the cinnamate- $\alpha$ CD inclusion interaction. The  $K_1$  value for cinnamic acid<sup>44</sup> is substantially outside the range exhibited by the fluorocinnamates and probably reflects the effect of substrate charge on the inclusion process.

(iii) <sup>19</sup>F Chemical Shifts.

While factors which influence proton chemical shifts are well known, less is understood of <sup>19</sup>F chemical shift behaviour.<sup>55</sup> The effect on <sup>19</sup>F chemical shifts of external factors such as susceptibility, hydrogen bonding and ring currents has not been as well documented or explained as in the case of proton shifts. There is no correlation between <sup>19</sup>F shifts as a function of structure and the proton chemical shift and structure relationship. For instance, whereas protons on aromatic rings resonate downfield of methyl protons, the reverse is true for fluorine nuclei in similar structures. The direction of induced shifts on complexation

have not been fully rationalized and are not easily predicted. Hydrogen bonding, while predicted to cause deshielding of the  $^{19}\text{F}$  nucleus which is usually observed, has also been used to explain upfield chemical shifts.<sup>56</sup> Also, studies of solvent effects on  $^{19}\text{F}$  chemical shifts show that transfer from water to nonpolar solvent usually induces substantial upfield shifts and yet the majority of observed shifts for fluorinated probe molecules complexed by proteins are downfield.<sup>32</sup>

Clearly the observed shifts are comprised of a number of contributions which are difficult to quantify, including magnetic anisotropy, van der Waals interaction and other specific chemical interaction effects, such as H-bonding. Although the origin of the  $^{19}\text{F}$  shifts on complexation may not be discernible in this work, the relative magnitudes of the shifts provide important information for discussion of the stereochemistry of the complex.

(iv) Stereochemistry of  $\alpha\text{CD}$  - fluorocinnamate complexes  
and Mechanistic Conclusions

The  $^{19}\text{F}$  chemical shift data in Table 2.2 show that:

(i) the formation of  $\text{S}(\alpha\text{CD})_2$  from  $\text{S}\alpha\text{CD}$  induces a greater shift change ( $\delta_2 - \delta_1$ ) than does the formation of  $\text{S}\alpha\text{CD}$  ( $\delta_1 - \delta_0$ ) and

(ii) the shift for  $\alpha\text{-F}$  is downfield for  $\text{S}\alpha\text{CD}$  and  $\text{S}(\alpha\text{CD})_2$  whereas the shifts for  $o\text{-F}$  and  $p\text{-F}$  are downfield and upfield for  $\text{S}\alpha\text{CD}$  and  $\text{S}(\alpha\text{CD})_2$ , respectively. In interpreting these shifts it must be remembered that whilst a given segment of the fluorocinnamate may be in close proximity to a particular segment of  $\alpha\text{CD}$  and will experience a strong local

solvational and electronic variation, the effects of this variation will be transmitted throughout the conjugated fluorocinnamate and will modify all  $^{19}\text{F}$  chemical shifts to some extent. The greatest environmental change experienced by the fluorocinnamates is in  $\text{S}(\alpha\text{CD})_2$ , in which space filling models (Figure 2.9) show fluorocinnamate to be completely encapsulated and where it appears that the fluorocinnamate hydration shell is probably totally lost. The polar carboxylate group of fluorocinnamate interacts more strongly with water than does the phenyl group and accordingly the solvational change experienced by the carboxylate group on transfer from water to the largely hydrophobic  $\alpha\text{CD}$  cavities of  $\text{S}(\alpha\text{CD})_2$  will be greater than that experienced by the phenyl group. Thus,  $\alpha\text{-F}$ , which is adjacent to the carboxylate group, should reflect solvational changes in  $\delta_2 - \delta_0$  more than  $o\text{-}$  and  $p\text{-F}$ . In contrast, the  $\delta_2 - \delta_0$  of  $o\text{-}$  and  $p\text{-F}$  are expected to reflect more strongly the dispersion-force interactions established between the  $\pi$  system of the phenyl group and the interior of the  $\alpha\text{CD}$  cavity, which are considered to be a major factor in the stabilization of cyclodextrin inclusion complexes as discussed in the introduction.

In the  $\text{S}\alpha\text{CD}$  complex one end of the fluorocinnamate is in a water environment whilst the other resides in the  $\alpha\text{CD}$  cavity. The  $p\text{-F}$  is furthest removed from the carboxylate group and exhibits the smallest values for  $\delta_1 - \delta_0$  and the most negative values for  $\delta_2 - \delta_1$ . Thus of  $o\text{-}$  and  $p\text{-F}$  the latter is least affected by the formation of  $\text{S}\alpha\text{CD}$  and most affected by the formation of  $\text{S}(\alpha\text{CD})_2$ . This suggests that the predominant  $\text{S}\alpha\text{CD}$  species formed is that in which the carboxylate group

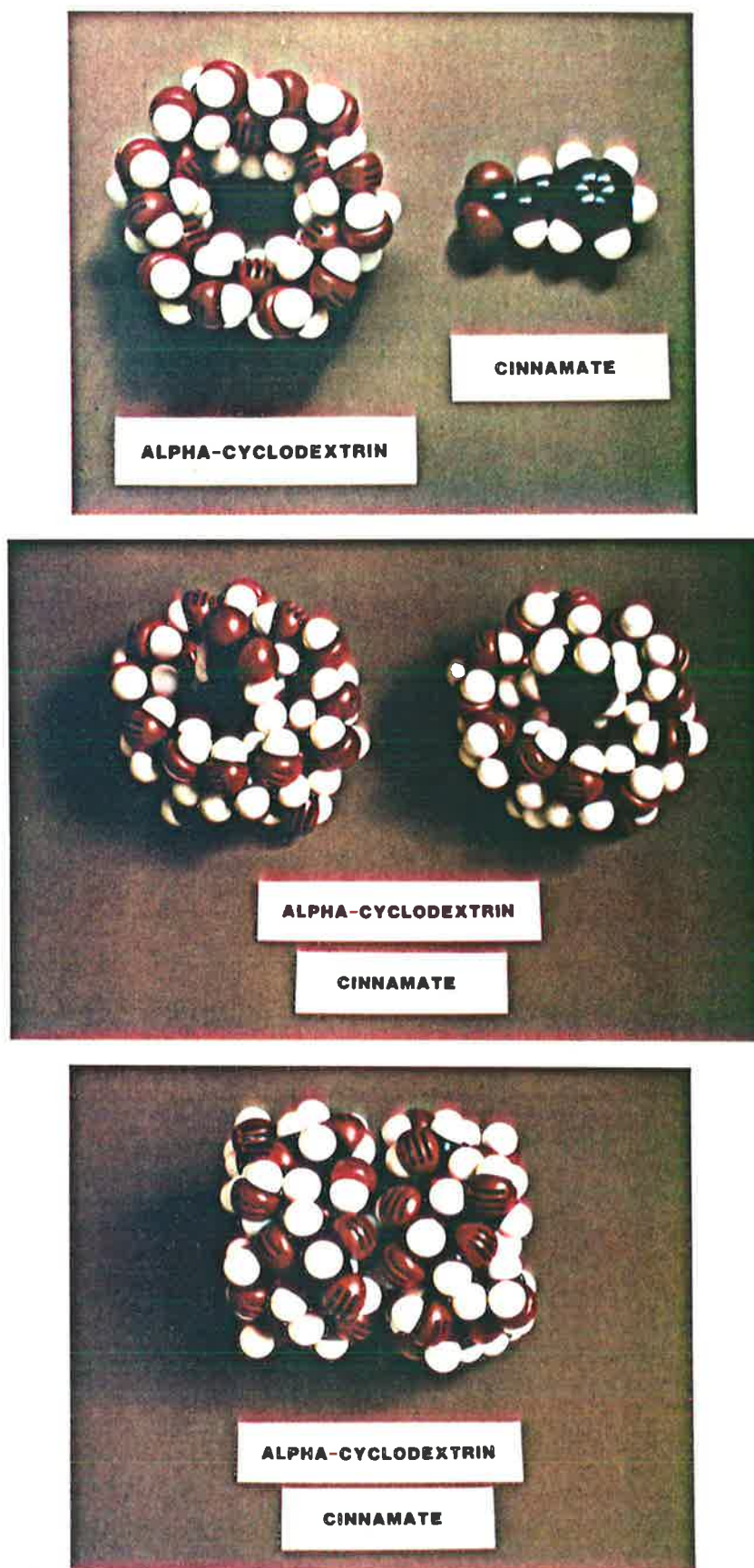


*Figure 2.9 CPK models of  $\alpha$ CD and the cinnamate anion (top), the two conformations of the binary  $\alpha$ -CD - cinnamate complexes (centre) and the ternary  $[S.(\alpha CD)_2]$  complex (bottom).*

enters the  $\alpha$ CD cavity as shown in the equilibrium characterised by  $K''_1$  in Figure 2.8. This deduction is reinforced by the observation that the fluorocinnamate carboxylate substituent bears substantial stereochemical and electronic similarities to the nitro and carboxylic acid groups of *p*- and *m*-nitrophenol and *p*-hydroxybenzoic acid, which were found to be inserted first into the  $\alpha$ CD cavity in S. $\alpha$ CD complexes in the previously discussed X-ray studies.<sup>53,54</sup>

The predominance of the binary complex with the carboxylate group inserted in the  $\alpha$ CD cavity is in accordance with the results of the  $^{13}\text{C}$  NMR study of *p*-methylcinnamate<sup>48</sup> and a range of other carboxylate containing substrates.<sup>27</sup> The overall driving force for formation of such complexes is probably dominated by dipolar or induced dipolar interactions, with other mechanisms making minor contributions only. Hydrophobic and apolar binding mechanisms are thought to be dominated by favorable entropy changes, whereas the formation of complexes in the above conformation is characterized by a favourable enthalpy term dominating an unfavourable entropy term.<sup>27</sup> While a study of the temperature dependence of the stability of the fluorocinnamate -  $\alpha$ CD complexes has not been undertaken, it is likely that the thermodynamics of this system would show similar characteristics to those of complexes investigated by Gelb et al.,<sup>27</sup> as indicated by the conformation of the predominant complex formed.

However, the formation of S. $(\alpha\text{CD})_2$  suggests that the alternative S. $\alpha$ CD complex characterised by  $K''_1$  in Figure 2.8 may well exist as a minor species. The formation of this complex indicates that the energetics of the inclusion of either end of fluorocinnamate in S. $\alpha$ CD in solution may not be



substantially different. The existence of  $S.(\alpha\text{CD})_2$  in the absence of any evidence for the dimerization of  $\alpha\text{CD}$  in the absence of  $S$ , is a demonstration of the substantial magnitude of the interaction established between the fluorocinnamate and  $\alpha\text{CD}$ . This ternary complex may be stabilized to some extent by intermacrocylic interactions formed between the wider rims of the two  $\alpha\text{CD}$  molecules.

### 2.3 Inclusion of Trifluoromethyl Substituted Cinnamates

The influence of substrate steric size and shape is of obvious importance to acquiring an understanding of spatial effects on inclusion by cyclodextrins. These effects have been utilized in studies of catalytic hydrolyses of phenyl esters<sup>16</sup> in which the rate of catalysis was found to be greatly increased for *meta*-substituted substrates relative to corresponding *para*-substituted phenyl esters. This was attributed to the influence of the steric bulk of the *meta*-substituent on the geometry of the inclusion complex, with the ester group being forced into closer contact with the secondary hydroxyl groups of the cyclodextrin.

The addition of a *para*-methyl group to cinnamate has a profound effect upon its inclusion by  $\alpha\text{CD}$ . The stabilities of both the 1:1 and 1:2 complexes formed with *p*-methylcinnamate<sup>48</sup> are increased by orders of magnitude compared to cinnamate, with the 1:2 complex being substantially predominant (Table 2.3). Therefore, it was of interest to investigate the complexation of trifluoromethylcinnamates by  $\alpha\text{CD}$ .

Figure 2.10 shows the variation of  $^{19}\text{F}$  chemical shifts of *p*-trifluoromethyl, *m*-trifluoromethyl and  $\alpha$ -fluoro-*p*-trifluoromethylcinnamates with  $[\alpha\text{CD}]$ . With the exception of *m*-trifluoromethylcinnamate, the  $^{19}\text{F}$  resonances undergo a dramatic downfield shift on the addition of approximately 3 to 8 molar equivalents of  $\alpha\text{CD}$  and then rapidly attain a constant limiting chemical shift, indicating the formation of a highly stable complex. The rapid chemical shift change is accompanied by a simultaneous linewidth variation, as exemplified by  $\alpha$ -fluoro-*p*-trifluoromethylcinnamate in Figure 2.11 where the  $\alpha$ - $^{19}\text{F}$  resonance broadens into the baseline, reappears ca. 10 ppm downfield, and then continues to narrow at high  $[\alpha\text{CD}]$ .

As in the case of the ring fluorinated cinnamates, the chemical shift variations are not monophasic but biphasic, indicating the presence of two complexed species. The overwhelming domination of the second complex formation has resulted in a deficiency in information describing  $\text{S}.\alpha\text{CD}$  over the concentration range studied in this experiment. Consequently, exhaustive attempts to fit the experimental data to equation (2.3) yielded results for the *p*-trifluoromethyl ( $p\text{-CF}_3$ )  $^{19}\text{F}$  chemical shifts only, with uncertain error limits and large standard deviations. The  $\alpha$ - $^{19}\text{F}$  shift curve could not be fitted to any degree, either simultaneously with the  $p\text{-CF}_3$  data or individually. A number of modifications to the algorithm described earlier were also unsuccessful, including attempts to incorporate the two individual  $\text{S}.\alpha\text{CD}$  complexes shown in Figure 2.8 as separate entities. This further exacerbated the problem of lack of data pertaining to the binary complexes.

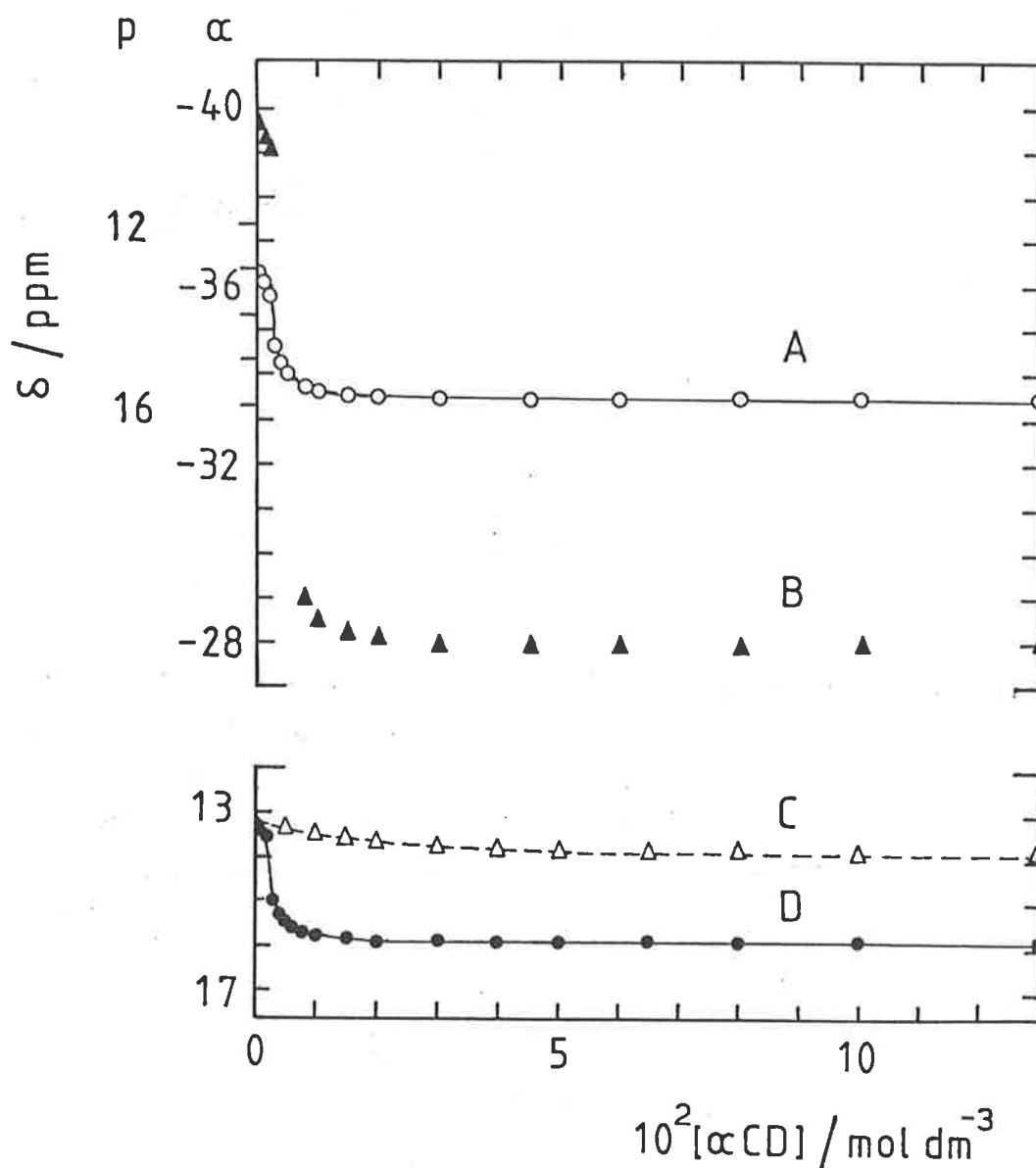


Figure 2.10. Variation of the  $^{19}\text{F}$  chemical shifts of trifluoromethylcinnamates with  $[\alpha\text{CD}]$ . The experimental data are shown as individual points. Curves A and D represent the best fit of the  $p\text{-CF}_3$  chemical shifts of  $\alpha$ -fluoro- $p$ -trifluoromethyl- and  $p$ -trifluoromethylcinnamates to equation 2.3. Curve C for  $m$ -trifluoromethylcinnamate represents the best fit of the data to equation 1.2. The data labelled B pertains to the  $\alpha$ -F resonance of  $\alpha$ -fluoro- $p$ -trifluorocinnamate.

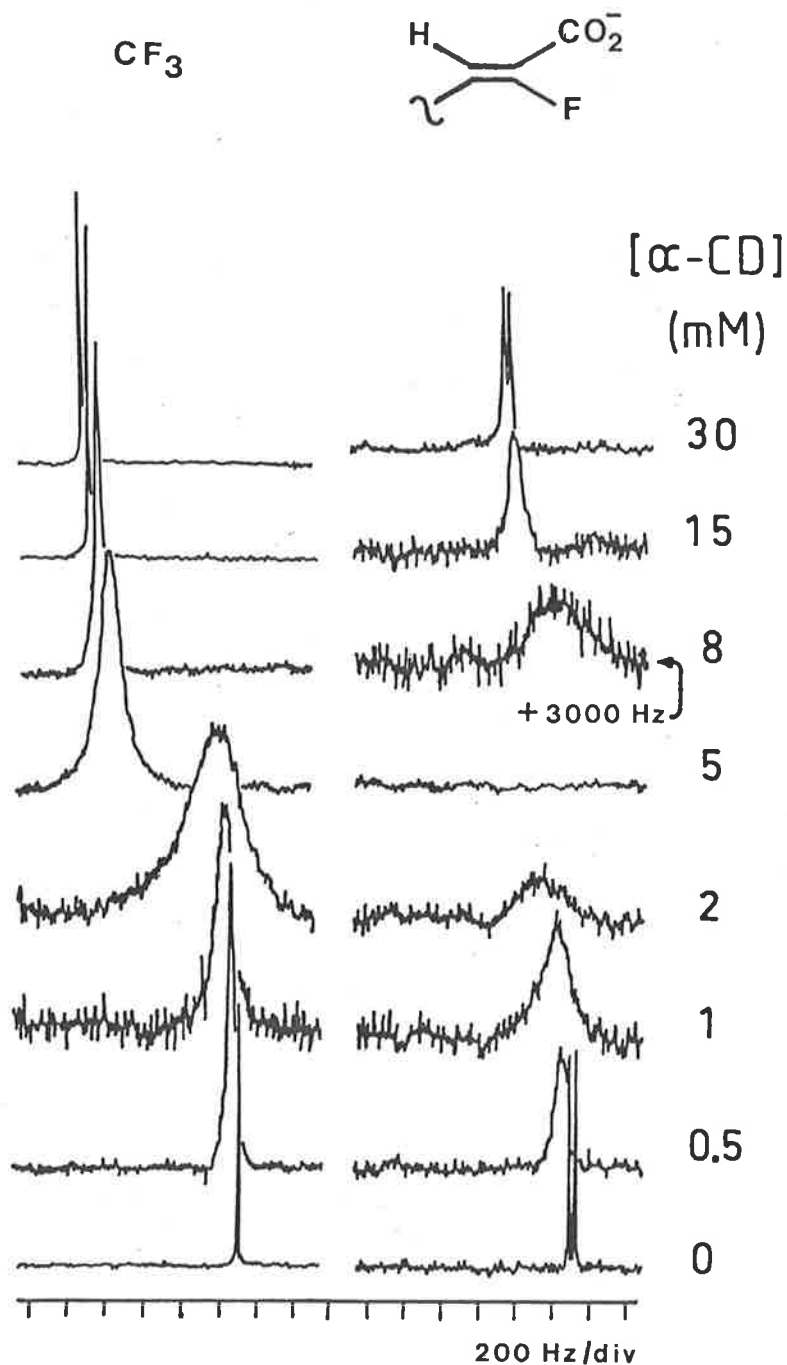


Figure 2.11. Variation of the 282.35 MHz  $^{19}\text{F}$  NMR spectrum of  $\alpha$ -fluoro-*p*-trifluoromethylcinnamate with  $[\alpha\text{CD}]$ . The doublet at high field ( $\delta$  -39.96 ppm) arises from the  $\alpha$ -F and the resonance at low field ( $\delta$  13.31 ppm) arises from the *p*- $\text{CF}_3$  group. The chemical shifts are measured relative to  $\text{CF}_3\text{COO}^-$ . The [cinnamate] was  $10^{-3}$  mol  $\text{dm}^{-3}$  and the aqueous solutions were 0.1 mol  $\text{dm}^{-3}$  in NaCl.

Bearing in mind these limitations, the values presented in Table 2.3 contain useful information pertaining to the complexation of these substrates. While the standard deviations of the parameters are large, the results do produce an acceptable simulation of the experimental data as shown in Figure 2.12 for *p*-trifluoromethylcinnamate in which the low  $[\alpha\text{CD}]$  data only is plotted. The linewidth variation of the  $\text{CF}_3$  resonance is also plotted and, as in the case of the other fluorocinnamates discussed previously, probably reaches a maximum coincident with the maximum binary complex concentration. Again the broadening is thought to arise due to transverse relaxation caused by exchange of the cinnamate between the environments of the three complexes present. The larger

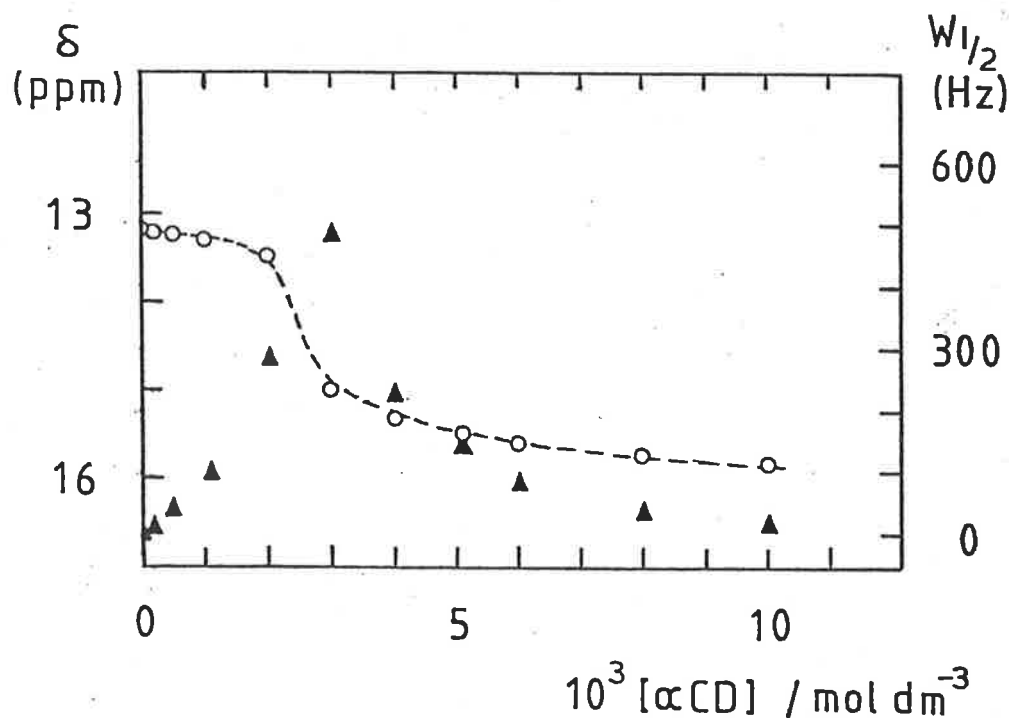


Figure 2.11. Variation of  $^{19}\text{F}$  chemical shift (circles) and  $W_{1/2}$  (triangles) of *p*-trifluoromethylcinnamate with  $[\alpha\text{CD}]$ . The experimental data are represented by individual points and the curve represents the best fit of the chemical shift data to equation 2.3.

Table 2.3. Equilibrium constants and  $^{19}\text{F}$  chemical shifts for Trifluoromethylcinnamates.<sup>a</sup>

<u>trans</u> -cinnamate	$K_1$ $\text{dm}^3\text{mol}^{-1}$	$K_2$ $\text{dm}^3\text{mol}^{-1}$	$\delta_0^b$ ppm	$\delta_1$ ppm	$\delta_2^c$ ppm	$\delta_1 - \delta_0$ ppm	$\delta_2 - \delta_0$ ppm
$\alpha\text{-F-}\underline{p}\text{-CF}_3$	714±1370	2962±3340	( <u>p</u> ) 13.31	9.29±5.6	16.09	-4.02	2.78
			( $\alpha$ )-39.96	-	-27.88	-	12.08
<u>p</u> -CF <sub>3</sub>	967±1400	4270±3300	13.39	9.97±3.5	15.94	-3.42	2.55
<u>m</u> -CF <sub>3</sub>	96±5	-	13.10	14.09±.01	-	0.99	-
<u>p</u> -CH <sub>3</sub> <sup>d</sup>	50	1995					

a Shifts are relative to  $\text{CF}_3\text{CO}_2^-$ . A negative sign indicates an upfield shift.

b Error is 0.01 ppm.

c Measured graphically

d Ref. 48.

linewidths are probably a consequence of a combination of a slower rate of exchange and the greater chemical shift differences between the complexes than those found in the case of the mono- and difluorinated cinnamates.

As noted in Table 2.3, the values of  $K_1$  and  $K_2$  found for *p*-methylcinnamate<sup>48</sup> are of the same order of magnitude as obtained here for both *p*-trifluoromethyl cinnamates. Thus the presence of the *p*-trifluoromethyl group has a similar influence on the complexation to that of the *p*-methyl group, indicating that there is probably no special contribution to the binding mechanism by the fluorine atoms such as hydrogen bonding.

The large increase in stability of the 1:2 complex is not well understood but may contain contributions from interactions between the secondary hydroxyl groups on the wider rims of the two  $\alpha$ CD molecules as mentioned earlier, and from increased van der Waals interactions. The increased axial length of the *p*-trifluoromethylcinnamate produces a substrate with almost "ideal" dimensions for the cavity formed by two  $\alpha$ CD molecules, resulting in an optimum spatial fit of the substrate and the formation of stronger intermolecular van der Waals forces. Presumably, the dipole-dipole interactions discussed previously also contribute to the binding in these complexes, probably to a similar extent to that in the other cinnamate- $\alpha$ CD complexes.

The *m*-trifluoromethylcinnamate  $^{19}\text{F}$  resonance showed a monophasic chemical shift variation with increasing  $[\alpha\text{CD}]$  (Figure 2.10), with no significant line broadening. This data could not be fitted to the algorithm for consecutive formation of 1:1 and 1:2 complexes (equation 2.3) but was simulated with

good precision by the algorithm described in the introduction for the formation of a binary complex only. The best fit is shown in Figure 2.10 and the  $K_1$  value in Table 2.3 pertains to the equilibrium shown in equation (2.1). The value obtained here is similar to that found for *m*-methylcinnamate<sup>43</sup> ( $132 \text{ dm}^3 \text{ mol}^{-1}$ ). It appears that the bulky *meta*- substituent precludes the formation of a stable  $S.(\alpha\text{CD})_2$  inclusion complex as is confirmed by inspection of space-filling models. The van der Waals axial diameter of *m*-trifluoromethylcinnamate is approximately  $8.6 \text{ \AA}$  as measured from CPK models, compared to the cavity diameter of  $5.2 \text{ \AA}$  at the position of the C(3) H atoms. While the observed  $K_1$  value is comprised of contributions from the formation of two complexes, where either the  $\text{CF}_3$  group or the carboxylate group is inserted into the  $\alpha\text{CD}$  cavity, it is likely that the latter conformation is largely dominant as indicated by the small chemical shift change relative to those observed for the *para*- $\text{CF}_3$  groups which are strongly included. Of interest to this discussion would be a study of the inclusion of  $\alpha$ -fluoro-*m*-trifluoromethylcinnamate to determine whether  $\alpha\text{CD}$  includes the cinnamate side chain to any extent as in the case of the other cinnamates.

#### 2.4 Conclusion

##### (i) A Comparison with Binding by $\alpha$ -Chymotrypsin

Although the cyclodextrins have been shown to catalyse various reactions in solution,<sup>1,2,18,19</sup> and are therefore considered as useful enzyme models, it is clear that their use as models for the study of enzyme - substrate binding must be



made with some caution. The factors controlling the complexation of substrates by  $\alpha$ CD are complex and are very sensitive to the nature of the substrate. While most of the driving forces for complexation postulated to be important for inclusion by cyclodextrins probably contribute to the mechanism of binding by enzymes to some extent, their relative importance is probably not as dependent upon the substrate.

$^{19}\text{F}$  NMR studies<sup>41,42</sup> of the binding of *o*-, *m*- and *p*-fluorocinnamates to  $\alpha$ -chymotrypsin showed that the complexes formed are 1 to 2 orders of magnitude more stable ( $K_1 = 909$ , 6250 and 3333 mol dm<sup>-3</sup> respectively) than the complexes formed with  $\alpha$ CD. Whereas  $\alpha$ -chymotrypsin forms dimers and trimers in solution and the substrates may then bind to any of the three forms, dimerization of  $\alpha$ CD occurs only after substrate complexation. The stereospecificity of  $\alpha$ CD complexation appears to be much lower than enzyme binding and mechanisms such as dipole-dipole binding, which are not usually thought to be as important as hydrophobic binding in enzyme systems, may become dominant allowing the inclusion of charged substituents.

Thus  $^{19}\text{F}$  NMR spectroscopy has provided information about the stereochemistry and stability of  $\alpha$ CD complexes, thereby giving some insight into the nature of the driving force for the formation of inclusion complexes in general. Studies to determine the effect of changing the hydrophobic nature of the cyclodextrin cavity, for example by methylation of the hydroxyl groups, are progressing in this laboratory.

CHAPTER 3EXPERIMENTAL3.1. General

Melting points were measured on a Reichert Kofler hot-stage melting point apparatus and are reported uncorrected.

Infrared spectra were recorded on a Jasco IRA-1 grating infrared spectrometer, using the  $1601\text{ cm}^{-1}$  band of polystyrene as a reference. The characteristics of the infrared bands are designated as s, strong; m, medium; w, weak; b, broad.

Mass spectra were measured with a Hitachi Perkin-Elmer RMU-7D double focussing or an AEI MS-30 mass spectrometer operating at 70 eV. The major fragments are given with relative abundances in parentheses.

Routine proton NMR spectra were recorded on either a Varian T-60 or a Jeol PMX-60 spectrometer operating at 60 MHz, with chemical shifts being measured relative to tetramethyl silane as an internal standard. Multiplets of resonances are given as s, singlet; d, doublet; t, triplet and m, complex multiplet. Samples were made up in  $\text{CDCl}_3$  unless otherwise stated.

Elemental analyses were performed by the Australian Microanalytical Service, Melbourne.

3.2. Solution Preparation

Solutions for the  $^{19}\text{F}$  NMR study were made up in  $\text{D}_2\text{O}$  and the pD was adjusted to  $8.5 \pm 0.1$  with  $\text{NaOD}/\text{D}_2\text{O}$  and  $\text{DCl}/\text{D}_2\text{O}$ . The total  $\alpha$ -cyclodextrin concentration,  $[\alpha\text{CD}]$ , varied in the range  $0\text{--}0.130\text{ mol dm}^{-3}$ , the fluorocinnamate concentration was constant at  $10^{-3}\text{ mol dm}^{-3}$  and all solutions were  $0.10\text{ mol dm}^{-3}$  in sodium chloride to keep the ionic strength constant.

### 3.3. NMR Spectra

$^{19}\text{F}$  NMR spectra were run on a Bruker CXP300 NMR spectrometer at 282.35 MHz and on a Bruker HX-90E NMR spectrometer at 84.67 MHz locked on the  $\text{D}_2\text{O}$  deuterium frequency. Spectra were obtained in quadrature detection FT mode and were accumulated into a 8192 point data base using various spectral widths. The Fourier pulse angle used was  $45^\circ$  and where appropriate, the 84.67 MHz  $^{19}\text{F}$  spectra were fully  $^1\text{H}$  decoupled by gating off the BB proton decoupler during acquisition of each data point. The samples in 5 mm o.d. NMR tubes (Wilmad 507-1PP) were thermostatted at  $294 \pm 0.3$  K using a Bruker B-VT 1000 variable temperature unit to control the probe temperature.

Chemical shifts were measured relative to a 2% sodium trifluoroacetate/ $\text{D}_2\text{O}$  solution sealed in a capillary. The use of such an external reference introduces the possibility of the incorporation of bulk susceptibility effects into the observed  $^{19}\text{F}$  chemical shifts. Accordingly, the bulk susceptibility variation introduced through the variation of  $[\alpha\text{CD}]$  was simulated by preparing a series of  $\text{D}_2\text{O}$  solutions containing D-glucose at six times the  $[\alpha\text{CD}]$  employed in the fluorocinnamate inclusion studies. The viscosity of such solutions were found to be approximately equal to those of the corresponding  $\alpha\text{CD}$  solutions at one sixth of the concentration.<sup>57</sup> The  $^{19}\text{F}$  shifts of these solutions measured relative to the reference capillary were used to produce a bulk susceptibility correction chart for the shifts observed in the fluorocinnamate studies. The shift difference between the internal and external trifluoroacetate resonances increases smoothly to a maximum of 0.07 ppm at  $[\text{D-glucose}] = 0.78$  mol  $\text{dm}^{-3}$ . Thus the bulk susceptibility corrections were very small

compared to the shift variation observed for the fluorocinnamates as  $[\alpha\text{CD}]$  varied. (Trifluoroacetate is included by  $\alpha\text{CD}$  and so cannot be used as an internal reference.) No significant shift or line width variation of the  $\alpha\text{-F}$  and  $p\text{-F}$  resonances of  $\alpha,p$ -difluorocinnamate were induced by up to  $0.78 \text{ mol dm}^{-3}$  [D-glucose] in  $\text{D}_2\text{O}$  solution and similar behaviour is assumed for the other fluorocinnamates. By measuring the  $^{19}\text{F}$  shifts of the fluorocinnamate and trifluoroacetate solutions with the applied field  $B_0$  parallel (CXP300) and perpendicular (HX 90-E) to the sample long axis, it was found that general bulk susceptibility effects were negligible.<sup>58</sup>

#### 3.4. Materials

$\alpha$ -Cyclodextrin (Sigma) was stored as the anhydrous material over  $\text{P}_2\text{O}_5$  in a vacuum desiccator prior to use.

The sodium fluorocinnamates were prepared by stoichiometric neutralization of the acids with sodium hydroxide and the solid product was obtained by freeze drying.

The fluorobenzaldehydes were purchased from Koch-Light and were redistilled before use.

$\text{D}_2\text{O}$  was supplied by AAEC and used without further purification.  $\text{CDCl}_3$  (MSD) was dried over Linde 4A molecular sieves.

All solvents employed in the preparative work were redistilled or purified and dried where necessary before use.<sup>59</sup>

### 3.5 Preparation of Fluorocinnamic Acids

#### (i) *o*-Fluorocinnamic acid

##### (a) Ethyl *o*-Fluorocinnamate

The method is a modification of that of Kucherov et al.<sup>45</sup> A solution of *o*-fluorobenzaldehyde (2.5 g, 0.02 mol) and carboethoxymethylidetriphenylphosphorane (16.1 g, 0.046 mol) in dry benzene (200 ml) was heated under reflux in a dry nitrogen atmosphere for 6 hours. The benzene was then removed under reduced pressure, the residue was stirred well with petroleum ether (X4) and filtered. Removal of the solvent and fractional distillation of the residue gave *ethyl o-fluorocinnamate* (3.4 g, 87%) as a colourless oil, b.p. 80-82°C/0.2 mm (lit.<sup>60</sup> 140-141°C/11 mm).

##### (b) *o*-Fluorocinnamic Acid

The ester (2.0 g, 0.01 mol) was saponified in refluxing aqueous 10% sodium hydroxide (30 ml) until the reaction mixture became homogeneous. The solution was cooled, acidified and the crude acid was collected by filtration. Recrystallization from aqueous acetic acid gave *o-fluorocinnamic acid* (1.43 g, 83%) as a white solid, m.p. 179-181°C (lit.<sup>60</sup> 175°C).

#### (ii) *m*-Fluorocinnamic Acid

*m*-Fluorobenzaldehyde (2.48 g, 0.02 mol) was reacted with the phosphorane (8.8 g, 0.025 mol) as described above to give *ethyl m-fluorocinnamate* (3.6 g, 92%), b.p. 74-75°C/0.1 mm (lit.<sup>61</sup> 137°C/11 mm).

Saponification of the ester (2.0 g, 0.01 mol) gave *m-fluorocinnamic acid* (1.43 g, 86%), m.p. 166-167°C (lit.<sup>62</sup> 166.5°C).

(iii) *p*-Trifluoromethylcinnamic Acid

*p*-Trifluoromethylbenzaldehyde (2.5 g, 0.0143 mol) was reacted with the phosphorane (5.7 g, 0.016 mol) as above to give the crude ester which was purified by 'flash' column chromatography<sup>63</sup> on silica (Merck, 230-400 mesh, 20% ether/X4) to give ethyl *p*-trifluoromethylcinnamate (3.2 g, 92%), as a white crystalline solid which was recrystallized from X4, m.p. 36-37°C. Calculated for C<sub>12</sub>H<sub>11</sub>F<sub>3</sub>O<sub>2</sub>: C, 59.02; H, 4.54; F, 23.33. Found: C, 59.33; H, 4.62; F, 23.0%.  $\nu_{\max}$  1710 s, 1640 m, 1325 s cm<sup>-1</sup>. <sup>1</sup>H NMR:  $\delta$  1.32 (3H, t, J 7 Hz, OCH<sub>2</sub>CH<sub>3</sub>), 4.23 (2H, t, J 7 Hz, OCH<sub>2</sub>CH<sub>3</sub>), 6.40 (1H, d, J 16 Hz, =CHCO<sub>2</sub>-), 7.50 (4H, m, Ar-H), 7.83 (1H, d, J 16 Hz, Ar-CH=).

Saponification of the ester (2.0 g, 0.0082 mol) gave *p*-trifluoromethylcinnamic acid (1.63 g, 92%) as a white solid, m.p. 228-229°C (lit.<sup>64</sup> 229.5-230°C).

(iv)  $\alpha$ ,*p*-Difluorocinnamic Acid(a) Ethyl  $\alpha$ ,*p*-difluorocinnamate

The method described is essentially that of Bergmann and Shahak.<sup>46</sup>

To a suspension of sodium hydride (2.40 g, 50% dispersion in oil, 0.05 mol) in dry xylene (50 ml) at 40-50°C, about 10 drops of dry ethanol were added, followed by diethyl oxalate (8.0 g, 0.055 mol) with stirring under a dry nitrogen atmosphere. Then a solution of ethyl fluoroacetate (5.3 g, 0.05 mol) in dry xylene (15 ml) was added dropwise, resulting in a vigorous reaction. After heating at 60°C for 1 hour, the temperature was increased to remove the ethanol by distillation, followed by a small amount of xylene (c.a. 5 ml). After cooling for 30 minutes, *p*-fluorobenzaldehyde (6.2 g, 0.05 mol)

in dry xylene (10 ml) was added dropwise and the reaction mixture was then heated at reflux for 30 minutes, cooled and poured into water (250 ml). This mixture was then extracted with ether (2 x 50 ml), the combined extracts were washed with 5% sodium carbonate solution (50 ml) and water (2 x 50 ml). The pale yellow ethereal solution was then dried over sodium sulphate, evaporated and the residue was fractionally distilled affording *ethyl  $\alpha$ , $p$ -difluorocinnamate* (4.3 g, 41%) as a colourless oil, b.p. 78–80°C/0.15 mm, which crystallized on standing, m.p. 20–22°C. Calculated for  $C_{11}H_{10}O_2F_2$ : C, 62.26; H, 4.75; F, 17.91. Found: C, 62.35; H, 5.02; F, 17.8%.  $\nu_{\max}$  1730 s, 1665 m, 1605 m, 1510 s  $cm^{-1}$ .  $^1H$  NMR ( $CCl_4$ ):  $\delta$  1.37 (3H, t, J 7 Hz,  $OCH_2CH_3$ ), 4.25 (2H, d, J 7 Hz,  $OCH_2CH_3$ ), 6.77 (1H, d,  $J_{H-F}$  41 Hz,  $CH=CF$ ), 6.8–7.6 (4H, m, Ar-H); m/e 212 ( $M^+$ , 100), 184(30), 167(44), 139(25).

(b)  **$\alpha$ , $p$ -Difluorocinnamic Acid**

Saponification of the ester (2.0 g, 0.009 mol) as described above yielded  *$\alpha$ , $p$ -difluorocinnamic acid* (1.51 g, 87%) as a white solid, m.p. 205–206°C.  $\nu_{\max}$  (nujol): 1680, 1650, 1595  $cm^{-1}$ .  $^1H$  NMR ( $d_6$ -DMSO):  $\delta$  7.00 (1H, d,  $J_{F-H}$  37 Hz,  $CH=CF$ ), 7.02–7.83 (4H, m, Ar-H), 12.2 (1H, s,  $CO_2H$ ). m/e 184 ( $M^+$ , 100), 164(19), 120(28).

(v)  **$\alpha$ -fluoro- $p$ -trifluoromethylcinnamic acid**

*p*-Trifluoromethylbenzaldehyde (2.0 g, 0.011 mol) was reacted with ethyl fluoroacetate (1.22 g, 0.011 mol) and diethyl oxalate (1.85 g, 0.013 mol) in the presence of sodium hydride (0.011 mol) as described above which afforded *Ethyl  $\alpha$ -fluoro- $p$ -trifluoromethylcinnamate* (1.54 g, 52%) as a colourless oil, b.p. 106–108°C/2.0 mm.  $\nu_{\max}$  1725 s, 1665 m, 1620 w,

1325 s  $\text{cm}^{-1}$ .  $^1\text{H}$  NMR:  $\delta$  1.37 (3H, t, J 7 Hz,  $\text{OCH}_2\text{CH}_3$ ), 4.32 (2H, q,  $\text{OCH}_2\text{CH}_3$ ), 6.83 (1H, d,  $J_{\text{H-F}}$  33 Hz, Ar-CH=), 7.57 (4H, m, Ar-H). Accurate mass: Calculated for  $\text{C}_{12}\text{H}_{10}\text{F}_4\text{O}_2$  262.0616924, found 262.062462; m/e 234 ( $\text{M}^+$ , 100%), 234(44), 233(25), 217(54), 189(29).

Saponification of the ester (0.27 g, 0.001 mol) as described previously afforded  $\alpha$ -fluoro-p-trifluoromethylcinnamic acid (0.217 g, 93%) as a white crystalline solid, m.p. 172-173°C.  $\nu_{\text{max}}$  (nujol): 1710 s, 1655 m, 1615 w  $\text{cm}^{-1}$ .  $^1\text{H}$  NMR ( $d_6$ -DMSO):  $\delta$  6.90 (1H, d,  $J_{\text{H-F}}$  34 Hz, Ar-CH=), 7.62 (4H, m, Ar-H). Accurate Mass: Calculated for  $\text{C}_{10}\text{H}_6\text{F}_4\text{O}_2$  234.0303923; found 234.030887. m/e 243 ( $\text{M}^+$ , 100%), 214(17), 197(15), 186(15).



REFERENCES

1. M.L. Bender and M. Komiyama, "Cyclodextrin Chemistry", Springer-Verlag, Berlin, 1978.
2. J. Szejtli, "Cyclodextrins and Their Inclusion Complexes", Akademiai Kiado, Budapest, 1982.
3. E.P. Kyba, R.C. Helgeson, K. Madan, G.W. Gokel, T.L. Tarnowski, S.S. Moore and D.J. Cram, *J. Am. Chem. Soc.*, **99**, 2564 (1977).
4. G.A. Melson, Ed., "Coordination Chemistry of Macrocyclic Compounds", Plenum Press, New York, 1979.
5. J-M. Lehn, *Accounts Chem. Res.*, **11**, 49 (1978).
6. J-M. Lehn, *Pure Appl. Chem.*, **51**, 979 (1979).
7. A. Villiers, *C.R. Acad. Sci.*, **112**, 536 (1891).
8. F. Schardinger, *Wien. Klin. Wochenschr.*, **17**, 207 (1904).
9. K. Freudenberg and M. Meyer-Delius, *Ber. Dtsch. Chem. Ges.*, **71**, 1596 (1938).
10. K. Freudenberg and F. Cramer, *Z. Naturforsch.*, **B 3**, 464, (1948).
11. A.O. Pulley and D. French, *Biochem. Biophys. Res. Commun.*, **5**, 11 (1961).
12. P.C. Manor and W. Saenger, *J. Am. Chem. Soc.*, **96**, 3630 (1974).
13. D.J. Wood, F.E. Hruska and W. Saenger, *J. Am. Chem. Soc.*, **99**, 1735 (1977).
14. W. Saenger, *Angew. Chem. Int. Ed. Eng.*, **19**, 344 (1980).
15. J. Szejtli, Ed., *Proc. 1st Int. Symp. Cyclodextrins, Budapest, Hungary, 1981*; D Reidel, Dordrecht, Holland, 1982.

16. R.L. Van Etten, J.F. Sebastian, G.A. Clowes and M.L. Bender, *J. Am. Chem. Soc.*, **89**, 3242 (1967).
17. R.L. Van Etten, G.A. Clowes, J.F. Sebastian and M.L. Bender, *J. Am. Chem. Soc.*, **89**, 3253 (1967).
18. I. Tabushi and Y. Kuroda, *Adv. Catalysis*, **32**, 417 (1983).
19. M. Komiyama and M.L. Bender, in *New Compr. Biochem.*, "The Chemistry of Enzyme Action", (M.I. Page, Ed.), Elsevier, 1984, pp. 505 - 527.
20. I. Iwakura, K. Uno, F. Toda, S. Onozuka, K. Hattori and M.L. Bender, *J. Am. Chem. Soc.*, **97**, 4432 (1975).
21. I. Tabushi, Y. Kuroda and T. Mizutani, *Tetrahedron*, **40**, 545 (1984).
22. K. Fujita, T. Shinoda and T. Imoto, *J. Am. Chem. Soc.*, **102**, 1161 (1980).
23. A.P. Croft and R.A. Bartsch, *Tetrahedron*, **39**, 1417 (1983).
24. I. Tabushi, Y. Kiyosuke, T. Sugimoto and K. Yamamura, *J. Am. Chem. Soc.*, **100**, 916 (1978).
25. F. Cramer, *Revs. Pure Appl. Chem.*, **5**, 143 (1955).
26. P.C. Manor and W. Saenger, *Nature (London)*, **237**, 392 (1972).
27. R.I. Gelb, L.M. Schwartz, B. Cardelino, H.S. Fuhrman, R.F. Johnson and D.A. Laufer, *J. Am. Chem. Soc.*, **103**, 1750 (1981).
28. G. Nemethy and H.A. Scheraga, *J. Chem. Phys.*, **36**, 3401 (1962).
29. W. Saenger, M. Noltemeyer, P.C. Manor, B. Hingerty and B. Klar, *Bioorg. Chem.*, **5**, 187 (1976).
30. I. Tabushi, *Tetrahedron*, **40**, 269 (1984).

31. T.M. Spotswood, J.M. Evans and J.H. Richards,  
*J. Am. Chem. Soc.*, **89**, 5052 (1967).
32. J.T. Gerig, *Biol. Magn. Reson.*, **1**, 139 (1978).
33. O. Jardetzky, *Adv. Chem. Phys.*, **7**, 499 (1964).
34. B.D. Sykes, *J. Am. Chem. Soc.*, **91**, 949 (1969).
35. H.J. Knight, E.H. Williams and T.M. Spotswood,  
*Aust. J. Chem.*, **31**, 2187 (1978).
36. M. Tsavalos, B.C. Nicholson and T.M. Spotswood,  
*Aust. J. Chem.*, **31**, 2179 (1978).
37. B.C. Nicholson and T.M. Spotswood, *Aust. J. Chem.*,  
**26**, 135 (1973).
38. B.C. Nicholson and T.M. Spotswood, *Aust. J. Chem.*,  
**31**, 2167 (1978).
39. (a) M.L. Bender, G.R. Schonbaum and B. Zerner,  
*J. Am. Chem. Soc.*, **84**, 2540 (1962).  
(b) *ibid*, **84**, 2550 (1962).
40. J.T. Gerig and J.D. Reinheimer, *J. Am. Chem. Soc.*,  
**92**, 3146 (1970).
41. J.T. Gerig, B.A. Halley and C.E. Ortiz, *J. Am. Chem. Soc.*,  
**99**, 6219 (1977).
42. J.T. Gerig, B.A. Halley, D.T. Loehr and J.A. Reimer,  
*Org. Magn. Reson.*, **12**, 352 (1979).
43. K. Uekama, M. Otagiri, Y. Kanie, S. Tanaka and K. Ikeda,  
*Chem. Pharm. Bull.*, **23**, 1421 (1975).
44. K.A. Connors and T.W. Rosanske, *J. Pharm. Sci.*,  
**69**, 173 (1980).
45. V.F. Kucherov, B.G. Kovalev, I.I. Nazarova and L.A.  
Yanovskaya, *Akad. Nauk SSSR, Izv. Otdel. Nauk*,  
1405 (1960).
46. E.D. Bergmann and I. Shahak, *J. Chem. Soc.*, 4033 (1961).

47. B.C. Nicholson, *Ph.D dissertation*, University of Adelaide, 1973.
48. R.I. Gelb, L.M. Schwartz and D.A. Laufer, *J. Am. Chem. Soc.*, **100**, 5875 (1978).
49. J.P. Behr and J.M. Lehn, *J. Am. Chem. Soc.*, **98**, 1743 (1976).
50. T.C. Farrar and E.D. Becker, "Pulse and Fourier Transform NMR", Academic Press, New York, 1971, p.46.
51. W.E. Hull and B.D. Sykes, *J. Mol. Biol.*, **98**, 121 (1975).
52. F. Cramer, W. Saenger and H-Ch. Spatz, *J. Am. Chem. Soc.*, **89**, 14 (1967).
53. K. Horata, *Bull Chem. Soc. Jpn.*, **50**, 1416 (1977).
54. K. Horata, H. Uedaira and J. Tanaka, *Bull. Chem. Soc. Jpn.*, **51**, 1627 (1978).
55. J.W. Emsley and L. Phillips, *Prog. NMR Spectrosc.*, **3**, 261 (1970).
56. R. Hauge and L.W. Reeves, *J. Phys. Chem.*, **70**, 2753 (1966).
57. N.J. Smith, *Honours Thesis*, University of Adelaide, 1984.
58. D.H. Live and S.I. Chan, *Anal. Chem.*, **42**, 791 (1970).
59. D.D. Perrin, W.L.F. Aramaego and D.R. Perrin, "Purification of Laboratory Chemicals", 2nd Ed., Pergamon, Oxford, 1980.
60. K. Kindler, *Liebigs Ann.*, **464**, 278 (1928).
61. K. Kindler, *Chem. Ber.*, **69**, 2792 (1936).
62. G. Schiemann and W. Winkelmueller, *J. Prakt. Chem.*, **135**, 101 (1932).
63. W.C. Still, M. Kahn and A. Mitra, *J. Org. Chem.*, **43**, 2923 (1978).
64. T.A. Wittstruck and E.N. Trachtenberg, *J. Am. Chem. Soc.*, **89**, 3803 (1967).

PART 2

A  $^{23}\text{Na}$  NMR STUDY OF SODIUM CRYPTATES

CHAPTER 4.STRUCTURAL ASPECTS OF CRYPTATES

## 4.1

CRYPTATES: GENERAL INTRODUCTION

The macrocyclic coordination chemistry of the alkali metal and alkaline earth metal ions has been the subject of intensive study in recent years.<sup>1-8</sup> Much of the interest in these metal ions arose from the discovery of their biological importance. For example, sodium and potassium ions constitute the major ionic component of intra- and extracellular fluids and the transport of these ions across cell membranes initiates the nerve impulse.

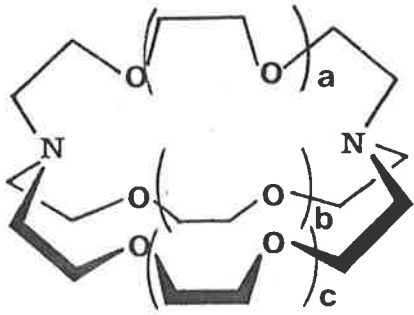
Various naturally occurring macrocyclic molecules selectively complex alkali metal cations by wrapping around the ion, completely isolating it from solvent molecules, as illustrated for the antibiotic valinomycin -  $K^+$  complex in the Figure in the foreword. Detailed studies of this complexation process<sup>9</sup> revealed a strong solvent dependence of the complex stability, indicating involvement of the solvent in the mechanism of complexation which entails sequential solvent displacement from the first solvation sphere of the metal ion and conformational changes in the valinomycin molecule. Two of these processes were detected in sound absorption kinetic studies,<sup>10</sup> one where a complex was formed in which the solvent was only partially displaced from the first solvation sphere of  $K^+$ , and the subsequent process of sequential displacement of remaining solvent synchronously with the formation of the valinomycin bracelet conformation around  $K^+$ . These mechanistic studies were important in the development of a model for the ionophoric action of the antibiotics and are discussed in more

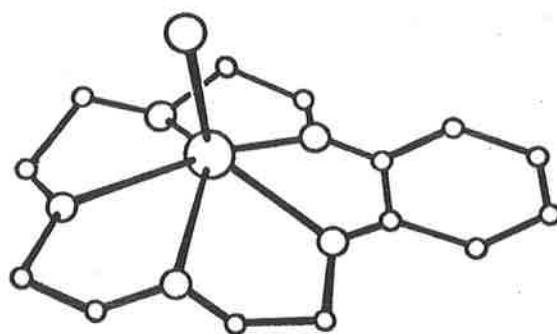
detail in reference to the cryptands in subsequent sections.

Synthetic macrocyclic polyethers, or crown ethers, were introduced in 1967<sup>11</sup> and showed similar complexation of metal cations. However, in these complexes the metal ion often remains in contact with solvent molecules or the associated anions, since the coordinating oxygen atoms of the crown ether form a circle around the metal ion, depending upon the size and flexibility of the ring. Thus benzo-[15]-crown-5 is too small and inflexible to completely displace water from the first coordination sphere of  $\text{Na}^+$ <sup>12</sup>, whereas the large crown ether dibenzo-[30]-crown-10 completely encloses  $\text{K}^+$  and excludes water from its solvation sphere,<sup>13</sup> as shown in Figure 4.1, closely resembling the complex formed by  $\text{K}^+$  and the antibiotic nonactin.

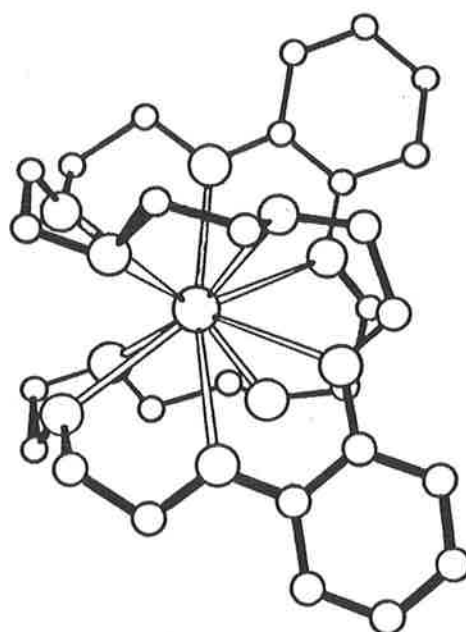
The design and preparation of ligands which completely encapsulate metal ions and thereby imitate the antibiotics,<sup>1</sup> was most successfully achieved by Lehn with the introduction of the diazapoloxamacrobicyclic ligands, or cryptands.<sup>14,15</sup> The general structure and naming of the cryptands are shown in Table 4.1

**Table 4.1** Cryptand Nomenclature.

	a	b	c	Cryptand
	0	0	0	C111
	1	0	0	C211
	1	1	0	C221
	1	1	1	C222
	2	2	2	C333
	1	1	3rd bridge $\text{C}_8\text{H}_{16}$	C22C <sub>8</sub>
				etc



(a)



(b)

Figure 4.1. a) The structure of  $[\text{Na}.\text{(B[15]C-5)}]^+$ . Sodium is the six coordinated central atom with the apical water molecule represented by a single sphere. The five oxygen atoms are shown as larger spheres and the smaller spheres represent the carbon atoms.<sup>12</sup>

b) The structure of  $[\text{K}.\text{(DB[30]C-10)}]^+$ . Potassium is the ten coordinated central atom. The ten oxygen atoms are represented by the larger spheres, and carbon atoms by small spheres.<sup>13</sup>



The cryptand structure delineates approximately spherical cavities containing both nitrogen and oxygen binding sites and the cavity size may be varied by altering the number of ethylene-oxy linkages in the nitrogen-nitrogen bridges. The cavity shape is also determined by the bridgehead nitrogen configurations. The ligand may exist in either of three forms, exo-exo, exo-endo or endo-endo which rapidly interconvert via nitrogen inversion. The endo-endo form shown in the figure in Table 4.1, is strongly favoured on complex formation as both nitrogens may participate in binding interactions. This is confirmed by the cryptate conformation found in all crystal structure determinations performed to date, examples of which are discussed in following sections.

The cryptands were found to form very highly stable complexes (cryptates) with metal cations which are of a size appropriate for the cryptand cavity. The properties of the cryptates are strongly dependent upon the cryptand structure and a number of structural modifications have been made in attempts to gain an understanding of the various factors which characterise the complexation process, and to enhance particular cryptate functions.

The properties of cryptates in general are well reviewed in the literature<sup>1,16-18</sup> and a number of important features are discussed in the introductions to the following sections. The aim of this work was to investigate structural, thermodynamic, kinetic and mechanistic aspects of the sodium cryptates of C211 and a structurally modified analogue, C21C<sub>5</sub>, which would complement existing information, thereby gaining further insight into cryptate complexation processes in general.

STRUCTURAL ASPECTS: INTRODUCTION

The relationship between the natures of the metal ion and the cryptand and the structure of the cryptate formed is fundamental to the general thermodynamic and kinetic properties of cryptates. Generally, the structure of metal ion - ligand complexes in the solid state cannot be assumed to represent the complex structure in solution, since various solvational and conformational changes may occur on dissolution. However, it has become apparent from studies mentioned below that in the case of alkali metal cryptates such a correlation may be made. This has proved particularly useful in aiding mechanistic discussion of cryptate equilibria in solution. The work in this section deals with various structural aspects of cryptates which are essential to the interpretation of kinetic and thermodynamic results presented in later sections.

**Determination of Cryptate Structure**

The cryptands may form complexes with alkali metal ions ( $M^+$ ) in which  $M^+$  resides in the centre of the cryptand cavity in an "inclusive" cryptate or in which  $M^+$  is located on the outside of a cryptand face defined by one of the polyoxadiazacycloalkane rings in an "exclusive" cryptate. (Perhaps a more appropriate term for the latter conformation is "addition" complex as this better describes the intermediate formed prior to inclusion. However, the exclusive terminology has been adopted in the literature and will be used here.) The inclusive cryptate is exemplified by  $[Li.C211]I$  and  $[Na.C221]NCS$  (Figure 4.2a), and the exclusive cryptate by  $[K.C221.NCS]$  (Figure 4.2b), whose structures have been determ-

ined by single crystal X-ray diffraction methods<sup>19,20</sup>. The solid state structure of [Na.C211.X] had not previously been determined. In the inclusive cryptates the Li<sup>+</sup> and Na<sup>+</sup> first coordination spheres are occupied solely by the binding groups of the cryptand, whilst in the exclusive cryptate the nitrogen of NCS<sup>-</sup> is within bonding distance of K<sup>+</sup> and accordingly the above formulae are adopted for these cryptates. In solution both inclusive and exclusive cryptates are shown as cations (e.g. [M.C221]<sup>+</sup>) as any anion in the M<sup>+</sup> first coordination sphere in the solid state is likely to be displaced by solvent on dissolution.

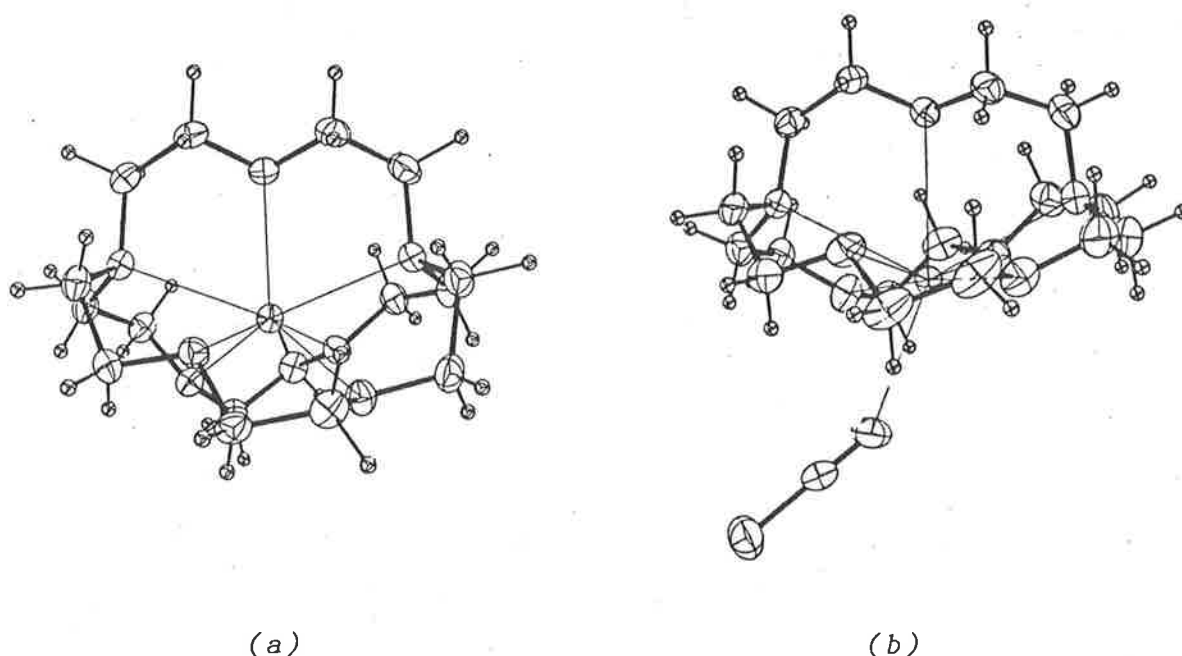
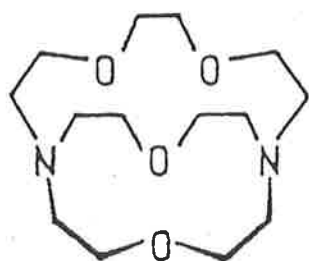


Figure 4.2. View of (a) [Na.C221]NCS and (b) [K.C221.NCS]. Hydrogen atoms are represented by spheres of arbitrary size and thermal ellipsoids are drawn at the 30% probability level.<sup>20</sup>

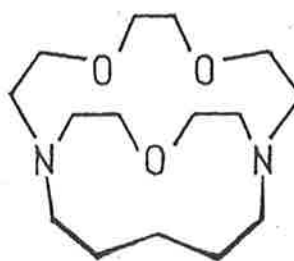
It has been deduced from <sup>13</sup>C NMR studies that these inclusive and exclusive structures are retained in solution.<sup>21</sup>

The  $^{13}\text{C}$  chemical shifts of the cryptand show characteristic variation on complexation by alkali metal ions, depending upon the type of cryptate formed. These results may then be correlated with the known solid state structure, which allows a prediction of the structure in solution.

Quite apart from its own intrinsic interest, a knowledge of the inclusive or exclusive nature of cryptates in solution can be important in mechanistic interpretation<sup>21</sup> of the kinetic parameters characterising  $\text{M}^+$  exchange between the fully solvated and the cryptate environment. As part of a wider structural and kinetic investigation of cryptates this study examines the structural effects of replacing an oxygen in one of the rings of C211 by a carbon to give C21C<sub>5</sub> (shown schematically below) on the  $\text{Na}^+$  cryptates in the solid state by X-ray diffraction, and on both  $\text{Na}^+$  and  $\text{Li}^+$  cryptates in solution by  $^{13}\text{C}$  NMR spectroscopy.



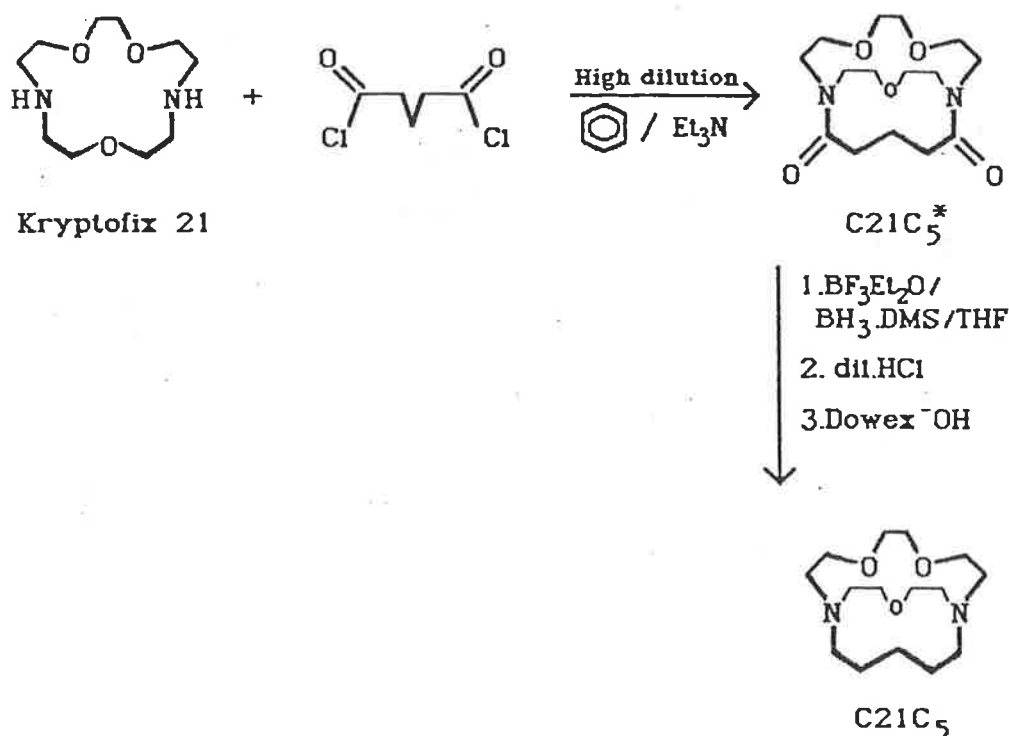
C211

C21C<sub>5</sub>

RESULTS AND DISCUSSION(i) Synthesis of Cryptand C21C<sub>5</sub>

The synthetic method for the preparation of cryptands was reported by Lehn<sup>22</sup> and involved the condensation of diamines with diacid chlorides under conditions of high dilution in moderate yield, followed by diborane reduction of the resultant diamide. This general method appeared to be convenient for our purposes of preparing C21C<sub>5</sub>, particularly as the immediate monocyclic diamine precursor (1,4,10-trioxa-7,13-diazacyclopentadecane) had become commercially available (Merck, Kryptofix 21).

The synthetic method used here is depicted in Scheme 4.1 and is essentially that of Lehn with some minor modifications.



Scheme 4.1. Synthetic route for C21C<sub>5</sub>. The asterisk indicates the bridge in the cryptand structure containing the diamide carbonyl groups.<sup>22</sup>

The high dilution condensation reaction was carried out with the use of motor driven syringes to allow very even addition rates of the two reactant solutions, which appeared to result in much improved yields of the diamide, typically up to 85 percent. In this way, the total volume of solvent required for the reactant solutions could also be reduced.

Reduction of the diamide was achieved with the more convenient borane-dimethylsulphide reagent introduced by Brown.<sup>23</sup> The preparation and properties of  $C_{21}C_5$  had not previously been reported in the literature, although it had been proposed<sup>24</sup> as an efficient ion carrier for  $Li^+$ , and rates of transport of  $Li^+$  and  $Na^+$  by  $C_{21}C_5$  through a chloroform membrane had been published.<sup>25</sup>

#### (i) X-ray Crystallography

The crystal structures of  $[Na.C_{21}C_5.NCS]$  and  $[Na.C_{21}C_5.NCS]$  were determined as described in the experimental section at the end of this chapter. The bond lengths and bond angles for  $[Na.C_{21}C_5.NCS]$  are given in Tables 4.2 and 4.3 in which the primed atoms represent the minor contributors to the disordered cryptand. The differences between the conformations of the primed and unprimed cryptand are insignificant and the structure of the latter and major contributor is shown together with the atom numbering system in Figure 4.3. Thus  $[Na.C_{21}C_5.NCS]$  is seen to exist as an exclusive cryptate with  $Na^+$  residing 0.14 Å outside the plane defined by O(1), O(2), and O(3) where the equation for the plane is :  $-0.2705x + 0.8136y + 0.5146z = 0.6059$ . The  $[Na.C_{21}C_5.NCS]$  cryptate also exists as the exclusive complex

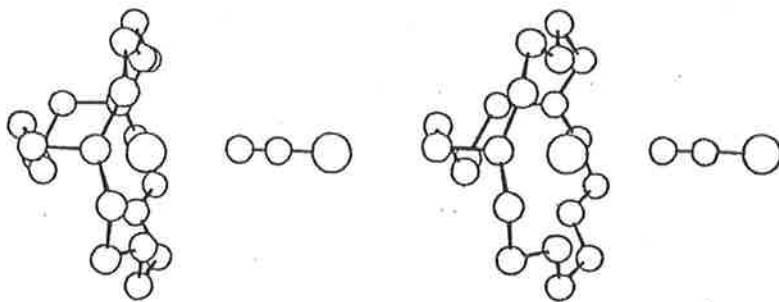
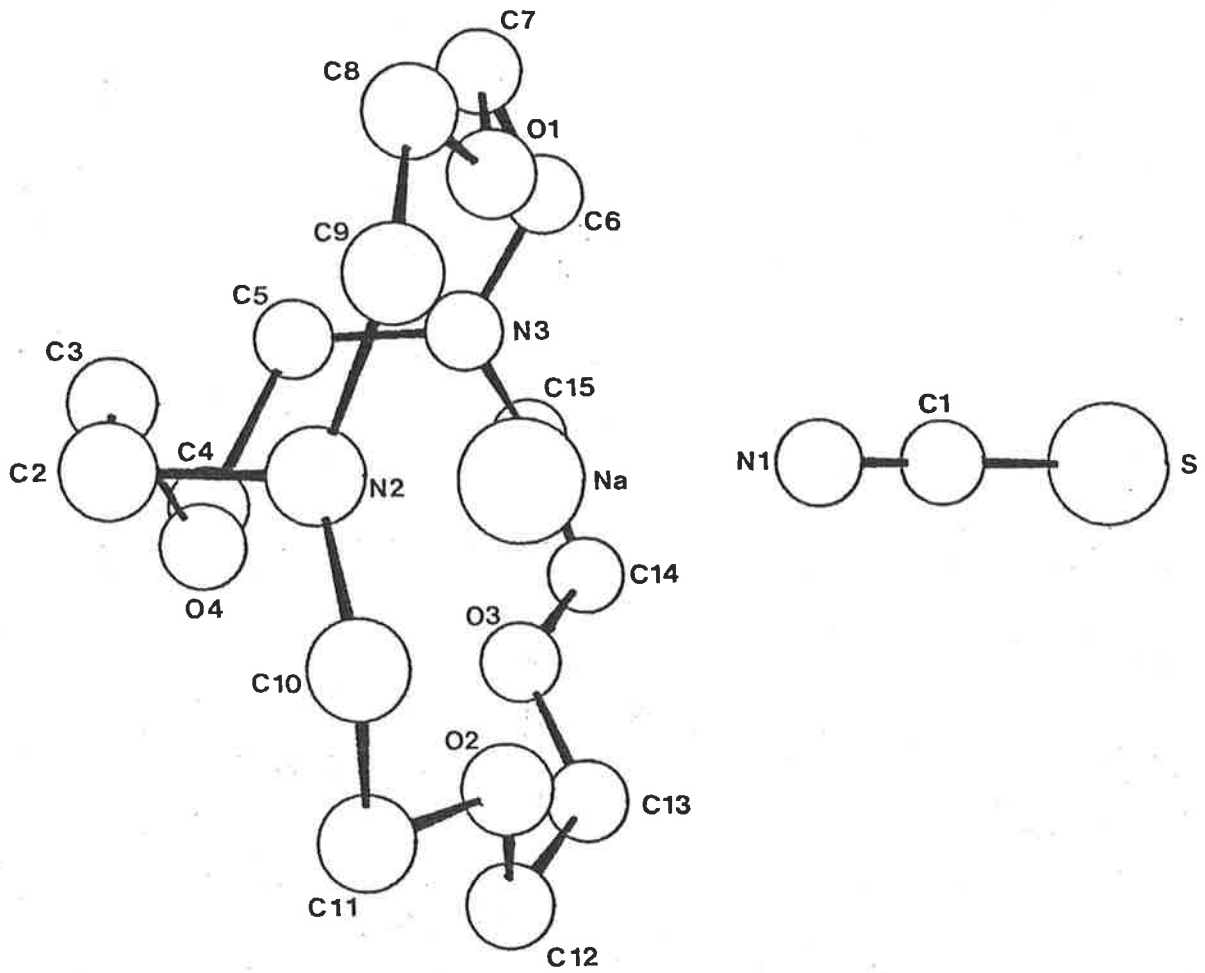


Figure 4.3. Perspective view (top), and stereoscopic view (bottom) of the  $[Na.C_{211}.NCS]$  crystal structure.

Table 4.2

Bond Lengths (Å) for [Na.C211.NCS]

O(1)	Na(1)	2.289(14)
O(2)	Na(1)	2.324(13)
O(3)	Na(1)	2.433(19)
O(4)	Na(1)	2.662(9)
N(1)	Na(1)	2.409(11)
N(2)	Na(1)	2.478(13)
N(3)	Na(1)	2.492(17)
C(1)	S(1)	1.616(28)
C(8)	O(1)	1.385(18)
C(7)	O(1)	1.374(59)
C(11)	O(2)	1.402(56)
C(12)	O(2)	1.370(38)
C(13)	O(3)	1.365(70)
C(14)	O(3)	1.299(42)
C(3)	O(4)	1.447(62)
C(4)	O(4)	1.408(31)
C(1)	N(1)	1.143(28)
C(2)	N(2)	1.504(41)
C(9)	N(2)	1.509(61)
C(10)	N(2)	1.474(38)
C(5)	N(3)	1.542(54)
C(6)	N(3)	1.306(53)
C(15)	N(3)	1.441(83)
C(3)	C(2)	1.617(70)
C(5)	C(4)	1.555(49)
C(7)	C(6)	1.701(74)
C(9)	C(8)	1.464(24)
C(11)	C(10)	1.557(49)
C(13)	C(12)	1.481(63)
C(15)	C(14)	1.341(62)
O(1')	Na(1)	2.290(21)
O(2')	Na(1)	2.348(19)
O(3')	Na(1)	2.316(23)
O(4')	Na(1)	2.594(19)
N(2')	Na(1)	2.450(22)
N(3')	Na(1)	2.422(26)
C(10)	O(2')	1.355(46)
C(12)	O(3')	1.319(58)
C(4)	O(4')	1.469(49)
C(8)	N(2')	1.455(27)
N(3')	O(3)	1.817(69)
C(6)	N(3')	1.496(39)
C(14)	N(3')	1.506(72)
C(5')	C(4)	1.448(62)
C(8')	C(8)	1.430(39)
C(10')	C(10)	1.493(73)
C(12')	C(12)	1.469(81)
C(14')	C(14)	1.672(86)
C(7')	O(1')	1.264(30)
C(8')	O(1')	1.443(43)
C(12')	O(2')	1.399(41)
C(14')	O(3')	1.204(40)
C(3')	O(4')	1.439(36)
C(2')	N(2')	1.524(33)
C(10')	N(2')	1.476(41)
C(5')	N(3')	1.461(32)
C(3')	C(2')	1.557(42)
C(7')	C(6')	1.782(37)



**Table 4.3**

Valence Angles (°) for [Na.C211.NCS]

---

N(1)	-C(1)	-S(1)	178.7(24)
C(1)	-N(1)	-Na(1)	160.4(11)
O(2)	-Na(1)	-O(1)	145.2(5)
O(3)	-Na(1)	-O(1)	140.7(6)
O(4)	-Na(1)	-O(1)	94.9(4)
O(3)	-Na(1)	-O(2)	72.8(6)
O(4)	-Na(1)	-O(2)	84.3(4)
O(4)	-Na(1)	-O(3)	75.4(5)
N(1)	-Na(1)	-O(1)	94.5(11)
N(1)	-Na(1)	-O(2)	92.2(4)
N(1)	-Na(1)	-O(3)	92.7(5)
N(1)	-Na(1)	-O(4)	168.1(4)
C(12)	-O(2)	-C(11)	113.9(34)
C(10)	-C(11)	-O(2)	109.5(35)
N(2)	-C(10)	-C(11)	110.0(25)
C(10')	-C(10)	-O(2')	110.8(35)
C(10)	-N(2)	-C(2)	112.5(27)
C(10)	-N(2)	-C(9)	112.4(32)
C(9)	-N(2)	-C(2)	113.4(31)
C(3)	-C(2)	-N(2)	109.8(33)
O(4)	-C(3)	-C(2)	102.1(38)
C(4)	-O(4)	-C(3)	108.9(32)
C(5)	-C(4)	-O(4)	112.4(26)
C(5')	-C(4)	-O(4')	107.0(36)
C(4)	-C(5)	-N(3)	113.2(35)
C(15)	-N(3)	-C(5)	107.5(44)
C(6)	-N(3)	-C(5)	123.6(49)
C(15)	-N(3)	-C(6)	112.8(49)
C(14)	-C(15)	-N(3)	127.5(59)
C(15)	-C(14)	-O(3)	112.2(43)
C(14')	-C(14)	-N(3')	102.6(45)
C(14)	-O(3)	-C(13)	121.0(45)
C(12)	-C(13)	-O(3)	118.6(48)
C(13)	-C(12)	-O(2)	106.1(33)
C(12')	-C(12)	-O(3')	103.6(44)
C(7)	-C(6)	-N(3)	110.0(42)
C(6)	-C(7)	-O(1)	105.8(38)
C(8)	-O(1)	-C(7)	118.6(17)
C(9)	-C(8)	-O(1)	113.1(13)
C(8')	-C(8)	-N(2')	115.8(19)
N(2')	-C(10')	-C(10)	111.3(25)
C(10')	-N(2')	-C(8)	115.6(24)
C(2')	-N(2')	-C(8)	102.1(21)
C(2')	-N(2')	-C(10')	117.8(24)
C(3')	-C(2')	-N(2')	112.3(24)
O(4')	-C(3')	-C(2')	99.1(23)
C(3')	-O(4')	-C(4)	112.1(17)
N(3')	-C(5')	-C(4)	115.5(23)
C(6')	N(3')	-C(5')	114.8(21)
O(3')	-C(14')	-C(14)	122.7(33)
C(14')	-O(3')	-C(12)	114.7(31)
O(2')	-C(12')	-C(12)	117.8(29)
C(7')	-C(6')	-N(3')	107.4(22)
O(1')	-C(7')	-C(6')	101.8(21)
C(8')	-O(1')	-C(7')	104.9(26)

---

as shown in Figure 4.4 which also shows the atom numbering system used for the bond lengths given in Table 4.4 and the bond angles in Table 4.5. In this cryptate  $\text{Na}^+$  is 0.37 Å outside the plane defined by O(1), O(2), and O(3) ( where the equation for the plane is :  $-0.0725x + 0.2022y + 0.9767z = 3.3146$  ) a substantially greater distance than that observed in [Na.C211.NCS].

In both cryptates the large size of  $\text{Na}^+$  relative to that of the cryptand cavity evidently dictates the formation of exclusive cryptates in contrast to [Li.C211]I which is an inclusive cryptate<sup>19</sup>. Complexation on the face of the fifteen membered ring of both cryptands brings  $\text{Na}^+$  into close proximity to three oxygens and two nitrogens. This together with the larger size of the cusp formed by this ring (and hence its greater ability to accomodate  $\text{Na}^+$  ) by comparison with that of the twelve membered ring is probably the major determinant of stereochemistry in both exclusive cryptates.

The closer proximity of  $\text{Na}^+$  to the O(1), O(2), O(3) plane in [Na.C211.NCS] probably reflects the interaction of  $\text{Na}^+$  with O(4) which is absent in [Na.C21C<sub>5</sub>.NCS]. In both cryptates N(1) of  $\text{NCS}^-$  is within bonding distance of  $\text{Na}^+$  and thus in [Na.C211.NCS] sodium is seven coordinate (bonding interactions with O(1), O(2), O(3), O(4), N(1), N(2), and N(3) ) whilst in [Na.C21C<sub>5</sub>.NCS] sodium is six coordinate (bonding interactions with O(1), O(2), O(3), N(1), N(2), and N(3) ). As a consequence of the Na(1)-O(4) bonding interaction a major stereochemical difference arises in the conformations of the C(2)-C(6) and C(2)-C(5) bridges of [Na.C21C<sub>5</sub>.NCS] and [Na.C211.NCS] respectively (Figures 4.3 and 4.2). Other stereochemical differences are the larger Na(1)-N(1) distance

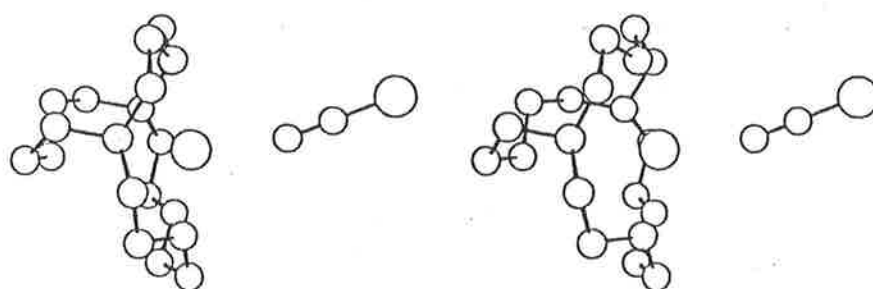
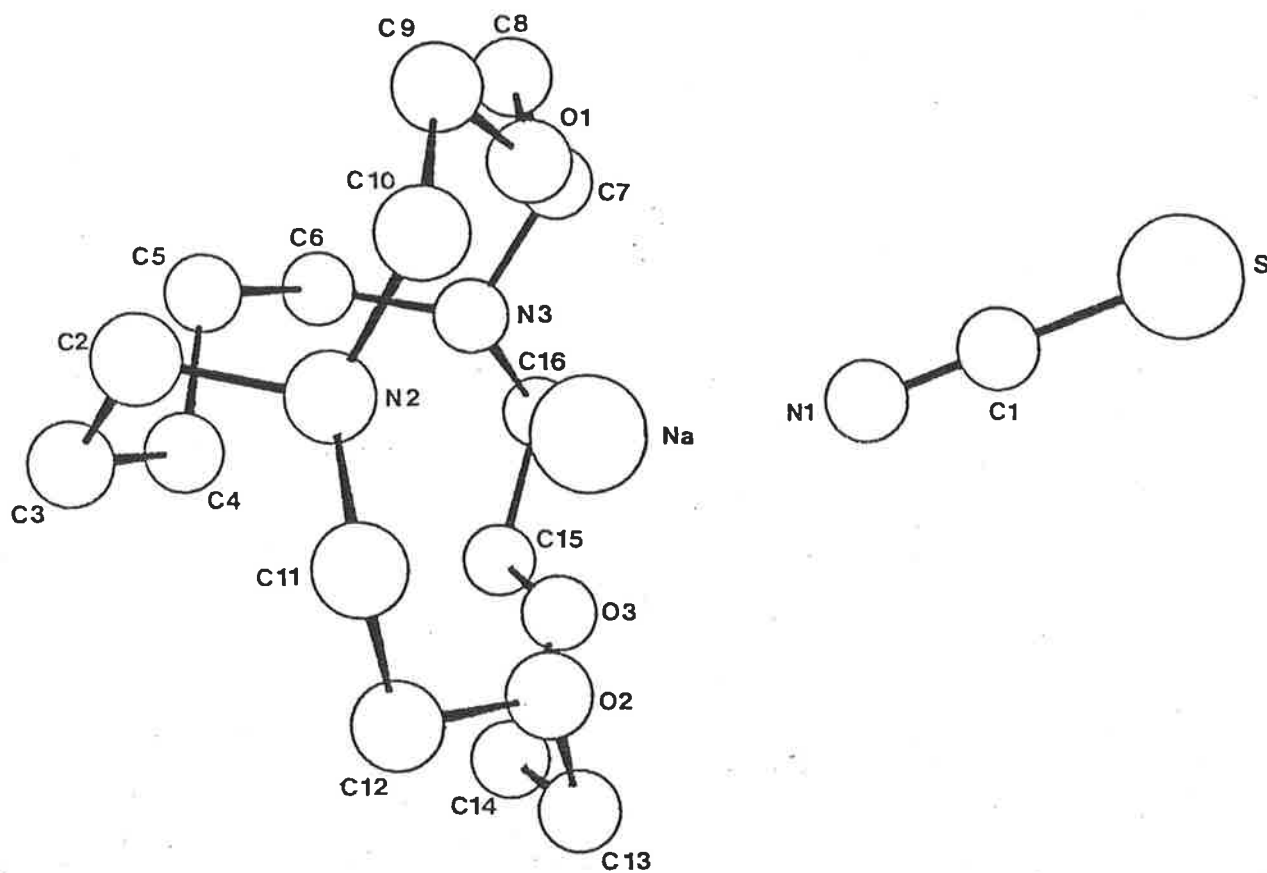


Figure 4.4. Perspective view (top) and stereoscopic view (bottom) of the [Na.C<sub>21</sub>C<sub>5</sub>.NCS] crystal structure.

Table 4.4Bond lengths (Å) for [Na.C<sub>21</sub>C<sub>5</sub>.NCS]

---

O(1) ---Na(1)	2.297(2)
O(2) ---Na(1)	2.340(3)
O(3) ---Na(1)	2.356(2)
N(1) ---Na(1)	2.358(4)
N(2) ---Na(1)	2.759(4)
N(3) ---Na(1)	2.576(3)
C(1) ---S(1)	1.609(5)
C(8) ---O(1)	1.416(4)
C(9) ---O(1)	1.429(4)
C(12)---O(2)	1.381(4)
C(13)---O(2)	1.427(4)
C(14)---O(3)	1.416(4)
C(15)---O(3)	1.421(4)
C(1) ---N(1)	1.167(5)
C(2) ---N(2)	1.471(4)
C(10)---N(2)	1.478(4)
C(11)---N(2)	1.465(4)
C(6) ---N(3)	1.475(4)
C(7) ---N(3)	1.466(4)
C(16)---N(3)	1.478(4)
C(3) ---C(2)	1.522(5)
C(4) ---C(3)	1.522(5)
C(5) ---C(4)	1.504(5)
C(6) ---C(5)	1.523(5)
C(8) ---C(7)	1.509(4)
C(10)---C(9)	1.502(5)
C(12)---C(11)	1.490(5)
C(14)---C(13)	1.492(5)
C(16)---C(15)	1.502(5)

---

**Table 4.5**Bond Angles (°) for [Na.C<sub>2</sub>1C<sub>5</sub>.NCS]

---

N(1) -C(1) -S(1)	179.5(3)
C(1) -N(1) -Na(1)	164.3(3)
O(2) -Na(1)-O(1)	136.7(1)
O(3) -Na(1)-O(1)	141.4(1)
O(3) -Na(1)-O(2)	72.2(1)
N(1) -Na(1)-O(1)	94.7(1)
N(1) -Na(1)-O(2)	103.6(1)
N(1) -Na(1)-O(3)	102.3(1)
C(9) -O(1) -C(8)	115.3(2)
C(13)-O(2) -C(12)	116.4(3)
C(15)-O(3) -C(14)	114.9(3)
C(10)-N(2) -C(2)	110.4(3)
C(11)-N(2) -C(2)	111.1(3)
C(7) -N(3) -C(6)	112.8(3)
C(11)-N(2) -C(10)	111.4(3)
C(16)-N(3) -C(6)	112.0(3)
C(16)-N(3) -C(7)	111.5(3)
C(3) -C(2) -N(2)	113.9(3)
C(4) -C(3) -C(2)	114.1(3)
C(5) -C(4) -C(3)	114.3(3)
C(6) -C(5) -C(4)	114.3(3)
C(5) -C(6) -N(3)	114.0(3)
C(8) -C(7) -N(3)	113.2(3)
C(7) -C(8) -O(1)	107.9(3)
C(10)-C(9) -O(1)	107.9(3)
C(9) -C(10)-N(2)	113.4(3)
C(12)-C(11)-N(2)	115.0(3)
C(11)-C(12)-O(2)	111.2(3)
C(14)-C(13)-O(2)	113.4(3)
C(13)-C(14)-O(3)	108.1(3)
C(16)-C(15)-O(3)	107.3(3)
C(15)-C(16)-N(3)	111.6(3)

---

and the smaller N(1) - Na(1) - O(2) and N(1) - Na(1) - O(3) angles observed for [Na.C211.NCS].

### (iii) Cryptate Structure in Solution - $^{13}\text{C}$ NMR Spectroscopy

In a  $^{13}\text{C}$  NMR study<sup>21</sup> of  $[\text{K.C221}]^+$  and  $[\text{Na.C221}]^+$  Popov and coworkers found that the chemical shifts of the cryptates varied markedly from those of the cryptand. The resonances of  $[\text{Na.C221}]^+$  which is an inclusive cryptate in the solid state, were all shifted upfield relative to those of the free ligand in deuterio-chloroform solution. (In this thesis, the terms 'upfield' and 'downfield' refer to shifts to lower frequency and higher frequency respectively.)  $[\text{K.C221}]^+$  is an exclusive complex in the solid state and its  $^{13}\text{C}$  resonances were also shifted upfield, but to a lesser extent and with the exception of the resonance assigned to the carbons next to nitrogen in the longer bridge. This peak shifted substantially downfield, separated from the other carbon adjacent to nitrogen by about 4.4 ppm. These chemical shift changes were attributed to differences in torsion angles of various bonds in the two different cryptate conformations.

On the basis of the optimisation of fit between the alkali metal ion and the cryptand cavity,  $[\text{Li.C211}]^+$  and  $[\text{Na.C211}]^+$  resemble  $[\text{Na.C221}]^+$  and  $[\text{K.C221}]^+$  respectively, and are inclusive and exclusive cryptates in the solid state as discussed earlier. The  $^{13}\text{C}$  NMR spectrum of  $[\text{Na.C211}]^+$  and that of its  $\text{Li}^+$  analogue shown in Figure 4.5 differ markedly and are very similar to the spectra of  $[\text{K.C221}]^+$  and  $[\text{Na.C221}]^+$ . This suggests  $[\text{Na.C211}]^+$  exists predominantly in the exclusive form and  $[\text{Li.C211}]^+$  in the inclusive form in deuterio-

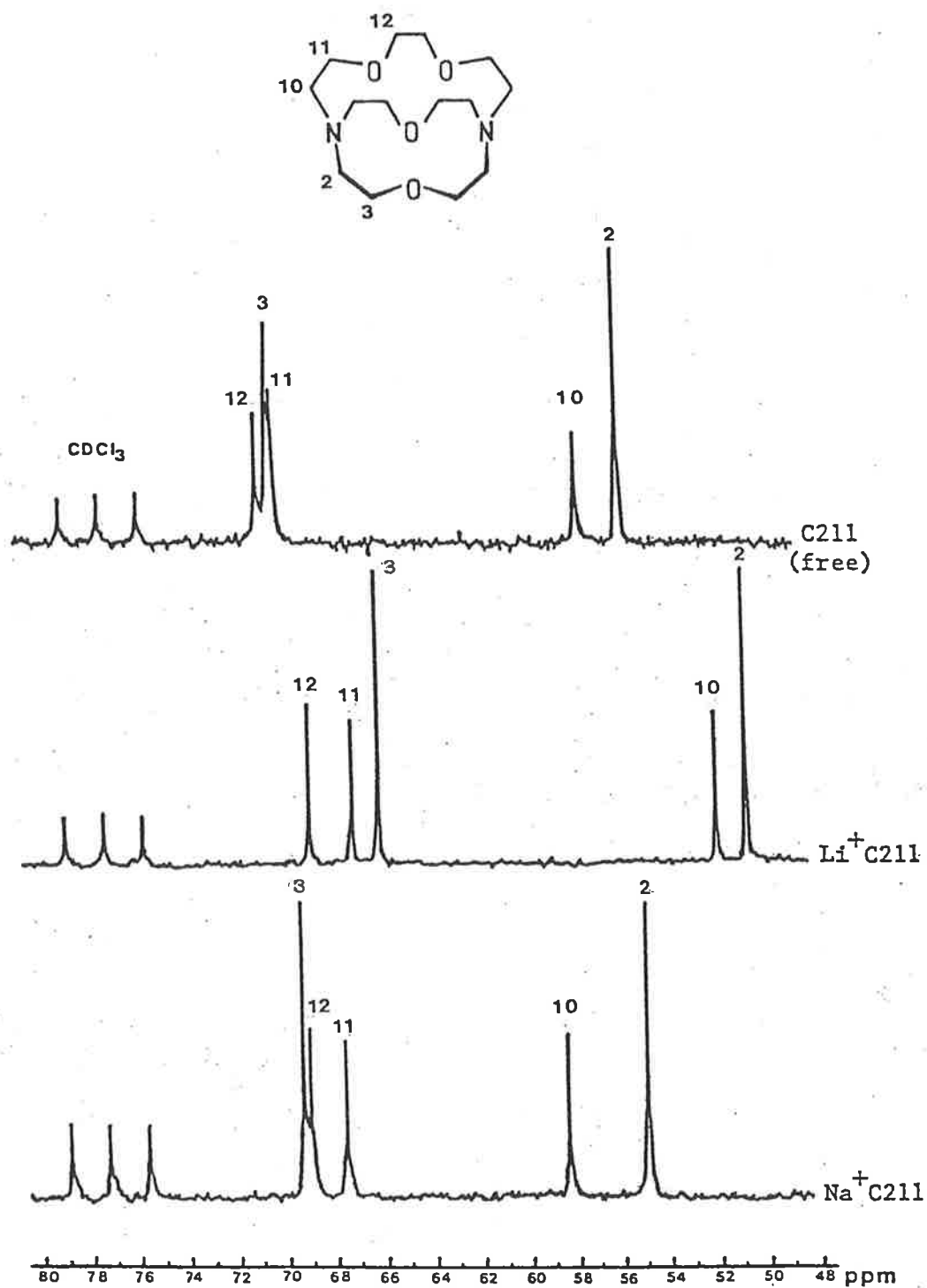


Figure 4.5.  $^{13}\text{C}$ - $\{^1\text{H}\}$  NMR spectra (20.1 MHz) of C211,  $[\text{Li}.\text{C211}]^+$  and  $[\text{Na}.\text{C211}]^+$  in  $\text{CDCl}_3$  solution at 305.2 K. The low field triplet arises from  $\text{CDCl}_3$ . The resonance numbering corresponds to that shown in the stylised C211 structure and is identical to that shown in Figure 4.3.

chloroform. The assignments of the resonances arising from carbons 3, 10, and 11 (where the numbering is the same as that used in the crystal structures discussed above) in C211 are self evident and those from carbons 11 and 12 are made by comparison to those reported for C221.<sup>21</sup> The shifts of all of the  $[\text{Li.C211}]^+$  resonances are upfield of those of  $[\text{Na.C211}]^+$  and the separations of the resonances in the two spectra differ substantially and qualitatively in a similar manner to those observed for  $[\text{Na.C221}]^+$  and  $[\text{K.C221}]^+$ .

The  $^{13}\text{C}$  NMR spectra of C21C<sub>5</sub> and its Na<sup>+</sup> and Li<sup>+</sup> cryptates are shown in Figure 4.6. The associated chemical shifts, and those of C211 and its Na<sup>+</sup> and Li<sup>+</sup> cryptates, are given in Table 4.6.

The resonances arising from C21C<sub>5</sub> are in three distinct groups: those of carbons adjacent to oxygen (C(9), C(12), C(13)), of carbons adjacent to nitrogen ((C(2), C(10), C(11))), and of carbons adjacent to carbon only (C(3), C(4)). The assignments of C(9), C(12), and C(13) are made by comparison to those made for C211 (as are those for the Na<sup>+</sup> and Li<sup>+</sup> cryptates)<sup>26</sup>, and the assignments of C(3) and C(4) are obvious. In principle, selective decoupling of the C(3) protons should distinguish the C(2) resonance from those of C(10) and C(11) and similar decoupling of C(9) and C(12) should distinguish the resonances of C(10) and C(11) from that of C(2). In practice, overlap of the proton coupled resonances of C(2), C(10), and C(11) rendered distinguishing between C(2) and C(11) a little uncertain for C21C<sub>5</sub> and  $[\text{Li.C21C}_5]^+$  but in the case of  $[\text{Na.C21C}_5]^+$  the assignment of the superimposing C(2) and C(11) resonances is unambiguous. The decoupling experiments do not distinguish between C(10) and C(11) but as



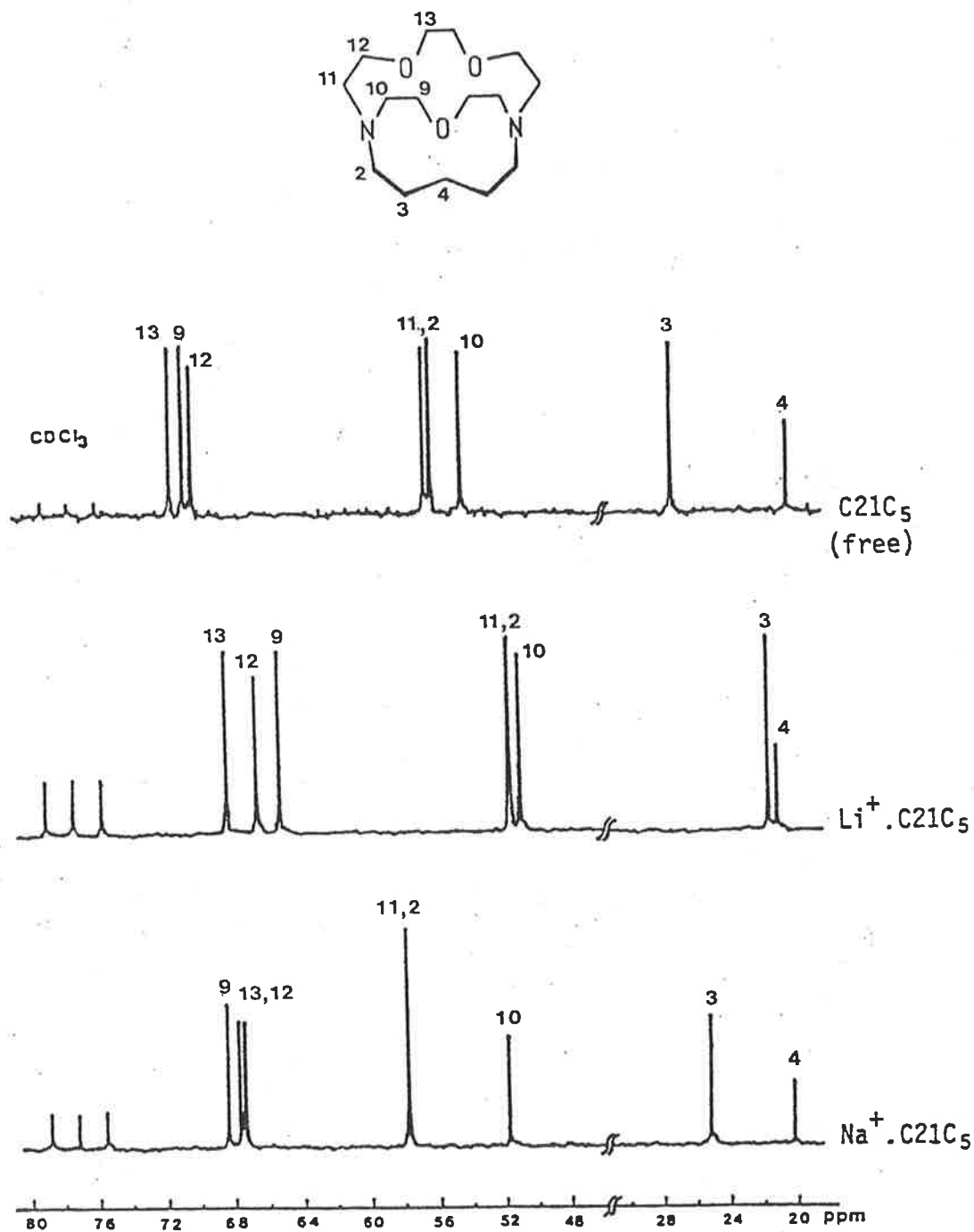


Figure 4.6.  $^{13}\text{C}$ - $\{^1\text{H}\}$  NMR spectra (20.1 MHz) of  $\text{C}_{21}\text{C}_5$ ,  $[\text{Li}.\text{C}_{21}\text{C}_5]^+$  and  $[\text{Na}.\text{C}_{21}\text{C}_5]^+$  in  $\text{CDCl}_3$  solution at 305.2 K. The low field triplet arises from  $\text{CDCl}_3$ . The resonance numbering corresponds to that shown in the stylised  $\text{C}_{21}\text{C}_5$  structure and is identical to that shown in Figure 4.4.

**Table 4.6**  $^{13}\text{C}$  NMR chemical shifts<sup>a</sup> for C211, C21C<sub>5</sub>  
and their Li<sup>+</sup>, and Na<sup>+</sup> cryptates at 305.2 K.

Carbon	C211	[Li.C211] <sup>+</sup>	[Na.C211] <sup>+</sup>	Carbon	C21C <sub>5</sub>	[Li.C21C <sub>5</sub> ] <sup>+</sup>	[Na.C21C <sub>5</sub> ] <sup>+</sup>
12	70.752	68.717	69.021	13	71.298	68.383	67.897
11	70.053	66.986	67.624	12	70.053	66.683	67.594
3,8	70.266	65.954	69.324	9	70.539	65.377	68.596
10	57.512	51.864	58.362	11	56.541	51.986	58.180
2,9	55.690	50.619	54.901	2	56.146	51.864	58.180
				10	54.354	51.287	52.229
				3	27.693	22.409	25.841
				4	20.891	21.893	21.013

a) Chemical shifts are referenced to the centre peak of CDCl<sub>3</sub> (77.25 ppm). The numbering system is that used in the structures shown in Figures 4.3 and 4.4. The cryptand and cryptate concentrations were 0.21 mol dm<sup>-3</sup>.

the resonance corresponding to C(10) in the spectra of C211 and its Na<sup>+</sup> and Li<sup>+</sup> cryptates (C(2)) has been unambiguously assigned as appearing at higher field than that of the carbon (C(10)) corresponding to C(11), it is unlikely that the relative chemical shifts of C(10) and C(11) will change in the very similar C21C<sub>5</sub> and its cryptates. The spectra in Figure 4.6 and Table 4.6 demonstrate that the changes in the chemical shifts of C21C<sub>5</sub> caused by complexation of Na<sup>+</sup> and Li<sup>+</sup> differ significantly as observed for C211 and follow similar patterns.

Thus it is generally observed that complexation of C222 by K<sup>+</sup>, Na<sup>+</sup>, and Li<sup>+</sup> <sup>26</sup>; of C221 by K<sup>+</sup>, Na<sup>+</sup>, and Li<sup>+</sup> <sup>21,26</sup>; and of C211 by Na<sup>+</sup> and Li<sup>+</sup> <sup>26</sup> produces an upfield shift of the cryptand  $^{13}\text{C}$  resonances with the exception of the C(11) resonance of [Na.C211]<sup>+</sup> and the equivalent resonance in [K.C221]<sup>+</sup>. This distinguishes these two exclusive cryptates

from the other cryptates which exist in the inclusive form. This difference in shift direction is also seen for the C(11) ( and C(2) ) resonances of  $[\text{Li.C}_{21}\text{C}_5]^+$  and  $[\text{Na.C}_{21}\text{C}_5]^+$  consistent with their existence as inclusive and exclusive cryptates respectively. The chemical shifts of C(3) and C(4) of  $[\text{Na.C}_{21}\text{C}_5]^+$  and  $[\text{Li.C}_{21}\text{C}_5]^+$  differ substantially, with those of the latter differing most from those of  $\text{C}_{21}\text{C}_5$ . This is consistent with C(3) and C(4) in the inclusive  $\text{Li}^+$  cryptate being in close proximity to  $\text{Li}^+$  and consequently experiencing a major change in environment, whilst in the exclusive  $\text{Na}^+$  cryptate C(3) and C(4) are more distant from  $\text{Na}^+$  (Figure 4.4) and their environment is more similar to that in  $\text{C}_{21}\text{C}_5$ .

One caveat to the above discussion, particularly with respect to the  $\text{Li}^+$  cryptates, is that the  $^{13}\text{C}$  NMR measurements were carried out in deuterio-chloroform solution only and generalising to other solvents may not be valid. It is conceivable that in a strongly coordinating solvent the exclusive form of the  $\text{Li}^+$  cryptates may exist to some extent, particularly in the case of  $[\text{Li.C}_{21}\text{C}_5]^+$ . However, the  $^7\text{Li}$  chemical shift of  $[\text{Li.C}_{21}\text{C}_5]^+$  in a range of solvents<sup>27</sup> was found to be insensitive to the nature of the solvent as expected for an inclusive cryptate. The observations that the  $^{23}\text{Na}$  chemical shift of  $[\text{Na.C}_{21}\text{C}_5]^+$  and  $[\text{Na.C}_{21}\text{C}_5]^+$  do vary with solvent (Table 4.7) is consistent with contact occurring between the complexed  $\text{Na}^+$  and solvent as anticipated for exclusive cryptates. (Under the experimental conditions of this study, the chemical shifts of  $[\text{Na.C}_{21}\text{C}_5]^+$  differ from those reported elsewhere<sup>28</sup> but the trends are similar.)

**Table 4.7.**  $^{23}\text{Na}$  Chemical Shifts for  $[\text{Na.C211}]^+$  and  $[\text{Na.C21C}_5]^+$ 

Solvent	Cryptand	Chemical Shift (ppm)	
		$\text{Na}^+(\text{solv.})$	$\text{Na}^+(\text{crypt.})$
$\text{H}_2\text{O}$	$\text{C211}^{\text{a}}$	-1.01	12.06
DMF	C211	-4.12	10.82
DMSO	C211	-0.24	10.52
DMF	$\text{C21C}_5^{\text{b}}$	0.0	9.18 <sup>c</sup>
MeCN	$\text{C21C}_5$	2.37	11.83
Pyridine	$\text{C21C}_5$	4.92	12.79
$\text{PC}^{\text{d}}$	$\text{C21C}_5$	-4.57	12.14
Acetone	$\text{C21C}_5$	-2.22	10.60
MeOH	$\text{C21C}_5$	1.68	12.57

a) Chemical shifts referenced to  $3.0 \text{ mol dm}^{-3}$  aqueous NaCl solution at 298 K and are corrected for bulk diamagnetic susceptibilities.<sup>29</sup> b) Chemical shifts referenced to  $0.1 \text{ mol dm}^{-3}$   $\text{NaClO}_4$  in DMF at 261.5 K since in some solvents  $\text{Na}^+$  was undergoing rapid exchange at room temperature. c) Value obtained by extrapolation from lower temperature spectra. (d) Propylene Carbonate.

In conclusion, it appears that the cryptate conformation formed in the solid state is also predominant in solution. The relationship between cavity size and metal ion diameter is important in determining whether the cryptate exists in the exclusive or inclusive form. Replacement of an oxygen binding site in C211 by a  $\text{CH}_2$  group resulted in a sodium cryptate in the solid state with the sodium ion residing at an increased distance from the centre of the cavity relative to the C211

cryptate. This difference should be reflected significantly in the thermodynamic and kinetic parameters of the two cryptates in solution. Further investigations into the structural properties of these cryptates are continuing, including the determination of the crystal structure of  $[\text{Li.C21C}_5]\text{NCS}$  and CP-MAS  $^{13}\text{C}$  solid state NMR studies. The CP-MAS  $^{13}\text{C}$  NMR spectrum of  $[\text{Na.C211.NCS}]$  showed two broad resonances, corresponding to the carbons adjacent to oxygen and those adjacent to nitrogen, but the individual resonances could not be resolved. This was presumably due to the disordered nature of the cryptate in the solid state as determined by X-ray diffraction studies.

## 4.4

EXPERIMENTAL

(i) Materials. NaSCN, LiSCN, and NaClO<sub>4</sub> were dried at 80 - 90°C under high vacuum for 48 hours and were stored over P<sub>2</sub>O<sub>5</sub> under vacuum. CDCl<sub>3</sub> and all other solvents were purified and dried where necessary by literature methods<sup>30</sup> and were stored over Linde 4A molecular sieves. Cryptand C211 (Merck) was distilled, dried under high vacuum for 24 hours and stored under dry nitrogen.

(ii) Preparation of C21C<sub>5</sub>(a) C21C<sub>5</sub>\*

## (16,20-Dioxo-4,7,13-Trioxa-1,10-diazabicyclo[8.5.5]eicosane)

The method described is a modification of the general method of Lehn.<sup>22</sup>

A solution of 1,4,10-trioxa-7,13-diazacyclopentadecane (Kryptofix 21, Merck) (2.0 g, 9.2 mmol) and triethylamine (2.5 g, 25.0 mmol) in dry benzene (100 ml), and a solution of glutaric acid dichloride (1.41 g, 8.34 mmol) in dry benzene (100 ml) were added simultaneously to dry benzene (1200 ml) over 8 hours at room temperature (22°C) with vigorous stirring under dry nitrogen using Perfusor motor driven syringes. After filtration and removal of the solvent under vacuum the residue was chromatographed on 'flash' silica<sup>31</sup> (Merck, 230 - 400 mesh, 4% methanol / dichloromethane, R<sub>f</sub> = 0.30), removal of the solvent and drying under high vacuum afforded the cryptand diamide C21C<sub>5</sub>\* as a white solid (2.2 g, 84%), m.p. 115 - 117°C;  $\nu_{\max}$  1630, 1130 cm<sup>-1</sup>; <sup>1</sup>H NMR (CDCl<sub>3</sub>):  $\delta$  1.8 - 5.2, a complex spectrum with large peaks at 3.55 and 3.60; m/e 314 (M<sup>+</sup>), 286, 271, 246, 239, 28 (100).

(b) C<sub>21</sub>C<sub>5</sub>

## (4,7,13-Trioxa-1,10-diazabicyclo[8.5.5]eicosane)

The diamide C<sub>21</sub>C<sub>5</sub>\* (1.3 g, 4.1 mmol) was dissolved in dry tetrahydrofuran (30 ml) and treated with boron trifluoride etherate (1.0 ml, 8.2 mmol) at 50°C under dry nitrogen. The reaction mixture was heated to reflux and borane-dimethylsulphide complex (Fluka, 10% dimethylsulphide, 1.2 ml, 10.9 mmol) was slowly added with a syringe. Heating was continued for 3 hours and ether and dimethylsulphide distilled off as they formed. After cooling, the solvent was removed under vacuum and the white residue was treated with 6M hydrochloric acid (25 ml). The resultant solution was heated at reflux for 12 hours and then evaporated to dryness. The crude cryptand was obtained from the hydrochloride salt after ion exchanging an aqueous solution on Dowex 1X8 (OH<sup>-</sup> form, 50 - 100 mesh), concentration of the basic eluent, extraction with chloroform (4 x 50 ml), and evaporation of the combined extracts. Fractional distillation of the residue yielded 4,7,13-trioxa-1,10-diazabicyclo[8.5.5]eicosane (1.1 g, 92 %) as a colourless oil, b.p. c.a. 110°C / 0.025 mm (Sublimation block). Calculated for C<sub>15</sub>H<sub>30</sub>N<sub>2</sub>O<sub>3</sub>: C, 62.90; H, 10.56; N, 9.78; Found: C, 62.93; H, 10.55; N, 9.88%. Accurate mass: Found 286.22448; Required m/e 286.225628; m/e 286 (M<sup>+</sup>,100), 269, 255;  $\nu_{\max}$  1460 (m), 1350 (m), 1125 (s), 1070 (m); <sup>1</sup>H NMR (CDCl<sub>3</sub>):  $\delta$  1.35 (6H, m, aliphatic -CH<sub>2</sub>- ), 2.50 (12H, m, -NCH<sub>2</sub>- ), 3.40 (12H, m, -OCH<sub>2</sub>- ).

(iii) X-ray Diffraction

Crystals of [Na.C211.NCS] and [Na.C21C<sub>5</sub>.NCS] were prepared by dissolving equimolar amounts of NaSCN and the cryptand in dry methanol and evaporating to dryness. The white solids were dissolved in dry acetone and the solutions were then equilibrated with dry hexane in a desiccator whereupon white crystals slowly formed.

## (a) X-Ray Crystallography of [Na.C211.NCS].

Crystal Data. C<sub>15</sub>H<sub>28</sub>N<sub>3</sub>NaO<sub>4</sub>S, M = 369.45, space group Pbca, a = 14.686(3), b = 15.699(4), c = 16.522(5) Å; U = 3809.2 Å<sup>3</sup>, Z = 8, D<sub>o</sub> = 1.28, D<sub>c</sub> = 1.288 g cm<sup>-3</sup>, F(000) = 1584, λ(Mo-K<sub>α</sub>) = 0.7107 Å, μ(Mo-K<sub>α</sub>) = 9.17 cm<sup>-1</sup>.

Data Collection. A crystal of dimensions 0.15 x 0.16 x 0.65 mm was mounted on a glass fibre and coated with cyano-acrylate super glue. (The crystal density was measured by floatation in a mixture of CCl<sub>4</sub> and petroleum spirit (100 - 120 °C).) Lattice parameters were determined at 295 K by a least-squares fit to the setting angles of 25 independent reflections, measured and refined by scans performed on an Enraf-Nonius CAD 4 four-circle diffractometer employing graphite monochromated Mo-K<sub>α</sub> radiation. Intensity data were collected in the range 1.3 < θ < 23° using a ω - n/3 θ scan, where n(=1) was optimised by profile analysis of a typical reflection. The ω scan angles and horizontal apertures employed were (1.85 + 0.35tanθ)<sup>o</sup> and (2.40 + 0.5tanθ) mm respectively. Three standard reflections, monitored after every 58 min. of data collection, indicated that by completion of the data collection no decomposition had occurred. Data reduction and



application of Lorentz and polarization corrections were performed using program SUSCAD<sup>32</sup>. Of the 2,944 reflections collected 1,417 with  $I > 2.5\sigma(I)$  were considered observed and used in the calculations.

Structure Solution and Refinement. The structure was solved by direct methods using the routines for non-centrosymmetric solution of program SHELX<sup>32</sup>. The solution was confirmed as being correct by analysis of the Patterson map. The thiocyanate ion, the sodium ion and two oxygen atoms were located in the E-map. Least-squares refinement and calculation of a series of difference maps resulted in the location of a set of atoms with the expected connectivities. However at this stage the discrepancy index  $R^*$  had only converged to 0.19, some atoms had unacceptably large thermal parameters, and a number of peaks (about  $2e\text{\AA}^{-3}$  in height) remained in the difference maps. Therefore a model with the cryptate disordered was developed. In this model there are contributors to all oxygen and nitrogen sites but five carbon sites overlap which explains why initially not all atoms had large thermal parameters. A group multiplicity parameter, defining the disorder, refined to 0.60(1) and in the final refinement all atoms had reasonable thermal parameters. The shift associated with the disorder is small with all oxygen and nitrogen atoms lying about 1  $\text{\AA}$  from their images, and presumably arises as a consequence of the approximately spherical form of the cryptand. Only those atoms present at full occupancy were refined anisotropically. Hydrogen atoms for both contributors were included at sites calculated assuming tetrahedral geometry about carbon ( C-H, 0.97  $\text{\AA}$  ). Full matrix least-

squares refinement converged ( all shifts  $< 0.1\sigma$  ) with  $R = 0.069$ ,  $R_w = 0.075^{**}$  and  $w = 5.33 / (\sigma^2(F_o) + 0.00044F_o^2)$ . The largest peak in a final difference map was  $0.3 \text{ e}\text{\AA}^{-3}$  in height. Final position parameters are listed in Table 4.8.

(b) X-Ray Crystallography of [Na.C21C<sub>5</sub>.NCS].

Crystal Data. C<sub>16</sub>H<sub>30</sub>N<sub>3</sub>NaO<sub>3</sub>S, M = 367.48, space group P2<sub>1</sub>/n, a = 9.947(2), b = 15.681(4), c = 12.460(3) Å;  $\beta = 95.27(2)^\circ$ , U = 1935.4 Å<sup>3</sup>, Z = 4, D<sub>o</sub> = 1.25, D<sub>c</sub> = 1.261 g cm<sup>-3</sup>, F(000) = 792,  $\lambda(\text{Mo-K}\alpha) = 0.7107 \text{ \AA}$ ,  $\mu(\text{Mo-K}\alpha) = 1.69 \text{ cm}^{-1}$ .

Data Collection. A crystal of dimensions 0.08 x 0.16 x 0.28 mm was mounted on a glass fibre and coated with cyano-acrylate super glue. The lattice parameters and the crystal density were determined as described above for [Na.C211.NCS]. Intensity data were collected in the range  $1.3 < \theta < 23^\circ$  using a  $\omega - n/3 \theta$  scan, where  $n(=1)$  was optimised by profile analysis of a typical reflection. The  $\omega$  scan angles and horizontal apertures employed were  $(1.85 + 0.35\tan\theta)^\circ$  and  $(2.40 + 0.5\tan\theta)$  mm respectively. Three standard reflections, monitored after every 58 min. of data collection, indicated that by completion of the data collection no decomposition had occurred. Data reduction and application of Lorentz and polarization corrections were performed using program SUSCAD<sup>32</sup>. Absorption corrections were applied with program ABSORB<sup>32</sup>. Maximum and minimum transmission factors were estimated to be 0.98 and 0.95 respectively. Of the 3,388 reflections collected 2,259 with  $I > 2.5\sigma(I)$  were considered observed and used in the calculations.

**Table 4.8**Final Positional Parameters ( $\times 10^3$ ) for [Na.C211.NCS]

	X	Y	Z
Na(1)	6035(2)	929(2)	2263(2)
S(1)	7463(2)	-1287(2)	400(2)
O(1)	7199(8)	1050(8)	3177(9)
O(2)	4560(9)	440(7)	2055(8)
O(3)	5498(13)	1553(11)	1003(12)
O(4)	5217(7)	2369(6)	2706(6)
N(1)	6682(7)	-285(7)	1583(7)
N(2)	5337(10)	844(9)	3626(7)
N(3)	7026(14)	2137(10)	1837(12)
C(1)	7010(7)	-692(6)	1089(7)
C(2)	5047(11)	1682(10)	3985(10)
C(3)	5558(20)	2455(28)	3523(27)
C(4)	5601(8)	3014(7)	2222(8)
C(5)	6658(13)	2973(12)	2203(14)
C(6)	7826(26)	1821(15)	2007(15)
C(7)	7898(14)	1606(13)	3014(26)
C(8)	6991(9)	872(8)	3977(8)
C(9)	6118(15)	433(14)	4075(12)
C(10)	4567(8)	256(7)	3507(8)
C(11)	4012(14)	522(11)	2475(12)
C(12)	4151(9)	713(8)	1356(9)
C(13)	4898(28)	927(28)	790(28)
C(14)	6221(10)	1700(11)	573(7)
C(15)	6843(23)	2157(29)	980(20)
O(1')	7483(14)	1286(12)	2648(11)
O(2')	4691(13)	258(10)	2695(13)
O(3')	4847(28)	1243(15)	1391(15)
O(4')	5902(26)	2446(12)	2876(13)
N(2')	6040(29)	949(15)	3746(13)
N(3')	6528(29)	2064(15)	1371(29)
C(2')	5779(25)	1805(29)	4110(20)
C(3')	5231(20)	2370(20)	3503(27)
C(5')	6256(20)	2934(28)	1572(29)
C(6')	7530(29)	1904(27)	1330(28)
C(7')	7948(28)	1882(27)	2343(29)
C(8')	7622(37)	1364(23)	3510(22)
C(10')	5459(22)	208(20)	3939(29)
C(12')	3962(25)	519(21)	2209(22)
C(14')	5124(24)	1480(38)	744(24)

Primes denote the minor contributors to the disordered ligand

Structure Solution and Refinement. The sodium, oxygen, nitrogen, and most of the carbon atom locations were determined using the direct method routine of the SHELX program. The remaining carbon atoms were located in the Fourier difference maps of successive full matrix least-squares refinements using the SHELX program. All hydrogen atoms were included at calculated positions (C-H, 0.97 Å) assuming tetrahedral geometry about the carbon atoms and their thermal parameters were refined as a common group factor. In the final full matrix least-squares calculations only the non-hydrogen atoms were modelled anisotropically. The refinement converged with  $R^* = 0.039$  and  $R_w^* = 0.045$ . The weighting scheme employed converged at  $w = 2.90/(\sigma^2 F_o + 0.0002 F_o * F_o)$ . The largest peak remaining in the final difference map was associated with the O (2) atom and was less than  $0.6 \text{ \AA}^{-3}$  in height. The final least squares positional parameters are given in Table 4.9.

All the calculations pertaining to [Na.C211.NCS] and [Na.C21C<sub>5</sub>.NCS] were performed using the scattering for the respective neutral atoms as tabulated in the International Tables for X-ray Crystallography<sup>33</sup>. The hydrogen atom parameters and the structure factor amplitudes are presented in Appendix 2.

(iv) NMR Spectroscopy. <sup>13</sup>C NMR spectra were recorded on a Bruker WP-80 NMR spectrometer operating at 20.1 MHz. The broad band and selectively proton decoupled <sup>13</sup>C spectra were run in anhydrous CDCl<sub>3</sub> solutions ca. 0.2 mol dm<sup>-3</sup> in cryptand or

Table 4.9Final Positional Parameters for [Na.C<sub>21</sub>C<sub>5</sub>.NCS]

	x	y	z
Na(1)	76782(11)	17255(7)	44974(10)
S(1)	76287(10)	3864(6)	82118(8)
O(1)	8397(2)	419(1)	3944(2)
O(2)	8565(3)	3106(1)	4667(2)
O(3)	5869(2)	2693(1)	4202(2)
N(1)	7515(4)	1298(2)	6295(3)
N(2)	9884(2)	1871(2)	3320(2)
N(3)	5821(2)	1050(2)	3189(2)
C(1)	7557(3)	914(2)	7100(3)
C(2)	10009(3)	1855(2)	2153(3)
C(3)	8933(4)	2372(2)	1494(3)
C(4)	7497(3)	2178(2)	1747(3)
C(5)	7069(4)	1268(2)	1545(3)
C(6)	5751(3)	1029(2)	2002(3)
C(7)	6034(3)	205(2)	3679(3)
C(8)	7401(3)	-167(2)	3521(3)
C(9)	9708(3)	301(2)	3586(3)
C(10)	10506(3)	1101(2)	3839(3)
C(11)	10471(3)	2651(2)	3811(3)
C(12)	9487(4)	3347(2)	3960(3)
C(13)	7515(4)	3701(2)	4823(4)
C(14)	6261(4)	3554(2)	4094(4)
C(15)	4743(3)	2434(2)	3493(3)
C(16)	4637(3)	1481(2)	3579(3)

Na and S coordinates x 10<sup>5</sup>, for the other atoms x 10<sup>4</sup>.

cryptate at 305.2 K in a standard microprobe using a deuterium lock. An average of 30,000 transients were accumulated into a 16,384 point data base.

$^{23}\text{Na}$  NMR spectra were measured on a Bruker CXP300 NMR spectrometer operating at 79.39 MHz. An average of 6000 transients were accumulated into a 2048 point data base using typically, a 2000 Hz spectral width. The sample temperature was controlled with a Bruker B-VT 1000 variable temperature unit to within  $\pm 0.3$  K.

CHAPTER 5.CRYPTATE STABILITY

## 5.1

INTRODUCTION

The cryptands were designed by Lehn with a view to producing ligands for metal ions which would exhibit considerable selectivity and high stability in complex formation,<sup>1</sup> properties important for their suitability as synthetic ion carriers or model antibiotics. A comprehensive appreciation of the mechanism of cryptate formation and dissociation requires a knowledge of cryptate thermodynamic behaviour. Factors affecting cryptate stability have been the subject of many studies and are generally well understood. While a comprehensive review is not attempted here, some of the major influences on cryptate stability are mentioned. More detailed discussion may be found in a number of published reviews.<sup>1,16,18,30,35</sup>

Varying the "topology" of the cryptand cavity by altering the length of the nitrogen - nitrogen bridges was found to markedly affect cryptate stability, such that the most stable cryptate for a given metal ion is formed with the cryptand having a cavity size approximately matched with the metal ion diameter. This is demonstrated in Table 5.1 for the overall equilibrium exemplified in Scheme 5.1 for C211 in which  $K_s = k_f/k_d$ .

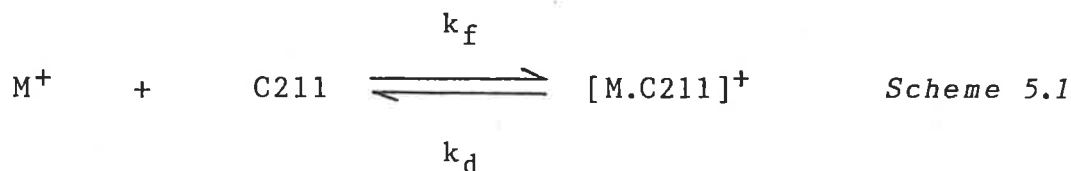


**Table 1.** Variation of Stability Constant,  $K_S$ , with Cavity Size and Metal Ion Diameter,  $d$ , in Aqueous Solution.<sup>34</sup>

Cryptand	Cavity Size		log K			
	(diameter)		Li <sup>+</sup>	Na <sup>+</sup>	K <sup>+</sup>	Cs <sup>+</sup>
	Å	d (Å)	1.56	2.24	2.88	3.3
C211	1.6		5.3	3.2	<2	<2
C221	2.2		2.5	5.4	3.9	<2
C222	2.8		<2	3.9	5.4	<2
C322	3.6		<2	1.6	2.2	2.0

As well as cavity size, the number of coordinating heteroatom binding sites in the cryptand affects the cryptate stability. For example, replacement of one or more oxygen atoms with CH<sub>2</sub> groups significantly reduces the stability constant and this has been shown for C22C<sub>8</sub><sup>34</sup> where the values for its Na<sup>+</sup> and K<sup>+</sup> complexes are 10<sup>4</sup>- 10<sup>5</sup> times smaller than those of C222. Studies of the variation with solvent<sup>35</sup> showed a large effect on stability, with the selectivity properties maintaining similar trends in different solvents and indicated that solvation of both the metal ion and the cryptand were important.

The structural properties of the sodium cryptates of C211 and C21C<sub>5</sub> were discussed in the previous section, and as part of the investigation into the influence of cryptand structure on thermo-kinetics of cryptates, the solvent variation of the stability of [Na.C21C<sub>5</sub>]<sup>+</sup> is presented here.

#### (i) Stability Constant Determination

Cryptate stability constants have been measured predominantly by two classical methods, potentiometric



titration with ion specific electrodes<sup>35-37</sup> and pH-metric titrations,<sup>34</sup> and also by analysis of NMR chemical shifts.<sup>38,39</sup> The method of choice is usually determined by the magnitude of stability constants to be measured and solvent considerations. pH-metric titrations are suited to measurements of high stability constants ( $\log K_s \geq 2$ ) in protic solvents and alkali-cation potentiometric titrations and NMR methods are suitable for measurements in most solvents where  $1 < \log K_s < 6$ . Due to the lower sensitivity of NMR measurements this technique was considered to be too expensive in cryptand and as the stability was to be studied in a range of solvents, it appeared that the potentiometric method would be most convenient for our purposes. A variation of the technique had been developed by Schneider and coworkers<sup>36</sup> allowing the indirect measurement of alkali metal cryptate stability constants greater than  $10^6$ .

Direct potentiometric measurement of metal ion concentration may be made with cation selective glass electrodes. The electrode potential is given by

$$E = E_0 + k \log [M^+] \quad (5.1)$$

where the coefficient  $k$  is determined by calibration measurements of solutions containing known metal ion concentration and may vary between 45 and 65 (where the emf is in mV). Having determined  $k$ , the concentration of free metal ion in a solution containing cryptand may be obtained directly, from which the stability constant may be calculated.

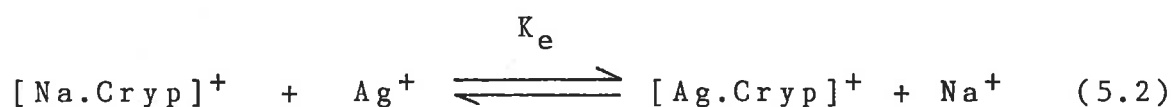
The sensitivity of sodium glass electrodes permits detection of free sodium where cryptate stabilities are in the

range 10 to  $10^8$ . The reported<sup>35</sup> stability constants for  $[\text{Na.C211}]^+$  are less than  $10^9$  and the values for  $[\text{Na.C21C}_5]^+$  were expected to be  $10^2 - 10^4$  less by comparison to the C222 and C22C<sub>8</sub> cryptates mentioned earlier. Therefore, it was envisaged that the  $[\text{Na.C21C}_5]^+$  stability constants could be measured in a variety of solvents employing this method.

## 5.2

RESULTS AND DISCUSSION

Early attempts to obtain the result of Schneider et.al.<sup>35</sup> for the stability constant of  $[\text{Na.C211}]^+$  in DMF using a sodium ion glass electrode were hampered by apparently capricious behaviour of the electrode in this solvent. Consequently, it was decided to employ the indirect method<sup>36</sup> of determining the stability constant for the formation of the  $\text{Ag}^+$  cryptate ( $K_{\text{Ag}}$ ) by direct titration using a  $\text{Ag}/\text{Ag}^+$  electrode, then monitoring the competitive equilibrium established between the  $\text{Ag}^+$  cryptate in the presence of  $\text{Na}^+$  in solution as shown below.



where

$$K_e = \frac{[\text{Ag.Cryp}^+][\text{Na}^+]}{[\text{Na.Cryp}^+][\text{Ag}^+]} \quad (5.3)$$

from which  $K_s$  is obtained since

$$K_s = K_{\text{Ag}} / K_e \quad (5.4)$$

Thus a solution of standard  $\text{Ag}^+$  is titrated with a solution of  $[\text{Na.Cryp}]^+$  and as the initial concentrations of these species are known, and the equilibrium concentration of  $\text{Ag}^+$  is determined from the potential of the  $\text{Ag}/\text{Ag}^+$  electrode, the value of  $K_e$  may be evaluated from the stoichiometry of the equilibrium. The total metal ion concentration is always in excess of that of the total cryptand concentration, under which conditions, the concentration of uncomplexed cryptand is assumed to be negligible.<sup>37</sup> The results are summarized in Table 5.2 and

values for C211 cryptates in some solvents<sup>35</sup> are included for comparison. Figure 5.1 shows a typical titration curve, for  $[\text{Ag.C21C}_5]^+$  in methanol (MeOH).

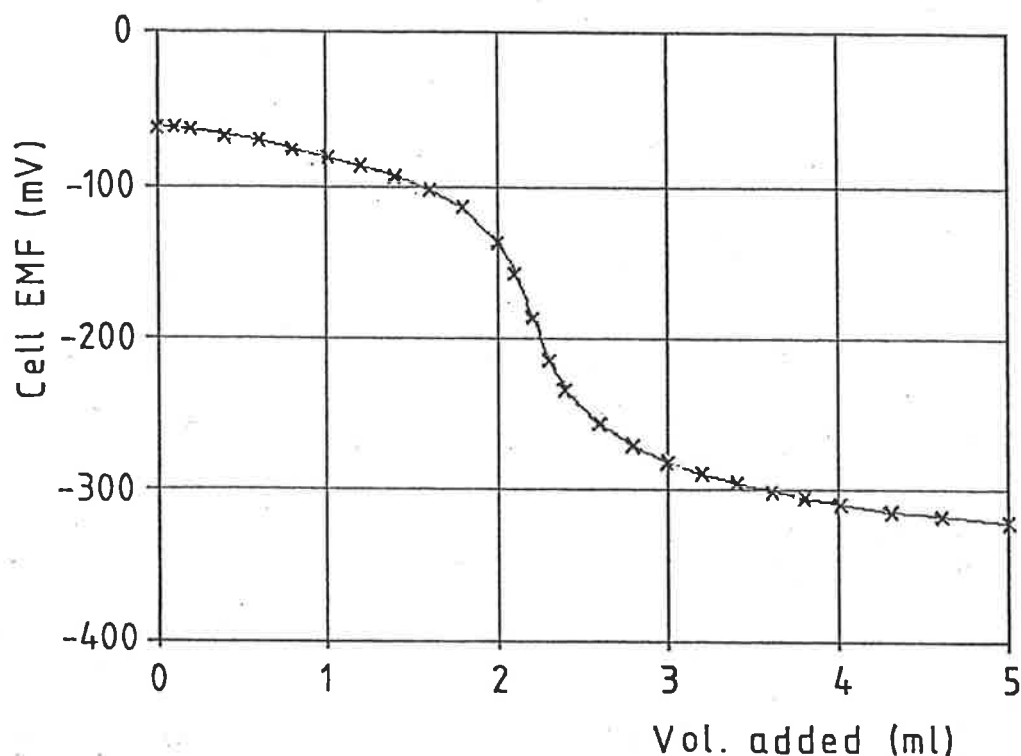


Figure 5.1. Curve obtained for the titration of  $10^{-3} \text{ mol dm}^{-3}$   $\text{AgNO}_3$  with  $10^{-2} \text{ mol dm}^{-3}$  C21C<sub>5</sub> in MeOH.

Surprisingly, C21C<sub>5</sub> is only sparingly soluble in water and its Na<sup>+</sup> cryptate was virtually insoluble. The stability constants for  $[\text{Ag.C21C}_5]^+$  could not be measured accurately in pyridine or propylene carbonate (PC). Only a small potential change was observed during the direct titration of Ag<sup>+</sup> with C21C<sub>5</sub> in pyridine indicating the formation of a relatively weak complex ( $\log K_{\text{Ag}} < 2$ ), presumably a result of the strong solvational interactions formed between Ag<sup>+</sup> and pyridine.

Solutions of  $\text{AgClO}_4$  in PC turned brown, even after repeated redistillation of the PC. The  $[\text{Na.C21C}_5]^+$  stability constants in pyridine and PC were subsequently measured by direct potentiometric titration monitored with a sodium glass electrode which performed consistently in these solvents. (The previous problems associated with this electrode were eventually attributed to impurities in the sample of background electrolyte (tetrabutylammonium perchlorate) being used and were overcome by the use of tetraethylammonium perchlorate in subsequent titrations.)

**Table 5.2. Stability Constants ( $\log K_s$ )<sup>a</sup> of Cryptates in Various Solvents at 298 K.**

Cryptate	Solvent					
	MeOH	DMF	MeCN	PC	Acetone	Pyridine
$[\text{Ag.C21C}_5]^+$	7.62	5.19	4.55	-	8.58	-
$[\text{Na.C21C}_5]^+$	3.76	2.87	5.08	5.12	3.98	3.72
$[\text{Ag.C211}]^+$	10.6	8.6	7.7	14.4	-	-
$[\text{Na.C211}]^+$	6.1	5.2	>9	8.7	-	-

a) Accuracy:  $\pm 0.1$  ( $\pm 0.2$  for  $[\text{Ag.C21C}_5]^+$  in MeOH)

Two points should be noted before further discussion of these results. The thermodynamic stability constant  $K_{th}$  is given by

$$K_{th} = \frac{f_C [\text{M.Cryp}^+]}{f_c [\text{Cryp}] f_{M^+} [\text{M}^+]} \quad (5.5)$$

where  $f_C$ ,  $f_c$  and  $f_{M^+}$  are the activity coefficients of the cryptate, cryptand and metal ion respectively. Since these quantities are generally unknown in the solvents studied, the stability constants reported here are concentration stability

constants  $K_s$ , such that

$$K_s = K_{th} \frac{f_c f_{M^+}}{f_C} = \frac{[M.Cryp^+]}{[Cryp][M^+]} \quad (5.6)$$

Also, the stability constants represent the overall equilibrium shown in Scheme 5.1 and include contributions from cryptand conformational changes and solvational equilibria.

The  $[Na.C21C_5]^+$  stability constant shows a similar variation (ca. 2.3 orders of magnitude) with solvent to that of  $[Na.C211]^+$ . The  $Ag^+$  cryptates exhibit a larger solvent variation in stability (ca. 4 orders of magnitude for  $[Ag.C21C_5]^+$ ) which is consistent with the known larger variations of free energy of solvent transfer<sup>40</sup> compared with alkali metal cations. The  $Ag^+$  cryptates are more stable than the  $Na^+$  cryptates in all solvents except acetonitrile (MeCN) and probably pyridine, due to the stronger ion - solvent interactions of  $Ag^+$  in the latter solvents.<sup>40</sup>

The trends in the stability constants are as predicted from ion - solvent interaction considerations. In solvents where alkali metal ion - solvent interactions are relatively weak, such as PC and MeCN the stability constants are greatest, whereas in solvents which exhibit strong interactions with cations, the stability of the cryptates are lower as is the case in DMF. If the stability of  $[Na.C21C_5]^+$  could be measured in water, it would be expected to be lower than in the non-aqueous solvents as observed for the other cryptates.

It is seen from Table 5.2 that  $K_s$  for  $[Na.C21C_5]^+$  in all solvents is markedly lower than for  $[Na.C211]^+$ , generally by factors of  $10^2$  to  $10^3$  for the  $Na^+$  cryptates and slightly

larger differences for the  $\text{Ag}^+$  cryptates. This significant reduction in stability of the cryptates of  $\text{C21C}_5$  relative to those of  $\text{C211}$  must be a consequence of the removal of one oxygen binding site and indicates the importance of this  $\text{Na}^+ - \text{O}$  bonding interaction, even in the exclusive  $[\text{Na}.\text{C211}]^+$  complex where the  $\text{Na}^+ - \text{O}(4)$  (Figure 4.3) is significantly longer than the other  $\text{Na}^+ - \text{O}$  bond lengths. The difference in stability between these two cryptates is less than found for  $\text{C222}$  and  $\text{C22C}_8$  where the stability constants differ by five orders of magnitude in methanol.<sup>34</sup> In this case a larger effect would be expected since two oxygen binding sites are replaced by  $\text{CH}_2$  groups and the cryptates are inclusive where the  $\text{Na}^+ - \text{O}$  bonding distances are shorter and interactions stronger.

Lehn<sup>34</sup> ascribed the very high stability of cryptates partly to the macrobicyclic topology of the cryptands or the "cryptate" effect. For example, it was noted that the formation of bicyclic topology in the ligand  $\text{C222}$ , caused an increase of  $10^5$  in its  $\text{K}^+$  complex stability in methanol compared to the monocyclic ligand derived by cleaving one end of a cryptand nitrogen - nitrogen bridge. This ligand has an equal number of binding sites to  $\text{C222}$ , the only difference being the structural spherical cavity of the cryptand which is well suited to forming complexes with spherical cations. The thermodynamic origin of this effect appears to be entirely enthalpic in nature.<sup>34b</sup> However, such an effect is not observed in the case of the  $\text{Na}^+$  and  $\text{K}^+$  complexes of  $\text{C22C}_8$  whose  $\log K_s$  values are 3.5 and 5.2 respectively.<sup>34</sup> The formation of the macrobicyclic cavity does not significantly increase the complex stability in these examples as  $\log K_s$

in methanol for the  $\text{Na}^+$  and  $\text{K}^+$  complexes of the monocyclic ligand [22-Me] (formed by methylation of both nitrogens in the monocyclic analogue of C222,  $\text{HN}(\text{CH}_2\text{CH}_2\text{OCH}_2\text{CH}_2\text{OCH}_2\text{CH}_2)_2\text{NH}$  ([22-H])), are 3.7 and 5.3 respectively.<sup>34</sup>

In the light of these observations it would be of interest to compare data for similar complexes of [21-Me] with the  $\text{C}_{21}\text{C}_5$  cryptate stabilities obtained in this work. Unfortunately, such studies have only been carried out in water and chloroform solvents<sup>41</sup> in the case of the alkali metal ions. However,  $\log K_s$  for the complex formed by [21-H] with  $\text{Ag}^+$  in methanol is 7.61<sup>42</sup> which is identical within experimental error to the value obtained in this work for  $[\text{Ag}.\text{C}_{21}\text{C}_5]^+$ . Here again there appears to be no further stabilization on formation of the macrobicyclic topology. This may not be unexpected in the case of exclusive cryptates such as  $[\text{Ag}.\text{C}_{21}\text{C}_5]^+$  where the added bridge introduces no increase in the number of binding heteroatoms, but the results for the inclusive  $\text{C}_{22}\text{C}_8$  cryptates mentioned above are surprising, particularly considering the magnitude of the cryptate effect observed for C222 and other cryptands. When making such direct comparisons of the cryptands and monocyclic analogues, it should be remembered that there are likely to be significant differences in conformational and solvational properties of the ligands which may influence the stability of their complexes.



CHAPTER 6. KINETIC AND MECHANISTIC ASPECTS OF THE  
CRYPTATES OF C211 AND C21C<sub>5</sub>

## 6.1

INTRODUCTION

The cryptands have attracted much attention as a result of their ability to form highly stable complexes with metal ions and to show high selectivity toward the metal cations in cryptate formation. Many of the proposed applications of these synthetic ligands, such as phase transfer catalysis, anion activation, extraction and isotope separation, are based on these thermodynamic properties. However, equilibrium studies generally only give information about the relative energetics of the reactant and the product states in the system. The kinetic properties of complexation also contain valuable information, for both mechanistic and practical considerations. Cryptate stability can be considered as the ratio of the rates of complexation and decomplexation and so insight into the kinetic basis for cation selectivity may be obtained from dynamic studies of cryptates. Kinetic factors are of obvious importance to the application of cryptates as metal ion carriers. Cryptands forming highly stable complexes do not necessarily perform as efficient ion carriers, that is, their function as either a metal ion receptor or a carrier is dependent upon both stability and cation exchange rates.

The alkali metal cryptates have consequently been the subject of a number of kinetic studies,<sup>43-51</sup> amongst which alkali metal ion NMR was shown to be a particularly useful technique. Various broad trends have been discerned from these

studies. The dissociation rates,  $k_d$ , decrease as cryptate stability increases. The most stable cryptates have dissociation rates which are several orders of magnitude slower than the naturally occurring antibiotic complexes. The variations of stability in a given solvent are reflected in the dissociation rates, with the rates of formation,  $k_f$ , varying over a relatively small range ( $10^6 - 10^9 \text{ mol}^{-1} \text{ dm}^3 \text{ s}^{-1}$ ), almost independent of stability in some cases.

However, it is apparent that the cryptands formed by C211 do not fit the broad kinetic pattern of those formed by the larger cryptands,<sup>46</sup> probably as a consequence of its smaller size and lower flexibility. Thus  $k_d$  for  $[\text{Li.C211}]^+$  (which has been well characterised<sup>43</sup> and for which most of the surprisingly few activation parameters for cryptate systems are available) is substantially less than expected from a simple comparison of the  $k_d$  values for the C221 and C222 cryptates. To a lesser extent this is also the case for the less studied  $[\text{Na.C211}]^+$  which is the subject of the first part of this variable temperature NMR investigation.

The objective of this work was to investigate the factors determining the lability of cryptates formed by C211 and the structurally modified cryptate,  $[\text{Na.C21C}_5]^+$ , thereby obtaining a better understanding of the mechanism of cryptate dissociation and formation.

## (i) Experimental Methods

### (a) $^{23}\text{Na}$ NMR Spectroscopy

Multinuclear NMR has become a very powerful technique in the study of ion - molecule interactions in solution, particularly in studies of alkali metal cryptates.<sup>52</sup>  $^{23}\text{Na}$  NMR

spectroscopy is a very convenient and direct method for investigating the exchange kinetics of sodium cryptates.<sup>44,53,54</sup>  $^{23}\text{Na}$  has a natural abundance of 100% and an intrinsic NMR sensitivity of one tenth of the proton<sup>53</sup>, or more than 500 times more sensitive than  $^{13}\text{C}$ , which has allowed its extensive use in studies of interactions with organic molecules and in direct investigations of biological systems.

The  $^{23}\text{Na}$  nucleus is quadrupolar with a spin number of 3/2. However, in the extreme narrowing conditions of rapid reorientational motion, the  $^{23}\text{Na}$  relaxation is characterised by a single exponential rate and gives rise to true Lorentzian lineshapes. The usual chemical shift range for  $^{23}\text{Na}$  cations is about 40 ppm which is relatively small for a heavy nucleus. The chemical shift is strongly solvent dependent and shows a linear correlation with the solvent Gutmann donor number.<sup>55</sup> Complexation by cryptands usually results in a considerable chemical shift change and if the rate of sodium ion exchange between the cryptate bound site and the free solution site is substantially less than the chemical shift separation, then individual resonances are observed for the two sites. These characteristics make sodium cryptate kinetics quite amenable to investigation by variable temperature  $^{23}\text{Na}$  NMR techniques and lineshape analysis.

#### (b) Lineshape Analysis

The theory and background of the NMR techniques for investigating rate processes in general have been reviewed by Lincoln.<sup>56</sup> The Bloch equations which describe the transverse components of magnetization in the rotating frame require modification under conditions of chemical exchange.<sup>57,58</sup> In the case of two site exchange, a useful model describing the

magnetization was proposed by Nakagawa<sup>59</sup> and further modified by Siddall et.al.<sup>60</sup> The algorithm applies only to cases where the system may be decomposed into a series of isolated coalescing doublets and is shown below.

The transverse magnetic moment component due to coalescing doublet  $i$ , is given by

$$M_{\nu i} = C \{ [(1+r_A p_A + r_B p_B)K + a(f+p_B-1)L] / (K^2+L^2) \} \quad (1)$$

and the total transverse magnetic moment at frequency  $\nu$  is therefore

$$M_{\nu} = \sum_{i=1}^n M_{\nu i} \cdot S_i \quad (2)$$

where  $n$  is the number of coalescing doublets

$S_i$  is an interdoublet scaling factor

$$\text{and } K = (r_A p_A + r_B p_B) - a(r_A r_B - f(f-1)) \quad (3)$$

$$L = f(1+r_A + r_B) - (a r_A + p_B) \quad (4)$$

$$C = -\nu H_1 M_0 / (2\pi |\nu_A - \nu_B|) \quad (5)$$

$$r_A = 1/2\pi T_{2A} |\nu_A - \nu_B| = \omega_A / (2|\nu_A - \nu_B|) \quad (6)$$

$$r_B = 1/2\pi T_{2B} |\nu_A - \nu_B| = \omega_B / (2|\nu_A - \nu_B|) \quad (7)$$

$$f = (\nu - \nu_A) / (\nu_B - \nu_A) = (\nu_A - \nu) / (\nu_A - \nu_B) \quad (8)$$

$$a = 2\pi\tau |\nu_A - \nu_B| \quad (9)$$

$$\tau = p_A \tau_B = p_B \tau_A \quad (10)$$

where  $\nu_j$  is the chemical shift of site  $j$  in the absence of exchange

$p_j$  is the relative population of site  $j$ , such that

$$\sum p_j = 1$$

$\omega_j$  is the width at 1/2 height of site  $j$  in the absence of exchange

$T_{2j}$  is the  $T_2$  of site  $j$  in the absence of exchange  
 $\tau$  is the exchange lifetime  
and  $\tau_j$  is the spin lifetime in site  $j$ .

Since the value of  $-\nu H_1 M_0 / 2\pi$  in (5) is a constant for a particular experiment,  $M_\nu$  is proportional to the experimental value ( $I_\nu$ ) of the absorption intensity at any frequency  $\nu$ . A theoretical spectrum proportional to the experimental spectrum may be calculated for a particular  $\tau$  value.

Spectra for a variety of  $\tau$  values must be generated and compared to the experimental one. This method of analysis is readily adapted for use on a minicomputer, and such a program, LINSHP,<sup>61</sup> was written for the BNC-12 computer of the HX-90E spectrometer and provided a convenient visual display of the fit.

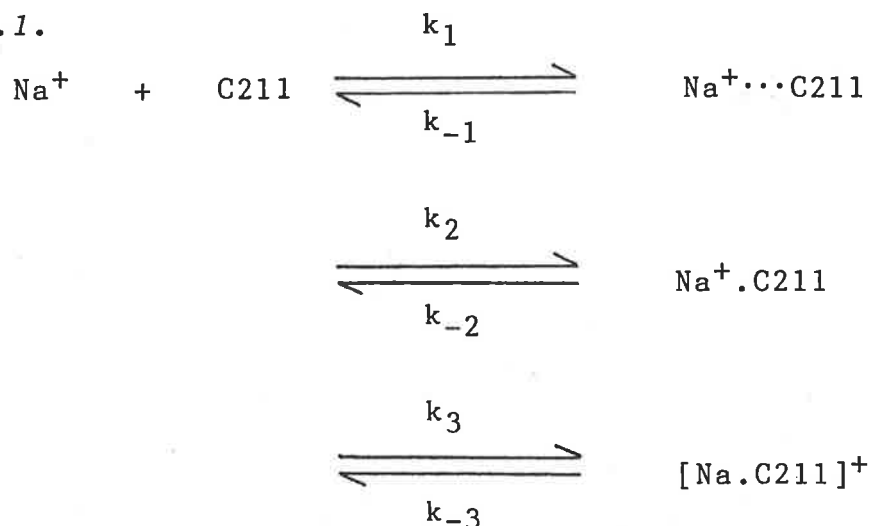
As described above, the lineshape analysis method requires a knowledge of the chemical shifts, line widths and populations of the site resonances in the absence of exchange. If these parameters are temperature dependent and vary through the region of coalescence where they cannot be measured directly, the variation must be established in conditions of no exchange and extrapolated into the exchange region. Alternatively, as in the case of ligand - metal ion exchange where the complex stability is sufficiently high, the temperature variation of the chemical shifts and linewidths may be determined from samples containing free metal ion or complexed metal ion only.

## 6.2

RESULTS AND DISCUSSION**(i) General Mechanistic Aspects**

Cryptate formation is the result of a complicated sequence of events involving solvational, conformational and coordination changes in the metal ion and cryptand in solution. However, a simplified mechanistic scheme may be constructed which encompasses many of these processes. In the case of sodium cryptates, the  $\text{Na}^+$  ion is bonded to two nitrogen atoms and a number of oxygen atoms. These bonds must be formed sequentially, accompanied by other complexation processes. The overall sequence involves the progressive desolvation of  $\text{Na}^+$  (solvated), conformational, and probably solvational changes in the cryptand, leading to the formation of the sodium cryptate in which, for C211 and C21C<sub>5</sub>, the  $\text{Na}^+$  ion is probably still partially solvated due to the exclusive structure of these cryptates. This process has become known as the Eigen-Winkler mechanism<sup>9</sup> on the basis of mechanisms proposed for the interactions of alkali metal ions with antibiotics. The mechanism may be schematically represented for  $[\text{Na.C211}]^+$  as shown below in Scheme 6.1 (the discussion applies equally well to  $[\text{Na.C21C}_5]^+$ ):

Scheme 6.1.



$k_1$  characterises the diffusion controlled formation of the encounter complex or collision complex in which both  $\text{Na}^+$  and C211 retain their complete solvational shell or sphere (probably associated with van der Waals interactions to some extent).  $k_2$  characterises the first  $\text{Na}^+$ -C211 bond formation which involves solvational and probably, conformational changes. All subsequent steps are incorporated in the final equilibrium and are represented by  $k_3$ . It should be remembered that this truncated scheme is almost certainly over simplified.

The identification of the rate determining step for the formation of  $[\text{Na.C211}]^+$  is not simple as desolvation of  $\text{Na}^+$  and C211, and conformational changes in C211 will contribute to the energetics of each step. As the solvating strength of the solvent changes or the cryptand structure is changed (e.g. from C211 to C21C<sub>5</sub>), the rate determining step in the sequence of events leading to  $[\text{Na.Cryp}]^+$  may change to an earlier or later step. Similarly, whilst the solvent may be the dominant contributor to the transition state energetics in one case, the cryptand may dominate the energetics in another solvent. Therefore, there will exist a sensitive balance between the dominance of the cryptand and of the solvent, depending on the solvating ability of the solvent. Thus broad generalisation concerning the formation of  $[\text{Na.Cryp}]^+$  and its dissociation are necessarily qualified by these considerations. In these NMR studies, only two rate constants are derived for the overall equilibrium shown in Scheme 5.1, where  $k_f / k_d = K_s$ . Therefore,  $k_f$  and  $k_d$  are closely related to the rate determining steps for the formation and dissociation reactions, which as previously noted, may change with solvent.

## (ii) Dynamics of C211 cryptates

At 298.2 K exchange of  $\text{Na}^+$  between  $[\text{Na.C211}]^+$  and the solvated state is slow on the NMR time scale in the solvents investigated ( $\text{H}_2\text{O}$ , DMSO, DMF, MeCN, pyridine, HMPA, acetone, propylene carbonate (PC) and MeOH). The  $^{23}\text{Na}$  resonance of the cryptate has a greater line width (Figure 6.1) than solvated sodium due to the quadrupolar induced relaxation arising from the non-cubic symmetry experienced by the nucleus in the cryptate environment. At 79.39 MHz coalescence of the resonances of the solvated and cryptate  $\text{Na}^+$  similar to that shown in Figure 6.1 is only observed for the water and DMSO systems. At the slower time scale available at 23.81 MHz this coalescence is also observed for the DMF system (Figure 6.1) but in the other solvents the exchange process is still too slow at this frequency to produce similar coalescences in the accessible temperature ranges. Subsequent discussion is accordingly restricted to water, DMSO and DMF solutions such that direct comparisons may be made with  $[\text{Li.C211}]^+$  under similar conditions. The mean lifetimes of  $[\text{Na.C211}]^+$ ,  $\tau_c$ , were derived using the complete lineshape analysis discussed in the previous section and typical best fit lineshapes are shown in Figure 6.1. The relationship between  $k_d$ , the dissociation rate constant and  $\tau_c$  is given by equation (6.1) in which  $\tau_s$  is the mean lifetime of solvated  $\text{Na}^+$ ,  $\chi_c$  and  $\chi_s$  are the appropriate mole fractions.

$$\begin{aligned} 1/\tau_c &= \chi_s/(\tau_s\chi_c) = k_d \\ &= (k_bT/h) \exp(-\Delta H^\ddagger/RT + \Delta S^\ddagger/R) \quad (6.1) \end{aligned}$$

where  $k_b$  is Boltzmann's constant

$h$  is Planck's constant

and  $R$  is the gas constant.



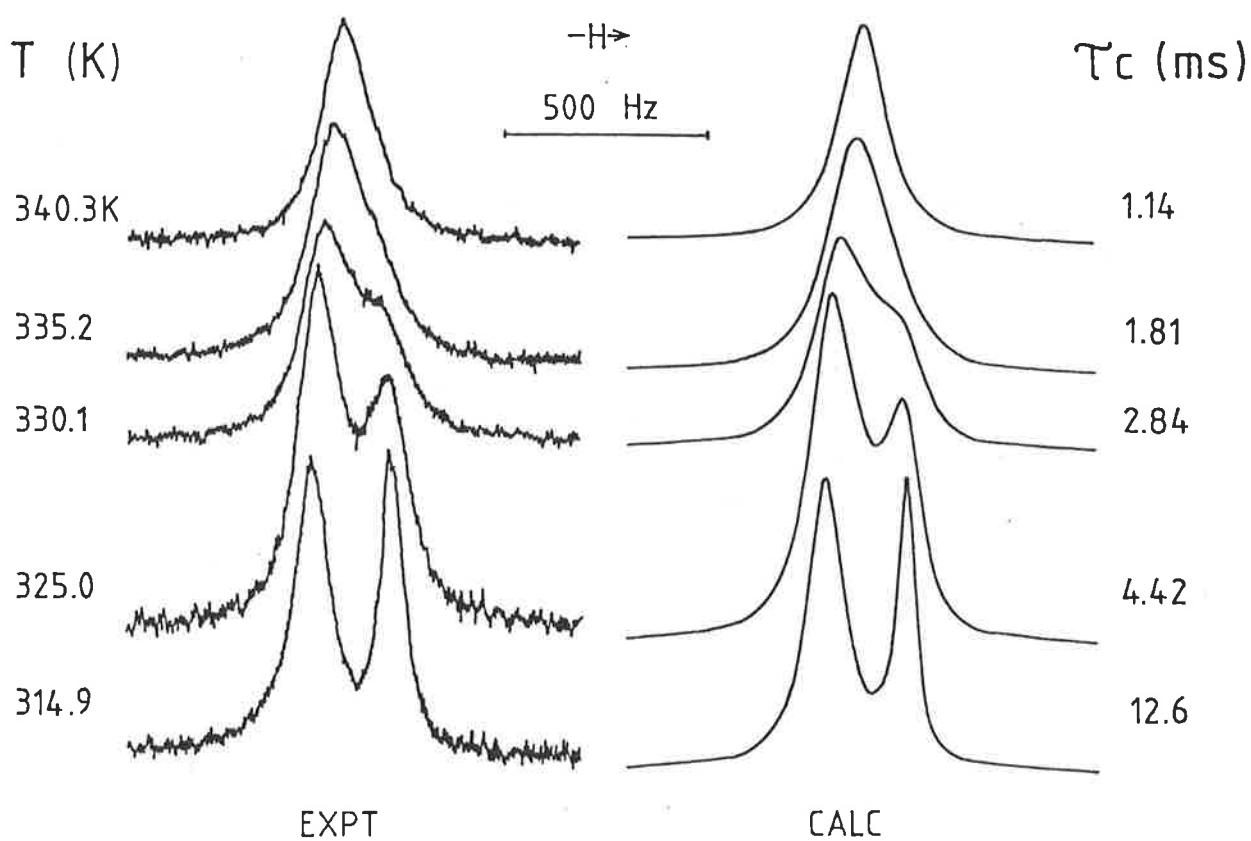


Figure 6.1. Typical exchange modified 23.81 MHz  $^{23}\text{Na}$  NMR spectra of a DMF solution of  $\text{NaClO}_4$  ( $0.100 \text{ mol dm}^{-3}$ ) and C211 ( $0.067 \text{ mol dm}^{-3}$ ). Experimental temperatures are shown to the left of the figure. Best fit lineshapes and derived  $\tau_c$  values appear to the right of the figure.

Kinetic data may be fitted to the Eyring relationship in this exponential form or in the more convenient linear form below

$$\ln(T\tau_c) = (\Delta H^\ddagger/R) / T + (\ln(h/k_b) - \Delta S^\ddagger / R) \quad (6.2)$$

The non-linear least squares program DATAFIT mentioned in section 2.2 was used to calculate the activation enthalpies and entropies using the above relationship. Eyring plots of  $T\tau_c$  against  $1/T$  are shown in Figure 6.2 and the derived  $k_d$ ,  $\Delta H^\ddagger$  and  $\Delta S^\ddagger$  values appear in Table 6.1 as do the compositions of the solutions studied. Within experimental error integration of the  $[\text{Na.C211}]^+$  and  $\text{Na}^+$  (solvated) resonances under slow exchange conditions showed all of the cryptand to be complexed consistent with reported stability constants  $\log K = 3.2, 4.6$  and  $5.2$  in water, DMSO and DMF, respectively.<sup>35</sup> The most reliable kinetic parameters are obtained in the midst of the coalescence temperature range when the width and amplitudes of the coalescing resonances are similar and this imposes a limitation on the range over which  $\chi_c$  and  $\chi_s$  may be varied. Thus  $\chi_c$  and  $\chi_s$  were varied from 0.30-0.63 and 0.70-0.37 respectively in water; 0.33-0.67 and 0.67-0.33 in DMSO; and 0.495-0.665 and 0.505-0.335 in DMF. It is seen from Figure 6.2 and Table 6.1 that  $k_d$  is invariant under these conditions which suggests that the rate determining step for exchange is the dissociation of  $[\text{Na.C211}]^+$  as has also been reported to be the case for  $[\text{Na.C222}]^+$ .<sup>44</sup> Protonation of both cryptates and cryptands can occur in water<sup>62</sup> and accordingly in addition to the three solutions of  $[\text{Na.C211}]^+$  studied in water at pH 10.5 another solution was studied at pH 11.8. It is seen from Table 6.1 that this pH variation induces no significant change in the kinetic parameters and it is concluded that the data

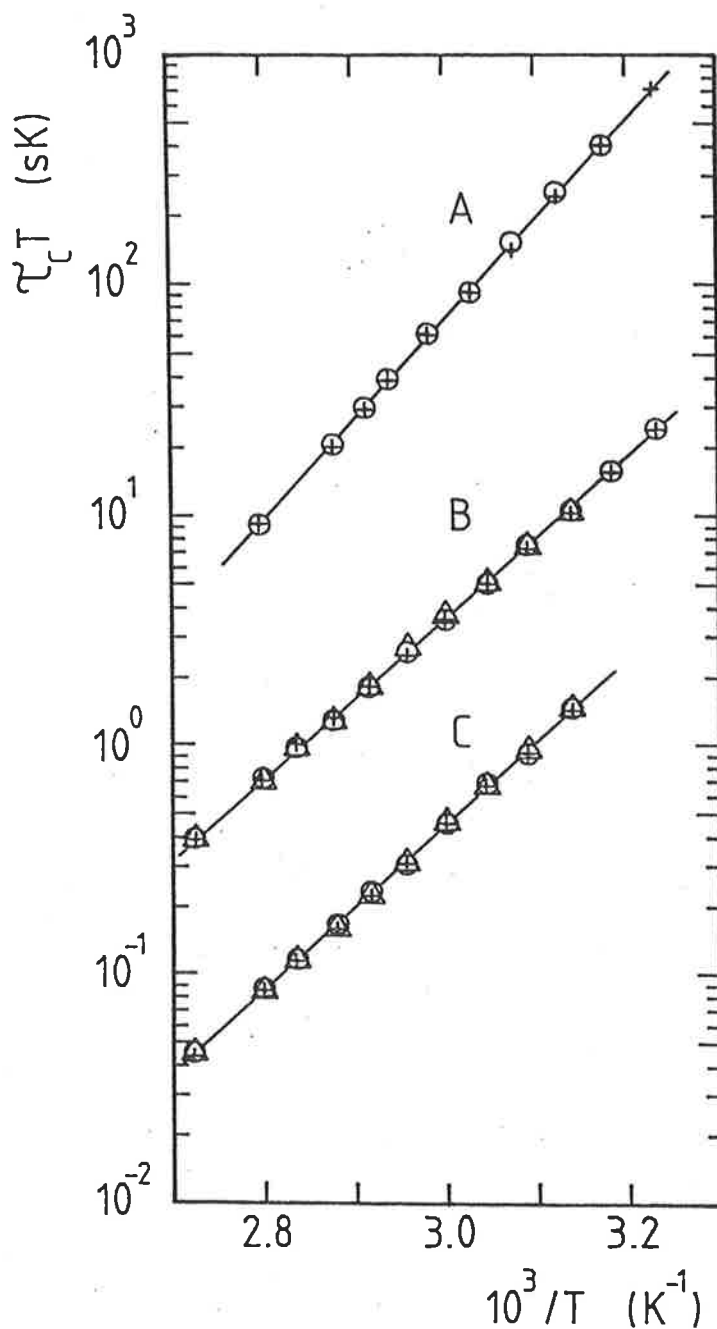


Figure 6.2. Plots of  $\tau_c T$  against  $1/T$  for (A) DMF ( $\times 10^2$ ), where solutions (viii) and (ix) are represented by  $\circ$  and  $+$ , respectively; (B)  $H_2O$  ( $\times 10$ ), where solutions (i), (ii) and (iii) are represented by  $\circ$ ,  $+$  and  $\Delta$ , respectively; and (C) DMSO, where solutions (v), (vi) and (vii) are represented by  $\circ$ ,  $+$  and  $\Delta$ , respectively.

Table 6.1. Solution composition and kinetic parameters for Na<sup>+</sup> exchange on [Na.C211]<sup>+</sup> in various solvents.<sup>a</sup>

Solvent	[Na <sup>+</sup> (solvated)] mol dm <sup>-3</sup>	[Na.C211] <sup>+</sup> mol dm <sup>-3</sup>	k <sub>d</sub> (335 K) s <sup>-1</sup>	ΔH <sup>‡</sup> kJ mol <sup>-1</sup>	ΔS <sup>‡</sup> J K <sup>-1</sup> mol <sup>-1</sup>	
i)	H <sub>2</sub> O (pH 10.5)	0.052	0.048	1054.8±8.2	67.5±0.5	13.5±1.3
ii)	H <sub>2</sub> O (pH 10.5)	0.037	0.063	1061.8±7.1	67.2±0.4	12.6±1.1
iii)	H <sub>2</sub> O (pH 10.5)	0.070	0.030	1044.4±4.8	66.9±0.3	11.7±0.9
i)-iii)	combined	-	-	1053.6±4.1	67.2±0.3	12.6±0.7
iv)	H <sub>2</sub> O (pH 11.8)	0.049	0.051	1058.3±9.5	67.3±0.1	12.9±1.6
v)	DMSO	0.051	0.049	837.4±6.2	69.1±0.5	16.4±1.4
vi)	DMSO	0.033	0.067	827.9±9.0	71.1±0.9	22.1±2.5
vii)	DMSO	0.067	0.033	840.3±8.2	68.3±0.7	14.0±1.8
v)-vii)	combined	-	-	832.7±5.0	69.5±0.4	17.4±1.2
viii)	DMF	0.052	0.048	550.2±3.0	84.2±0.4	57.7±1.3
ix)	DMF	0.033	0.067	558.3±5.0	83.1±0.7	54.9±1.8
viii)-ix)	combined	-	-	554.8±3.2	83.5±0.5	55.9±1.2

a) Kinetic parameters were determined from DATAFIT analysis. Errors quoted represent one standard deviation.

reported here pertains to the unprotonated form of  $[\text{Na.C211}]^+$ .

Comparisons between the kinetic parameters characterising  $[\text{Na.C211}]^+$  may be made from the data collected in Table 6.2. The positive  $\Delta S^\ddagger$  values characterising  $[\text{Na.C211}]^+$  contrast with the negative values characterising  $[\text{Li.C211}]^+$  and are the sole source of the greater  $[\text{Na.C211}]^+$   $k_d$  values in DMSO and DMF solvents. In water the greater  $k_d$  value characterising  $[\text{Na.C211}]^+$  arises from both a smaller  $\Delta H^\ddagger$  and more positive  $\Delta S^\ddagger$  value than are observed for  $[\text{Li.C211}]^+$ . These differences in the activation parameters characterising the  $\text{Li}^+$  and  $\text{Na}^+$  cryptates probably reflect the different sizes and solvation of the two metal ions to some extent, but in addition may also reflect the differing propensities of the two cryptates to exist in the exclusive and inclusive forms as is discussed below. The modest dependence of  $k_d$  characterising both  $[\text{Na.C211}]^+$  and  $[\text{Li.C211}]^+$  on the nature of the solvent indicates some involvement of solvent in the transition state, but the dependence of  $k_f$  ( $=Kk_d$ , Table 6.2) on the nature of the solvent is greater. This suggests that the transition state for alkali metal ion exchange resembles  $[\text{M.C211}]^+$  more closely than solvated  $\text{M}^+$  and C211, and that in the formation reaction  $\text{M}^+$  becomes substantially desolvated. Also, any C211 solvational changes are close to completion when the transition state is attained. These observations are contrary to those made for the larger and more flexible cryptands and reflect the greater rigidity of the C211 structure by comparison to its larger homologues.<sup>46</sup> Discussion of these data is complicated by the multistep nature of the cryptate formation process and it is now appropriate to consider the mechanistic aspects in more detail.

Table 6.2. Kinetic parameters for Li<sup>+</sup> and Na<sup>+</sup> exchange on cryptate in various solvents

M <sup>+</sup>	cryptand	solvent	10 <sup>-3</sup> k <sub>f</sub> (298.2K) <sup>a</sup> dm <sup>3</sup> s <sup>-1</sup> mol <sup>-1</sup>	k <sub>d</sub> (298.2K) s <sup>-1</sup>	ΔH <sup>‡</sup> kJ mol <sup>-1</sup>	ΔS <sup>‡</sup> J K <sup>-1</sup> mol <sup>-1</sup>	Ref.
Li <sup>+</sup>	C211	H <sub>2</sub> O	1.55	0.0049±0.002	86.6±4.6	1.7±13.0	b
Li <sup>+</sup>	C211	DMSO	16.1	0.0232±0.0054	64.8±2.5	-57.7±5.8	b
Li <sup>+</sup>	C211	DMF	127	0.013 ±0.0033	64.4±2.5	-63.2±5.8	b
Na <sup>+</sup>	C211	H <sub>2</sub> O	75.4	47.6±0.5	67.2±0.3	12.6±0.7	c
Na <sup>+</sup>	C211	DMSO	1450	34.0±0.7	69.5±0.4	17.4±1.2	c
Na <sup>+</sup>	C211	DMF	1920	12.1±0.2	83.5±0.5	55.8±1.2	c
Na <sup>+</sup>	C221	H <sub>2</sub> O	3600	14.5	-	-	d
Na <sup>+</sup>	C221	DMSO	7200	0.75	-	-	d
Na <sup>+</sup>	C221	DMF	18000	0.25	-	-	d
K <sup>+</sup>	C221	H <sub>2</sub> O	18000	2000	-	-	d
Na <sup>+</sup>	C222	H <sub>2</sub> O	1400	147.6±2.6	67.4±0.8	22.2±3.3	e
K <sup>+</sup>	C222	H <sub>2</sub> O	2000	7.5	-	-	d

a)  $k_f = k_d K$  using values from ref. 35.

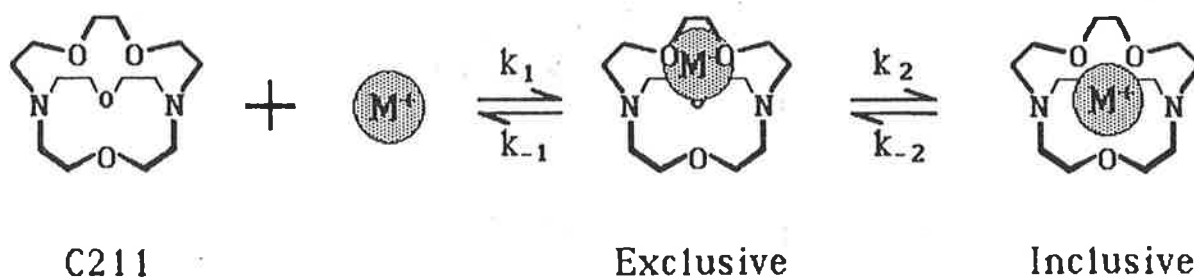
b) Ref. 43 Ref. 46 quotes  $k_d = 0.025, 0.0212$  and  $0.0145 \text{ s}^{-1}$  for H<sub>2</sub>O, DMSO and DMF respectively. These values were determined using a stopped-flow technique and the origin of the discrepancy between the H<sub>2</sub>O values is not obvious. However, this discrepancy does not affect the arguments presented.

c) This study. For H<sub>2</sub>O and DMSO refs. 62 and 46 respectively quote  $k_d(298.2K) = 140$  and ca  $5 \text{ s}^{-1}$ , determined by temperature-jump spectrophotometric and stopped-flow spectrophotometric methods. The origins of these discrepancies are not apparent but they do not affect the arguments presented.

d) Ref. 46.

e) Ref. 44.

As cryptates exist in exclusive and inclusive forms in solution, a minimum of two steps, as shown in Scheme 6.2, must be considered in discussion of dissociation and formation processes.



Scheme 6.2

This scheme is over simplified as it does not specifically include solvational and conformational changes, and the diffusion controlled formation of the encounter complex generally considered to precede metal complex formation reactions is not shown. Nevertheless, Scheme 6.2 provides a convenient basis for ensuing mechanistic discussion, and clearly raises the possibility that the rate determining step for dissociation of  $[M.C211]^+$  may involve either the exclusive or the inclusive cryptate as the nature of  $M^+$  is varied (or the nature of the cryptate is varied). The previously discussed data indicate that  $[Na.C211]^+$  exists predominantly in the exclusive form in solution such that  $k_2 \ll k_{-2}$ . Under these circumstances it is probable that  $k_{-1}$  characterises the rate determining step for dissociation of  $[Na.C211]^+$ , and as shown below,  $k_d \approx k_{-1} / (k_2 / k_{-2} + 1) \approx k_{-1}$  and similarly,  $k_f = K.k_d \approx k_1$ .

$$K = [M.C211]_{in}^+ / [M^+][C211] = k_1 k_2 / k_{-1} k_{-2} \quad (6.3)$$

$$k_1 / k_{-1} = [M.C211]_{ex}^+ / [M^+][C211] \quad (6.4)$$

and  $k_2 / k_{-2} = [M.C211]_{in}^+ / [M.C211]_{ex}^+ \quad (6.5)$

Now if  $k_{-1}$  characterises the rate determining step, then

$$k_d = k_{-1} \{ [M.C211]_{ex}^+ / ([M.C211]_{ex}^+ + [M.C211]_{ex}^+) \}$$

$$= k_{-1} \{ 1 / (1 + ([M.C211]_{in}^+ / [M.C211]_{ex}^+)) \}$$

and substituting from (6.5) gives

$$= k_{-1} / (k_2/k_{-2} + 1) \quad (6.6)$$

(It should be noted that if significant amounts of  $[Na.C211]^+$  exist in the inclusive form and  $k_{-1} > k_{-2}$  the  $^{23}Na$  resonance of this species would appear superimposed on the coalescing resonances of  $Na^+$  and  $[Na.C211]^+$ .)

In contrast,  $[Li.C211]^+$  exists predominantly in the inclusive form such that  $k_2 \gg k_{-2}$ . A stopped flow calorimetric study of the formation of  $[Li.C211]^+$  in water detected two kinetic processes consistent with the fast formation of the exclusive form followed by the slower formation of the inclusive form.<sup>45</sup> It was not possible to separate individual rate constants from these data and the  $k_d$  values determined by  $^7Li$  NMR<sup>43</sup> (Table 6.2) cannot be unambiguously identified with  $k_{-1}$  or  $k_{-2}$  in Scheme 6.2. Intuitively it seems plausible that as a consequence of the smaller ionic radius of  $Li^+$  compared to that of  $Na^+$ , the rate determining step in the dissociation of the  $Li^+$  cryptate involves inclusive  $[Li.C211]^+$  such that  $k_d \approx k_{-2}$ . (An alternative possibility that  $k_{-1}$  characterises the rate determining step results in  $k_d \approx k_{-1}k_{-2}/k_2$ .) When  $\log k_d$  is plotted against  $\log K$  the  $[Li.C211]^+$   $k_d$  values are found to be  $10^3 - 10^4$  smaller than expected by comparison to similar data for the dissociation of  $Na^+$  and  $K^+$  from larger cryptates and this has been



attributed<sup>46</sup> largely to the lower flexibility of C211. In DMF, DMSO and water,  $k_d$  for  $[\text{Na.C211}]^+$  is found to be  $10^{-10}$  smaller than anticipated from a similar comparison. These observations are consistent with the earlier deduction (based on the solvent dependence of  $k_f$  being greater than of  $k_d$ ) that both  $\text{Li}^+$  and  $\text{Na}^+$  in the transition state are substantially desolvated. Thus it appears that the relative rigidity of C211 restricts the sequential displacement or acquisition of solvent molecules in the metal ion solvation sheath by comparison to more flexible complexones, and as a consequence  $k_f$  and  $k_d$  characterising  $[\text{Li.C211}]^+$  and  $[\text{Na.C211}]^+$  are quite small.

The discussion is now extended to include the data pertaining to the other  $\text{Na}^+$  and  $\text{K}^+$  cryptates in Table 6.2. A comparison of the  $k_f$  and  $k_d$  values determined in water for  $[\text{Na.C221}]^+$  and  $[\text{K.C221}]^+$  (which  $^{13}\text{C}$  NMR studies indicate exist predominantly in the inclusive and exclusive forms respectively in solution<sup>21</sup>) shows that the  $k_f$  and  $k_d$  values characterising  $[\text{Na.C221}]^+$  are substantially less than those for  $[\text{K.C221}]^+$ . It is expected that for  $[\text{K.C221}]^+$   $k_d \approx k_{-1}$  and for  $[\text{Na.C221}]^+$   $k_d \approx k_{-2}$  on the basis of the arguments advanced for the C211 cryptates. In both pairs of exclusive and inclusive cryptates the latter is seen to be the least labile towards exchange of  $\text{M}^+$  between the solvated and complexed environments.

The  $k_d$  and  $k_f$  values characterising  $[\text{K.C222}]^+$ , which is expected to exist predominantly in the inclusive form, are decreased relative to those for  $[\text{K.C221}]^+$  consistent with the above observations. However, such comparisons between cryptates formed with different cryptands must be made with

caution as the flexibility of the cryptand increases with size. Thus it is seen that in contrast to  $[\text{Na.C211}]^+$  and  $[\text{Li.C211}]^+$  the  $k_d$  values obtained for  $[\text{Na.C221}]^+$  are more dependent on the nature of the solvent (Table 6.2) than are the  $k_f$  values consistent with the transition state for  $\text{Na}^+$  exchange resembling the solvated  $\text{Na}^+$  and the cryptand more than the cryptate, as compared with the C211 cryptates where the reverse situation prevails. It is therefore likely that the variation of the  $k_d$  and  $k_f$  values in water for  $[\text{Na.C211}]^+$ ,  $[\text{Na.C221}]^+$  and  $[\text{Na.C222}]^+$  not only reflects the change from the exclusive to the inclusive species on going from the first to the second cryptand, but also the increasing flexibility of the cryptand with size and the non-optimal fit of  $\text{Na}^+$  into the large cavity of C222. This discussion is based on data obtained in a limited range of solvents but it is nevertheless apparent that the predominance of the factors determining the lability of the cryptates varies as the structural properties of the metal ion and the cryptand are varied. Extension of the discussion pertaining to the relative solvent dependence of  $k_f$  and  $k_d$  to a broader solvent range is presented in section 6.2 (iv).

### (iii) Kinetics of $[\text{Na.C21C}_5]^+$

The previous section dealt with the effect on general cryptate dynamics of factors such as ionic radius, cryptand cavity size and flexibility in terms of the exclusive or inclusive nature of the cryptate structural conformation. In this section, the effect of changing the structural binding features of the cryptand are examined by a comparison of the kinetic parameters of  $[\text{Na.C211}]^+$  and  $[\text{Na.C21C}_5]^+$ .

In the solid state structure of  $[\text{Na.C21C}_5]^+$ , the sodium ion was found to be bound less closely to the cryptand cavity than in the C211 analogue since there is no binding interaction with the all carbon bridge. In the structure of  $[\text{Na.C211}]^+$  the sodium ion is in binding contact with the oxygen of the bridge on the opposite side of the cryptand, as indicated by the conformation of the bridge where the oxygen is directed towards the cavity and sodium ion. These differences in structures are manifest in the solution stabilities of the two cryptates with the C21C<sub>5</sub> cryptate being substantially less stable than the C211 cryptate since the solvent may compete more effectively in the coordination of  $\text{Na}^+$  in the former cryptate. In line with the behaviour of cryptates in general, such a reduction in complex stability should result in increased rates of dissociation for  $[\text{Na.C21C}_5]^+$ .

The variable temperature  $^{23}\text{Na}$  NMR studies of  $[\text{Na.C21C}_5]^+$  revealed that the rate of exchange of  $\text{Na}^+$  was increased in all solvents. The coalescence temperatures were substantially reduced relative to those found for  $[\text{Na.C211}]^+$  such that the coalescence of the two resonances was observed within the accessible temperature ranges for a wider range of solvents; DMF, MeOH, propylene carbonate (PC), acetone, pyridine at

79.39 MHz and MeCN at 23.81 MHz. The exchange rate was fast on the NMR time scale in DMSO at its melting temperature and as mentioned previously, the cryptand and its  $\text{Na}^+$  cryptate are insoluble in water. The mean lifetimes of  $[\text{Na.C21C}_5]^+$ ,  $\tau_c$ , were derived from complete lineshape analysis as described in section 6.1 and typical best fit lineshapes and the experimental  $^{23}\text{Na}$  NMR spectra for  $[\text{Na.C21C}_5]^+$  in MeOH and MeCN are shown in Figures 6.3 and 6.4 respectively. Eyring plots of  $T\tau_c$  against  $1/T$  are shown in Figures 6.5 and 6.6 and the solution compositions, derived  $k_d$  and activation parameters are given in Table 6.3. Again it can be seen from Table 6.3 and Figures 6.5 and 6.6 that  $k_d$  is independent of the ratio of  $\text{Na}^+(\text{solvated})$  to  $[\text{Na.C21C}_5]^+$  indicating that the rate determining step for exchange is the dissociation of the cryptate.

A summary of the kinetic parameters for  $[\text{Na.C21C}_5]^+$  is presented in Table 6.4 and  $k_d$  values for  $[\text{Na.C211}]^+$  in common solvents are included for comparison. Clearly the  $k_d$  values for  $[\text{Na.C21C}_5]^+$  show a strong solvent dependence and with the exception of the nitrogen donor solvents, pyridine and MeCN, the  $k_d$  values rise steeply with increasing Gutmann donor number (DN), although  $\log k_d$  is not linearly dependent on DN as found for  $[\text{K.C222}]^+$ .<sup>46</sup> (The Gutmann donor number<sup>63</sup> represents a quantitative measure of the electron donating ability of a solvent, and is given by the heat of formation of the complex between  $\text{SbCl}_5$  and the solvent in 1,2-dichloroethane.) The  $k_f$  values also show some solvent variation, but by a factor of only 43 over the range of solvents as compared to a factor of greater than 1500 for the  $k_d$  values. This suggests that in the case of  $[\text{Na.C21C}_5]^+$ , the transition state

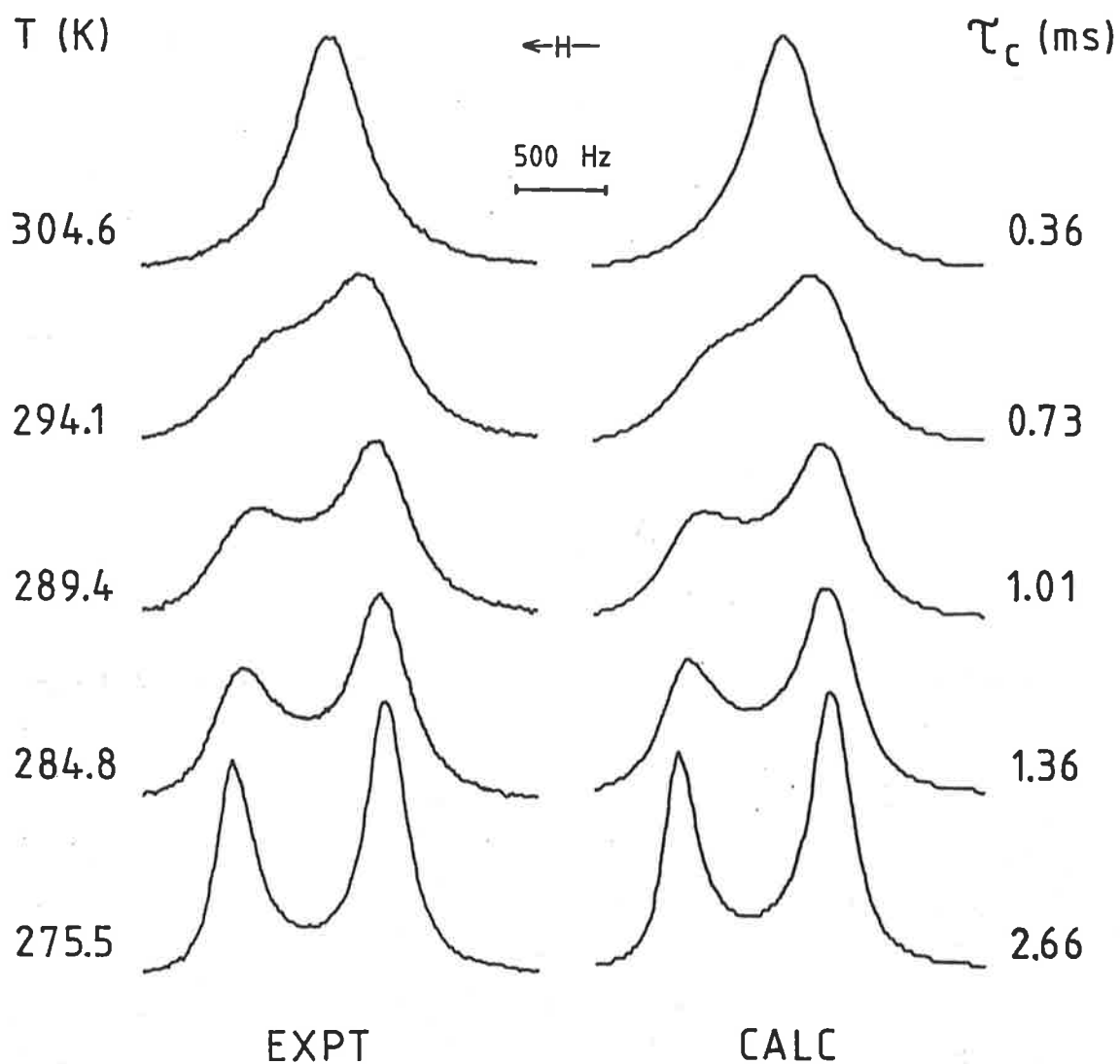


Figure 6.3. Typical exchange modified 79.39 MHz  $^{23}\text{Na}$  NMR spectra of a MeOH solution of  $\text{NaClO}_4$  ( $0.099 \text{ mol dm}^{-3}$ ) and  $\text{C}_{21}\text{C}_5$  ( $0.066 \text{ mol dm}^{-3}$ ). Experimental temperatures are shown to the left of the figure, and best fit lineshapes and derived  $\tau_c$  values appear to the right of the figure.

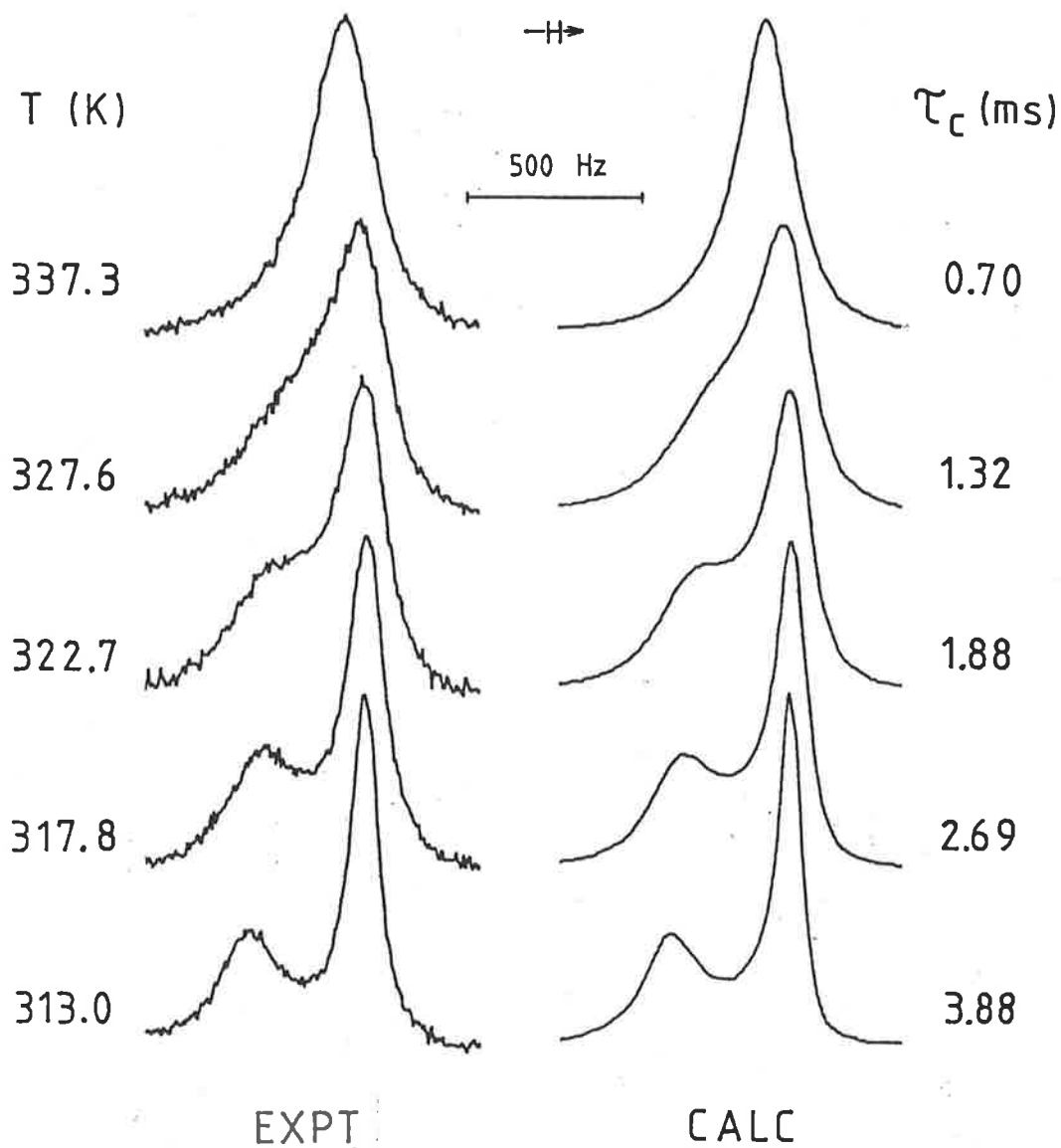


Figure 6.4. Typical exchange modified 23.81 MHz  $^{23}\text{Na}$  NMR spectra of a MeCN solution of  $\text{NaClO}_4$  ( $0.105 \text{ mol dm}^{-3}$ ) and  $\text{C}_{21}\text{C}_5$  ( $0.053 \text{ mol dm}^{-3}$ ). Experimental temperatures are shown to the left, and best fit lineshapes and derived  $\tau_c$  values appear to the right of the figure.

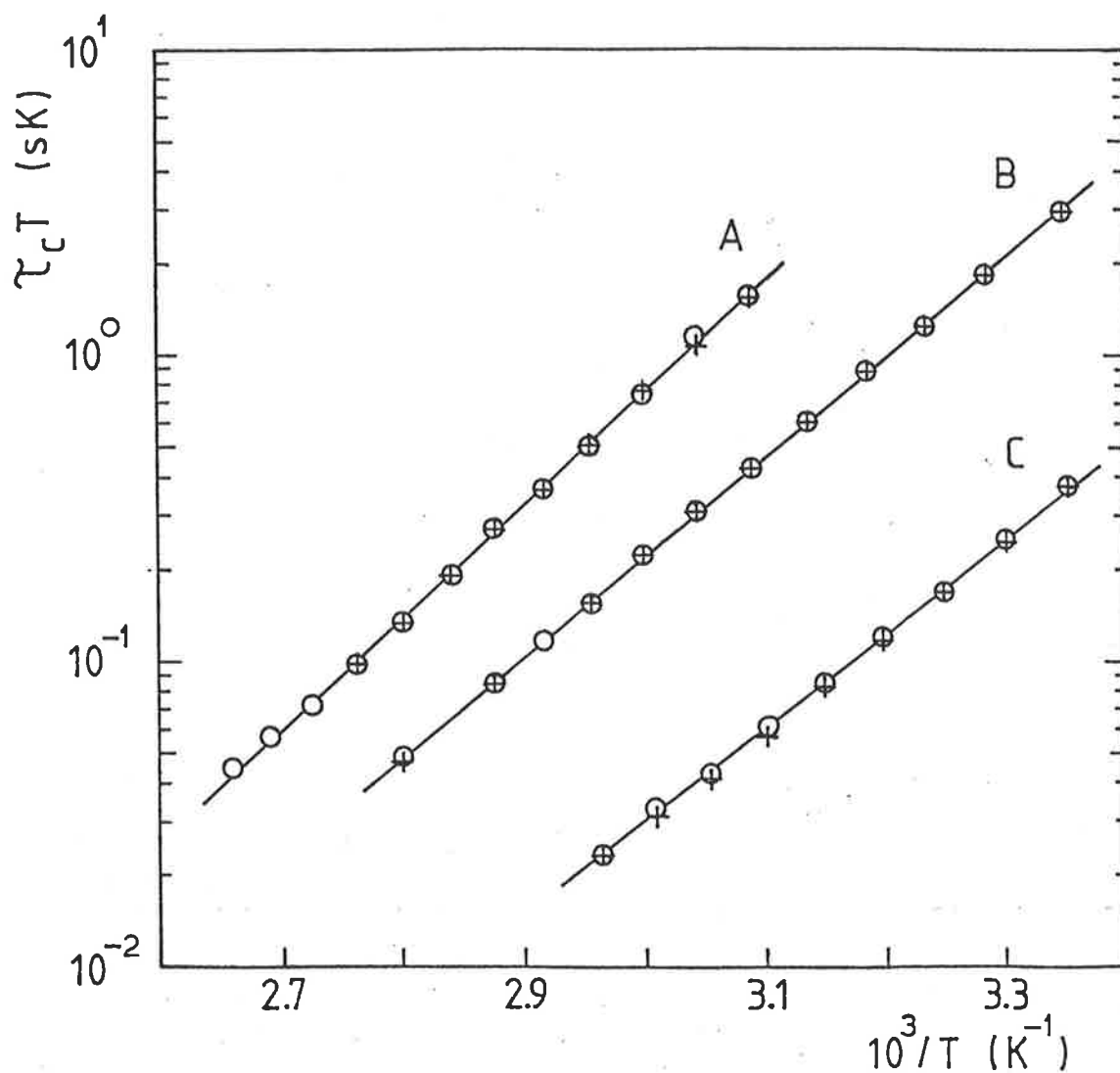


Figure 6.5. Plots of  $\tau_c T$  against  $1/T$  for (A) PC, where solutions (ix) and (x) are represented by  $\circ$  and  $+$ , respectively; (B) pyridine, where solutions (i) and (ii) are represented by  $\circ$  and  $+$ , respectively, and (C) MeCN, where solutions (vii) and (viii) are represented by  $\circ$  and  $+$  respectively.

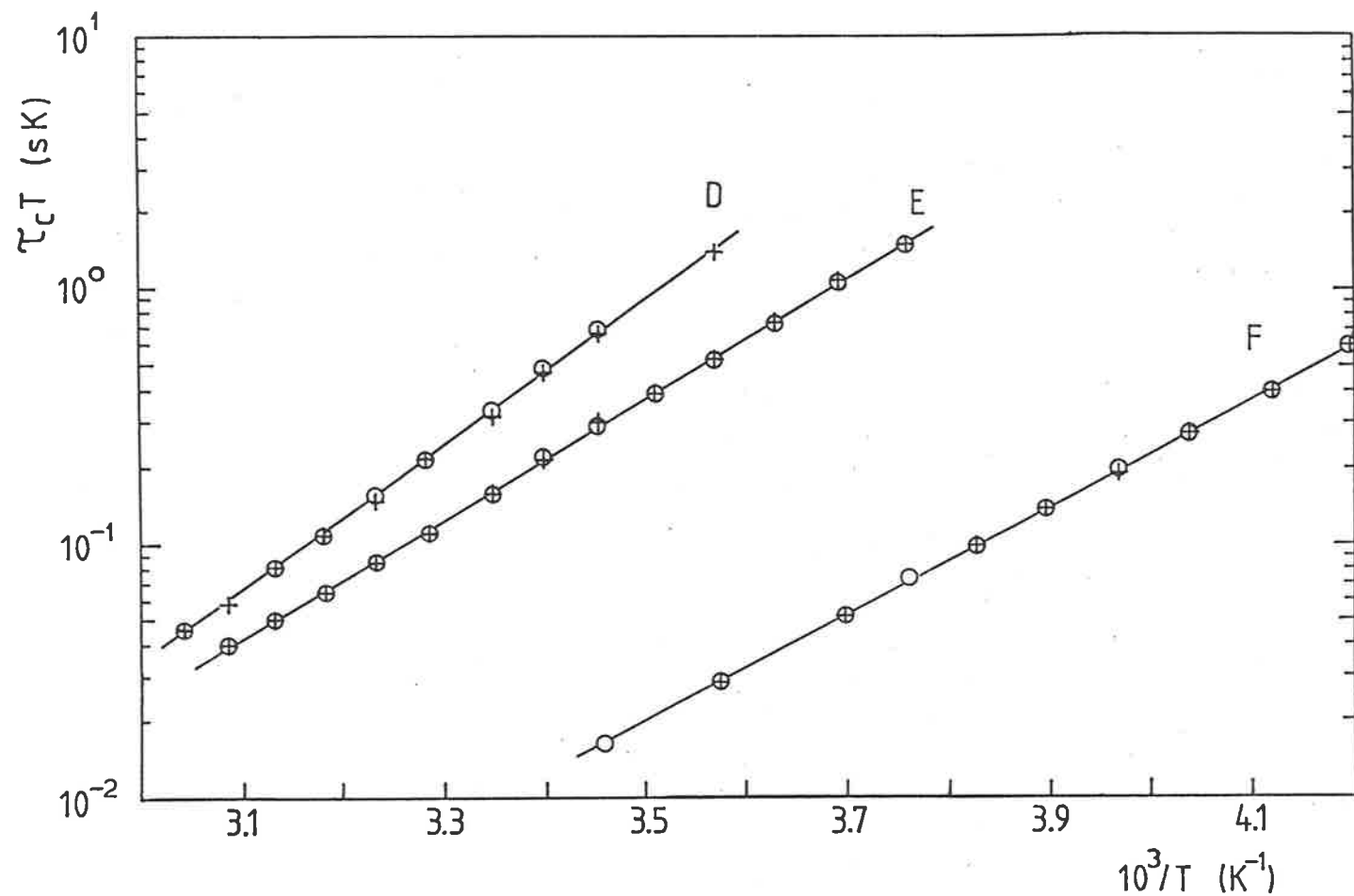


Figure 6.6. Plots of  $\tau_c T$  against  $1/T$  for (D) acetone, where solutions (iii) and (iv) are represented by  $\circ$  and  $+$ , respectively; (E) MeOH, where solutions (v) and (vi) are represented by  $\circ$  and  $+$ , respectively, and (F) DMF, where solutions (xi) and (xii) are represented by  $\circ$  and  $+$ , respectively.



ix)	PC	0.051	0.050	19.4±0.8	70.2±0.7	15.2±2.0
x)	PC	0.033	0.068	19.1±0.6	70.7±0.7	16.7±1.9
ix)-x)	combined	-	-	19.4±0.5	70.3±0.5	15.3±1.4
xi)	DMF	0.053	0.053	28819±343	40.1±0.2	-25.0±0.8
xii)	DMF	0.035	0.071	28871±337	40.0±0.2	-25.4±0.7
xi)-xii)	combined	-	-	28818±242	40.0±0.1	-25.3±0.5

---

a) Kinetic parameters determined from DATAFIT analysis. Errors quoted represent one standard deviation.

Table 6.4. Kinetic Parameters Summary for Na<sup>+</sup> exchange on Cryptate in Various Solvents

Solvent	DN <sup>a</sup>	Cryptand	10 <sup>-3</sup> k <sub>f</sub> <sup>b</sup> dm <sup>3</sup> s <sup>-1</sup> mol <sup>-1</sup>	k <sub>d</sub> (298K) s <sup>-1</sup>	ΔH <sup>‡</sup> kJ mol <sup>-1</sup>	ΔS <sup>‡</sup> J K <sup>-1</sup> mol <sup>-1</sup>
MeCN	14.1	C21C <sub>5</sub>	10195.2	84.8±1.6	57.9±0.7	-13.8±2.1
PC	15.1	C21C <sub>5</sub>	25574.1	19.4±0.5	70.3±0.5	15.3±1.4
Acetone	17.0	C21C <sub>5</sub>	8398.2	879.4±6.4	54.4±0.4	-6.1±1.2
MeOH	19.0	C21C <sub>5</sub>	10370.0	1802.1±4.8	44.9±0.1	-31.9±0.4
DMF	26.6	C21C <sub>5</sub>	21363.1	28818 ±242	40.0±0.1	-25.3±0.5
Pyridine	33.1	C21C <sub>5</sub>	490.7	93.5±0.5	62.8±0.2	3.3±0.5
DMF <sup>c</sup>		C211	1920	12.1±0.2	83.5±0.5	55.8±1.2
MeOH <sup>d</sup>		C211	3100	2.5	-	-
PC <sup>d</sup>		C211	21000	0.036	-	-

a) Gutmann donor number; b) k<sub>f</sub> = k<sub>d</sub>K<sub>S</sub> values from section 5.2; c) From Table 6.2; d) Values taken from Ref. 46.

for complex formation strongly resembles  $\text{Na}^+(\text{solvated})$  and cryptand rather than the cryptate. The greater solvent dependence of  $k_d$  values in this range of solvents is contrary to the situation found for the  $[\text{Li.C211}]^+$  and  $[\text{Na.C211}]^+$  cryptates in the solvents discussed in section 6.2 (ii).

It is also noted from Table 6.4 that the  $k_d$  values for  $[\text{Na.C21C}_5]^+$  are 2 to 3 orders of magnitude larger than those for the C211 cryptate in the same solvent. This increase is much larger than the increase in  $k_f$  values, for example, in DMF the  $k_d$  value differs by a factor of over 2000, whereas the  $k_f$  value varies by a factor of approximately 20. Thus the overall reduction in stability of the  $\text{C21C}_5$  cryptates relative to the C211 cryptates is reflected almost completely in the dissociation rates. Indeed, a plot of  $\log K_s$  vs  $\log k_d$  is approximately linear and the values for  $[\text{Na.C21C}_5]^+$  are coincident with the plot obtained for the C222 and C221 cryptates of various metal ions in various solvents.<sup>46</sup>

$[\text{Na.C21C}_5]^+$  exists as an exclusive cryptate as shown previously and so the mechanistic arguments presented for  $[\text{Na.C211}]^+$  in terms of the equilibrium shown in Scheme 6.2 are also appropriate for this cryptate. Thus  $k_{-1}$  is substantially increased and  $k_1$  slightly increased relative to  $[\text{Na.C211}]^+$ , destabilizing the exclusive cryptate. The loss of an oxygen binding site has led to a reduction in the lifetime of the sodium residing on the face of the cryptand containing three oxygen binding sites. There is no evidence that the sodium ion binds to either face containing the all carbon bridge.

It is of interest to extend these studies to other alkali metal cations and preliminary 116.64 MHz  $^7\text{Li}$  NMR investig-

ations of the kinetics of  $[\text{Li.C21C}_5]^+$  have been carried out. As in the case of  $[\text{Li.C211}]^+$ <sup>43</sup>, the rate of  $\text{Li}^+$  exchange is slow on the NMR time scale at 298 K in the solvents studied (DMF, DMSO, acetone, MeOH and PC). Of these solvents, only in DMF and DMSO was coalescence obtained within the accessible temperature ranges and to date, the data obtained for DMF only has been subjected to complete lineshape analysis.<sup>65</sup> The  $k_d$  value obtained in DMF was  $145 \text{ s}^{-1}$  at 298 K, substantially lower than for  $[\text{Na.C21C}_5]^+$  ( $28818 \text{ s}^{-1}$ , Table 6.4). This difference reflects the change in cryptate structure from exclusive  $[\text{Na.C21C}_5]^+$  to the presumably inclusive  $[\text{Li.C21C}_5]^+$ . (Although the latter cryptate was shown to be inclusive by  $^{13}\text{C}$  NMR in  $\text{CDCl}_3$  in section 4.3, it is possible that in the more strongly solvating DMF, the exclusive form may exist in significant amounts.) The variation of a factor of 200 between these two cryptates compares to a difference in  $k_d$  of a factor of 920 for the two C211 cryptates (Table 6.2). This smaller difference in the C21C<sub>5</sub> cryptate dissociation rates may indicate the presence of a significant amount of exclusive  $\text{Li}^+$  cryptate. However, a more detailed investigation of the kinetics of  $[\text{Li.C21C}_5]^+$  in a wider range of solvents is required before any such mechanistic conclusions can be made.

The  $k_d$  value for  $[\text{Li.C21C}_5]^+$  is much higher than that for  $[\text{Li.C211}]^+$  ( $0.013 \text{ s}^{-1}$ , Table 6.2), again a consequence of the loss of an oxygen binding site. The variation (4 orders of magnitude) is larger than for the two  $\text{Na}^+$  cryptates (just over 3 orders of magnitude, Table 6.4), which again reflects the difference between the inclusive cryptates where the interaction between  $\text{Li}^+$  and all oxygen binding sites are strong and so loss of one site would be expected to affect the exchange

rate to a greater extent than in the exclusive cryptates where the bonding interaction with the third bridge of the cryptand is weaker. In the absence of stability information for  $[\text{Li}.\text{C}21\text{C}_5]^+$  and kinetic data in other solvents, a detailed mechanistic discussion is not possible. Determination of this information is part of continuing work in the study of cryptates in this laboratory.

#### (iv) General Mechanistic Conclusions

In summarizing the preceding kinetic and mechanistic discussion, two important features of cryptate formation emerge. Firstly, the possibility that the cryptate may exist predominantly in either of the two structural conformations, inclusive or exclusive, depending upon the relative sizes of the metal ion and the cryptand cavity. In the cases of  $[\text{Li}.\text{C}211]^+$  and the  $\text{Na}^+$  cryptates of C211 and C21C<sub>5</sub>, the inclusive and exclusive forms respectively dominate completely, there being no kinetic or spectroscopic evidence for the presence of the other form in either case. However, the importance of consideration of such factors in analysing kinetic and thermodynamic data is strongly emphasised by the example of  $[\text{Cs}.\text{C}222]^+$ . <sup>133</sup>Cs chemical shift studies<sup>38,66,67</sup> revealed a temperature dependence of the position of the equilibrium between the exclusive and inclusive forms of this cryptate. At room temperature the <sup>133</sup>Cs chemical shift is markedly solvent dependent, indicating interaction of the Cs<sup>+</sup> ion with solvent as expected for an exclusive cryptate. However, on decreasing the temperature to -100° C, the chemical shifts in a range of solvents converge to a value which is independent of solvent, indicative of the predom-

ance of the inclusive form. This is clearly good evidence for the formation of a relatively stable, exclusive intermediate in the formation of  $[\text{Cs.C222}]^+$  and, in conjunction with the observations made for the C211 and similar cryptates, illustrates the effects of cryptand size and flexibility on the energetics of cryptate formation.

The other important conclusions to be drawn from these kinetic studies pertain to the mechanistic aspects of cryptate formation and dissociation revealed by the solvent dependence of these processes. In previous work<sup>46</sup> interpretation of the variation of  $k_d$  and  $k_f$  with solvent was generalised over a range of solvent types and conclusions made concerning the structure of the transition state of formation. However, as mentioned in section 6.2 (ii), the results obtained for  $[\text{Na.C211}]^+$  in the solvents studied in this work are apparently at variance with these conclusions. A more detailed analysis of the available data, in terms of the donor strength of the solvents and its effect on the energetics of the transition state gives further insight into the mechanism of cryptate dynamics and incorporates these findings.

As described at the beginning of this chapter, application of the Eigen-Winkler mechanism to cryptate formation would lead to the expectation that the structure of the transition state of the rate determining step should be dependent upon solvent coordination strength. Eyring, Petrucci and coworkers have interpreted kinetic data obtained from ultrasonic absorption studies in terms of this mechanism for the complexation of  $\text{Ba}^{2+}$ ,  $\text{Li}^+$ ,  $\text{Na}^+$  and  $\text{K}^+$  by [18]-crown-6 and analogous crown ethers.<sup>68-71</sup> In Scheme 6.1, the  $k_2$  step involves partial conformational change in the crown ether and

partial desolvation of  $M^+$ , and the  $k_3$  step involves further desolvation and encapsulation of the cation. The rate determining factor for the  $k_3$  step varied depending upon the solvent. In water the desolvation process was found to be important, whereas in methanol the crown ether conformational change was the rate determining factor. This variation with solvent is also observed in the formation of the cryptates studied in this work.

As previously noted,  $k_d$  for  $[Na.C211]^+$  shows a significantly smaller solvent dependence than  $k_f$  in DMF, DMSO and water, all strongly coordinating solvents (Table 6.4). This also applies to  $[Li.C211]^+$ . This suggests that in the rate determining step for the formation reaction the transition state more closely resembles the product cryptate than the reactants, implying that  $Na^+$  has almost reached its final (partially) desolvated state. Conversely, for  $[Na.C211]^+$  in methanol and PC (Table 6.4),  $k_d$  exhibits the greater solvent dependence and the transition state for the rate determining step is probably more similar to solvated  $Na^+$  and cryptand. Thus as the solvent varies from water to PC, the transition state for formation becomes more like the reactants and  $k_f$  increases while  $k_d$  decreases. Generally,  $k_f$  increases as the solvent donor strength decreases and  $k_d$  decreases with the same solvent variation.

Hence, in simplistic terms, the stronger the solvation of  $Na^+$ , the greater is the barrier to formation of  $[Na.C211]^+$  and greater is the ability of the strong donor solvent to compete for binding sites on  $Na^+$  in the cryptate. Consequently, the magnitude of  $k_d$  will be greater in these solvents. It appears that in weak donor solvents the formation of  $Na^+$  - cryptand

bonds makes a relatively larger contribution to the transition state energetics than in the presence of strong donor solvents, and the rate determining step for cryptate formation involves the first  $\text{Na}^+$  - cryptand bond (or a step close thereafter). In strong donor solvents the rate determining step appears to occur somewhat later in the inclusion process, possibly involving removal of final solvent molecules.

That the position of the transition state may vary along the reaction coordinate with solvent thereby changing the rate determining step, is evidenced by the mechanism of exchange of  $\text{Ca}^{2+}$ ,  $\text{Sr}^{2+}$ ,  $\text{Ba}^{2+}$  and  $\text{Pb}^{2+}$  between different cryptands in a range of solvents.<sup>72</sup> In strongly solvating water, DMF and DMSO, the rate determining step was found to be the dissociation of the metal ion from the cryptate, whereas in the weak donor solvents methanol and PC, the attack of a second cryptand on the cryptate is important in the rate determining step.

The preceding arguments also apply to  $[\text{Na}.\text{C21C}_5]^+$  where most solvents studied were weakly coordinating. From Table 6.4 it can be seen that  $k_d$  varies with solvent to a greater extent than  $k_f$  amongst the weak donor solvents, as would be predicted from the above discussion. As such, the transition state presumably resembles the reactants in the formation reaction, which suggests that the rate determining step for dissociation of the cryptate occurs late in the cryptand -  $\text{Na}^+$  bond breaking process. Relative to C211, the total bonding strength of C21C<sub>5</sub> is reduced by the loss of an oxygen binding site and this should result in a significant decrease in the rate of dissociation as is observed. If the rate determining factor for cryptate formation involves the formation of the first



cryptand -  $\text{Na}^+$  bond as mentioned above, the influence of the oxygen binding site on the opposite face of the cryptand would be expected to be less and this is reflected in the smaller difference in  $k_f$  between  $[\text{Na.C211}]^+$  and  $[\text{Na.C21C}_5]^+$ .

In summary, the kinetic parameters for  $\text{Na}^+$  exchange on  $[\text{Na.C211}]^+$  and  $[\text{Na.C21C}_5]^+$  have been determined by dynamic  $^{23}\text{Na}$  NMR spectroscopy in a range of solvents. The results have been interpreted in terms of stepwise formation of the cryptate and discussion has been extended to include other cryptates. The mechanistic discussion has incorporated the effects of metal ion size, and cryptand cavity size, flexibility and binding sites on cryptate formation and dissociation.

6.3.

EXPERIMENTAL

(i) Materials. Cryptand C211 (Merck) was redistilled, then dried under high vacuum for 24 hours before use and stored under nitrogen. Sodium, lithium and silver perchlorate salts were dried under high vacuum for 24 hours. All solvents were purified and dried using literature methods<sup>30</sup> and were stored over Linde 4A molecular sieves under nitrogen. Tetraethylammonium perchlorate (TEAP) was prepared by ion exchange of tetraethylammonium chloride (BDH) on Amberlite IRA-400 resin (OH<sup>-</sup> form) to give an aqueous solution of the hydroxide which was acidified with perchloric acid resulting in the precipitation of TEAP. The crude material was twice recrystallized from water (no precipitate was observed on the addition of AgNO<sub>3</sub> to an aqueous solution) and dried under high vacuum at 60° C for 24 hours.

(ii) Stability Constant Measurements. The stability constants of Ag<sup>+</sup> cryptates were measured by direct potentiometric titration. Cell potentials were measured using an Orion Research 701A digital ionalyser and were accurate to ±0.2 mV. Typically, 10<sup>-3</sup> mol dm<sup>-3</sup> AgNO<sub>3</sub> solution (25 ml) was titrated with 10<sup>-2</sup> mol dm<sup>-3</sup> C21C<sub>5</sub> solution (approximately 5 ml) and the Ag<sup>+</sup> concentration was monitored with a silver wire electrode. For all titrations, the reference electrode was a Ag wire in 10<sup>-2</sup> mol dm<sup>-3</sup> AgNO<sub>3</sub> solution (AgClO<sub>4</sub> in the cases of acetone and PC) and all solutions were 0.05 mol dm<sup>-3</sup> in TEAP to keep the Ag<sup>+</sup> activity coefficient constant. The sample cell was separated from the reference cell by a salt bridge containing the TEAP background electrolyte solution. The titrations were carried out with stirring and a slow stream of

nitrogen passing through the sample solution contained in a Princeton Applied Research polarographic cell with a water jacket for thermostating at 298K. The electrode response was calibrated in each solvent by measuring the potential of solutions containing known  $\text{Ag}^+$  concentration, usually by adding  $10^{-2} \text{ mol dm}^{-3} \text{ AgNO}_3$  solution to the TEAP solution (25 ml). Plots of potential vs.  $\log [\text{Ag}^+]$  were linear with slopes varying from 55 to 65 (emf in mV). Readings were taken after 5 - 10 minutes equilibration time when no further change in emf was observed.

The indirect determination of  $\text{Na}^+$  cryptate stability constants was carried out by titration of  $10^{-3} \text{ mol dm}^{-3} \text{ AgNO}_3$  (25 ml) with a solution  $10^{-2} \text{ mol dm}^{-3}$  in both cryptand and  $\text{NaClO}_4$ , monitoring the  $[\text{Ag}^+]$  with a Ag wire electrode. The stability constants were calculated as described in section 5.2.

The direct potentiometric titrations of  $\text{NaClO}_4$  solutions with cryptand were carried out in a similar manner to the  $\text{Ag}^+$  titrations described above using a Radiometer G502Na sodium glass electrode which was also calibrated in solutions of known  $\text{Na}^+$  concentration. Typically, ten points on the titration curve after equivalence point, where the error in  $K_s$  is lowest, were used in the calculations and the results averaged to give the quoted  $K_s$  value.<sup>64</sup>

(iii) NMR Spectroscopy.  $^{23}\text{Na}$  NMR spectra were recorded on a Bruker CXP-300 NMR spectrometer operating at 79.39 MHz or on a modified Bruker HX-90E NMR spectrometer at 23.81 MHz.  $^7\text{Li}$  NMR spectra were also run on the CXP-300 spectrometer operating at 116.64 MHz. An average of 6000 transients were accumulated into a 2048 point data base using a 2000 Hz spectral width.

The sample temperature was controlled to within  $\pm 0.3$  K with a Bruker B-VT 1000 variable temperature unit which was calibrated using a copper-constantan thermocouple and checked periodically using the temperature dependence of the  $^1\text{H}$  resonances of methanol and ethylene glycol.<sup>73</sup> Data obtained on the CXP-300 was transferred from the Aspect 2000 computer to the Nicolet BNC-12 computer of the HX-90E using the Bruker program, SPECNET, for lineshape analysis.

Solutions of the sodium cryptates were prepared under dry nitrogen, degassed and sealed under vacuum in 5 mm o.d. NMR tubes according to the compositions in Tables 6.1 and 6.3. All operations were performed in a dry box under nitrogen to exclude moisture.

Refer to section 3.1 for general experimental details and to section 4.4 for details of the preparation of  $\text{C}_{21}\text{C}_5$ .

## REFERENCES

1. J.-M. Lehn, *Struct. Bonding (Berlin)*, **16**, 1 (1973).
2. M.R. Truter, *ibid*, **16**, 71 (1973).
3. W.E. Morf and P.Ch. Meier, *ibid*, **16**, 113 (1973).
4. R.M. Izatt, D.J. Eatough and J.J. Christensen, *ibid*, **16**, 161 (1973).
5. W. Burgermeister and R. Winkler-Oswatitsch, *Topics in Current Chem.*, **69**, 91 (1977).
6. F. Vogtle and E. Weber in "The Chemistry of Ethers, Crown Ethers, Hydroxyl Groups and Their Sulphur Analogues", Supp. E, Part 1, in "The Chemistry of the Functional Groups", S. Patai (Ed), John Wiley, New York, 1980, p59.
7. G.A. Melson (Ed.), "Coordination Chemistry of Macrocyclic Compounds", Plenum Press, New York, 1979.
8. R.M. Izatt and J.J. Christensen, "Progress in Macrocyclic Chemistry", John Wiley, New York, 1979.
9. E. Grell, T. Funck and F. Eggers, in "Membranes", Vol. 3, G. Eisenman (Ed.), Dekker, New York, 1975.
10. E. Grell, F. Eggers and T. Funck, *Chimica*, **26**, 632 (1972).
11. C.J. Pedersen, *J. Am. Chem. Soc.*, **89**, 7017 (1967).
12. M.A. Bush and M.R. Truter, *J.C.S. Perkin II*, 341 (1972).
13. M.A. Bush and M.R. Truter, *ibid*, 345 (1972).
14. B. Dietrich, J.-M. Lehn and J.P. Sauvage, *Tetrahedron Lett.*, 2885 (1969).
15. B. Dietrich, J.-M. Lehn and J.P. Sauvage, *ibid*, 2889 (1969).
16. J.-M. Lehn, *Acc. Chem. Res.*, **11**, 49 (1978).
17. J.-M. Lehn, *Pure Appl. Chem.*, **50**, 871 (1978).
18. J.-M. Lehn, *ibid*, **49**, 857 (1977).
19. D. Moras and R. Weiss, *Acta Crystallogr.*, **B29**, 400 (1973).

20. F. Mathieu, B. Metz, D. Moras, and R. Weiss,  
*J. Am. Chem. Soc.*, **100**, 4412 (1978).
21. E. Schmidt, J.-M. Tremillon, J.-P. Kintzinger, and  
A.I. Popov, *J. Am. Chem. Soc.*, **105**, 7563 (1983).
22. B. Dietrich, J.-M. Lehn, J.P. Sauvage, and J. Blanzat,  
*Tetrahedron*, **29**, 1629 (1973).
23. H.C. Brown, S. Narasimhan, and Y.M. Choi,  
*Synthesis*, 996 (1981).
24. J.-M. Lehn, *Neurosci. Res. Prog. Bull.*, **14**, 133 (1976).
25. J.-M. Lehn, *Pure Appl. Chem.*, **51**, 979 (1979).
26. L. Echegoyen, A. Kaifer, H.D. Durst, and G.W. Gokel,  
*J. Org. Chem.*, **49**, 688 (1984).
27. Y.M. Cahen, J.L. Dye and A.I. Popov, *J. Phys. Chem.*,  
**79**, 1289 (1975).
28. J.D. Lin and A.I. Popov, *J. Am. Chem. Soc.*,  
**103**, 3773 (1981).
29. D.H. Live and S.I. Chan, *Anal. Chem.*, **42**, 791 (1970).
30. D.D. Perrin, W.L.F. Aramaego, and D.R. Perrin,  
"Purification of Laboratory Chemicals", 2nd. Ed.,  
Pergamon, Oxford, 1980.
31. W.C. Still, M. Kahn, and A. Mitra, *J. Org. Chem.*,  
**43**, 2923 (1978).
32. Programs used include SUSCAD and ABSORB "Data reduction  
programs for the CAD 4 diffractometer.", University of  
Sydney, 1976; and SHELX, "Program for crystal structure  
determination", G.M. Sheldrick, 1976.
33. "International Tables for Crystallography" Vol 4,  
pp 99-149, Kynoch Press, Birmingham, 1974.
34. (a) J.-M. Lehn and J.P. Sauvage, *J. Am. Chem. Soc.*,  
**97**, 6700 (1975).

- (b) E. Kauffmann, J.-M. Lehn and J.P. Sauvage,  
*Helv. Chim. Acta*, **59**, 1099 (1976).
35. B.G. Cox, J. Garcia-Rosas and H. Schneider,  
*J. Am. Chem. Soc.*, **103**, 1384 (1981).
36. J. Gutknecht, H. Schneider and J. Stroka, *Inorg. Chem.*,  
**17**, 3326 (1978).
37. B.G. Cox, H. Schneider and J. Stroka, *J. Am. Chem. Soc.*,  
**100**, 4746 (1978).
38. E. Mei, L. Liu, J.L. Dye and A.I. Popov,  
*J. Solution Chem.*, **6**, 771 (1977).
39. J.S. Shinard and A.I. Popov, *Inorg. Chem.*,  
**19**, 1689 (1980).
40. B.G. Cox, *Ann. Rep. Prog. Chem., Sect. A, Phys. Inorg. Chem.*, **70**, 249 (1973).
41. P. Gramain and Y. Frere, *Nouv. J. de Chimie*, **3**, 53 (1979).
42. B. Spiess, F. Arnaud-Neu and M.J. Schwing-Weill,  
*Helv. Chim. Acta.*, **63**, 2287 (1980).
43. Y.M. Cahen, J.L. Dye and A.I. Popov, *J. Chem. Phys.*,  
**79**, 1292 (1975).
44. J.M. Ceraso, P.B. Smith, J.S. Landers and J.L. Dye,  
*J. Phys. Chem.*, **81**, 760 (1977).
45. G.W. Leisegang, *J. Am. Chem. Soc.*, **103**, 953 (1981).
46. B.G. Cox, J. Garcia-Rosas and H. Schneider,  
*J. Am. Chem. Soc.*, **103**, 1054 (1981).
47. J.-M. Lehn, J.P. Sauvage and B. Dietrich,  
*J. Am. Chem. Soc.*, **92**, 2916 (1970).
48. J.M. Ceraso and J.L. Dye, *J. Am. Chem. Soc.*,  
**95**, 4432 (1973).
49. J.P. Kintzinger and J.-M. Lehn, *J. Am. Chem. Soc.*,  
**96**, 3313 (1974).

50. V.M. Loyola, R.G. Wilkins and R. Pizer, *J. Am. Chem. Soc.*, **97**, 7382 (1975).
51. B.G. Cox and H. Schneider, *J. Am. Chem. Soc.*, **99**, 2809 (1977).
52. A.I. Popov, *Pure Appl. Chem.*, **51**, 101 (1979).
53. B. Lindman and S. Forsen, in "NMR and the Periodic Table", R.K. Harris and B.E. Mann (Eds.), Academic Press, London, 1978, p. 129.
54. P. Laszlo, *Angew. Chem. Int. Ed. Eng.*, **17**, 254 (1978).
55. R.H. Erlich and A.I. Popov, *J. Am. Chem. Soc.*, **93**, 5620 (1971).
56. S.F. Lincoln, *Prog. React. Kinetics*, **9**, 1 (1977).
57. H.S. Gutowsky, D.M. McCall and C.P. Slichter, *J. Chem. Phys.*, **21**, 279 (1953).
58. H. M. McConnell, *J. Chem. Phys.*, **28**, 430 (1958).
59. T. Nakagawa, *Bull. Chem. Soc. Jap.*, **39**, 1006 (1966).
60. T.H. Siddall, W.E. Stewart and F.D. Knight, *J. Phys. Chem.*, **74**, 3580 (1970).
61. E.H. Williams, *Ph.D. dissertation*, University of Adelaide, 1980.
62. K. Henco, B. Tümmeler and G. Maass, *Angew. Chem.*, **89**, 567 (1977).
63. V. Gutmann, "Coordination Chemistry in Nonaqueous Solutions", Springer-Verlag, Vienna, 1968,
64. F.J. Rossotti and H. Rossotti, "Determination of Stability Constants", McGraw-Hill, New York, 1961.
65. I.M. Brereton, A. Abou-Hamdan, A.M. Hounslow and S.F. Lincoln, unpublished results.
66. E. Mei, A.I. Popov and J.L. Dye, *J. Am. Chem. Soc.*, **99**, 6532 (1977).



67. E. Kauffmann, J.L. Dye, J.-M. Lehn and A.I. Popov,  
*J. Am. Chem. Soc.*, **102**, 2274 (1980).
68. W. Wallace, E.M. Eyring and S. Petrucci, *J. Phys. Chem.*,  
**83**, 6353 (1984).
69. K.J. Maynard, D.E. Irish, E.M. Eyring and S. Petrucci,  
*ibid*, **88**, 729 (1984).
70. C. Chen, W. Wallace, E.M. Eyring and S. Petrucci,  
*ibid*, **88**, 2541 (1984).
71. W. Wallace, C. Chen, E.M. Eyring and S. Petrucci,  
*ibid*, **89**, 1357 (1985).
72. B.G. Cox, N. van Truong, J. Rzeszotarska and H. Schneider,  
*Faraday Trans. I*, **80**, 3285 (1984).
73. D.S. Raiford, C.L. Fisk and E.D Becker, *Anal. Chem.*,  
**51**, 2050 (1979).

PUBLICATIONS

1. "Fluorine-19 Nuclear Magnetic Resonance Study of the Inclusion of Fluoro- and Difluoro-trans-cinnamates by  $\alpha$ -Cyclodextrin", by I.M. Brereton, T.M. Spotswood, S.F. Lincoln and E.H. Williams, *J. Chem. Soc., Faraday Trans. 1*, **80**, 3147 (1984).
  
2. "A Nuclear Magnetic Resonance Study of the Sodium Cryptate formed by 4,7,13,18-tetraoxa-1,10-diazabicyclo[8.5.5]-eicosane (C211) in Various Solvents", by S.F. Lincoln, I.M. Brereton and T.M. Spotswood, *J. Chem. Soc., Faraday Trans. 1*, in press.
  
3. "A Structural Study of the Complexation of the Sodium Ion by the Cryptands 4,7,13,18-Tetraoxa-1,10-diazabicyclo[8.5.5]eicosane (C211) and 4,7,13-Trioxa-1,10-diazabicyclo[8.5.5]eicosane (C21C<sub>5</sub>)", by S.F. Lincoln, I.M. Brereton, E. Horn, T.W. Hambly, M.R. Snow and T.M. Spotswood, *J. Chem. Soc., Dalton Trans.*, submitted for publication.

APPENDIX 1  $^{19}\text{F}$  Chemical Shifts of Fluorocinnamates in the  
Presence of Varying  $[\alpha\text{CD}]$

(Chemical shifts are referenced to  $\text{CF}_3\text{COO}^-$  (2% w/v in  $\text{D}_2\text{O}$ ) and are corrected for bulk susceptibility variations (see 3.3))

$\alpha$ -FLUOROCINNAMATE

$[\alpha\text{-CD}]$ $\text{mol dm}^{-3}$	shift ppm
.0010	-42.342
.0030	-41.655
.0050	-41.121
.0081	-40.570
.0102	-40.264
.0152	-39.721
.0204	-39.317
.0250	-38.964
.0301	-38.679
.0352	-38.435
.0401	-38.240
.0503	-37.727
.0600	-37.419
.0701	-37.090
.0802	-36.858
.0902	-36.641
.1000	-36.401
.1201	-36.001

$p$ -FLUOROCINNAMATE

$[\alpha\text{-CD}]$ $\text{mol dm}^{-3}$	shift ppm
.0005	-36.686
.0010	-36.634
.0020	-36.582
.0030	-36.565
.0038	-36.547
.0060	-36.621
.0080	-36.726
.0100	-36.831
.0153	-37.173
.0202	-37.483
.0252	-37.771
.0302	-38.014
.0399	-38.405
.0503	-38.765
.0602	-38.994
.0802	-39.328
.0902	-39.453
.1000	-39.537
.1150	-39.696
.1304	-39.814

*o*-FLUOROCINNAMATE

[ $\alpha$ -CD]	shift
mol dm <sup>-3</sup>	ppm
.0004	-41.394
.0010	-41.349
.0020	-41.276
.0030	-41.210
.0039	-41.171
.0059	-41.088
.0081	-41.038
.0102	-41.017
.0153	-41.031
.0202	-41.095
.0249	-41.181
.0301	-41.269
.0402	-41.460
.0501	-41.606
.0601	-41.725
.0800	-41.910
.0901	-41.989
.1024	-42.062
.1148	-42.137
.1304	-42.191

*m*-FLUOROCINNAMATE

[ $\alpha$ -CD]	shift
mol dm <sup>-3</sup>	ppm
.0005	-38.271
.0010	-38.248
.0020	-38.209
.0031	-38.161
.0040	-38.127
.0060	-38.062
.0080	-37.985
.0101	-37.948
.0152	-37.833
.0201	-37.729
.0249	-37.648
.0301	-37.584
.0401	-37.466
.0503	-37.382
.0601	-37.314
.0800	-37.225
.0900	-37.193
.1001	-37.159
.1151	-37.124
.1300	-37.124

*o,p*-DIFLUOROCINNAMATE

[ $\alpha$ -CD] mol dm <sup>-3</sup>	<i>o</i> -FLUORINE	<i>p</i> -FLUORINE
	shift	shift
	ppm	ppm
.0005	-37.095	-33.142
.0010	-37.061	-33.148
.0020	-37.013	-33.178
.0031	-36.952	-33.218
.0038	-36.924	-33.258
.0060	-36.841	-33.382
.0080	-36.792	-33.518
.0100	-36.753	-33.699
.0152	-36.745	-34.162
.0202	-36.759	-34.546
.0252	-36.754	-34.817
.0301	-36.780	-35.039
.0401	-36.852	-35.393
.0502	-36.908	-35.634
.0603	-36.967	-35.794
.0800	-37.037	-35.976
.0901	-37.078	-36.067
.1003	-37.106	-36.129
.1152	-37.136	-36.193
.1298	-37.150	-36.218

 $\alpha,p$ -DIFLUOROCINNAMATE

[ $\alpha$ -CD] mol dm <sup>-3</sup>	$\alpha$ -FLUORINE	<i>p</i> -FLUORINE
	shift	shift
	ppm	ppm
.0002	-44.041	-36.774
.0005	-43.926	-36.756
.0010	-43.712	-36.705
.0020	-43.308	-36.608
.0030	-42.968	-36.577
.0040	-42.619	-36.548
.0060	-41.982	-36.571
.0100	-40.932	-36.699
.0150	-39.954	-36.951
.0182	-39.395	-37.168
.0203	-39.086	-37.270
.0223	-38.878	-37.430
.0272	-38.351	-37.660
.0319	-37.897	-37.897
.0395	-37.202	-38.203
.0453	-36.931	-38.455
.0540	-36.439	-38.739
.0757	-35.535	-39.289
.0811	-35.473	-39.400
.0950	-34.897	-39.739
.1100	-34.660	-39.962
.1249	-34.871	-39.886

$\alpha$ -FLUORO-*p*-TRIFLUOROMETHYLCINNAMATE

[ $\alpha$ -CD] mol dm <sup>-3</sup>	$\alpha$ -FLUORINE	<i>p</i> -TRIFLUOROMETHYL
	shift	shift
	ppm	ppm
.0002	-39.856	13.131
.0005	-39.766	13.165
.0011	-39.598	13.291
.0020	-39.326	13.597
.0031	-	14.817
.0039	-	15.200
.0050	-	15.437
.0080	-28.866	15.742
.0101	-28.427	15.831
.0151	-28.144	15.926
.0200	-28.014	15.951
.0300	-27.915	15.981
.0451	-27.861	15.987
.0602	-27.861	15.987
.0798	-27.860	15.988
.100	-27.860	15.988
.130	-27.859	15.989

*p*-TRIFLUOROMETHYLCINNAMATE

[ $\alpha$ -CD] mol dm <sup>-3</sup>	shift ppm
.0002	13.193
.0005	13.242
.0011	13.298
.0020	13.472
.0030	14.998
.0040	15.320
.0051	15.479
.0060	15.590
.0080	15.735
.0102	15.813
.0149	15.877
.0204	15.903
.0302	15.911
.0401	15.906
.0501	15.900
.0650	15.892
.0800	15.884
.1001	15.866
.1304	15.842

*m*-TRIFLUOROMETHYLCINNAMATE

[ $\alpha$ -CD]	shift
mol dm <sup>-3</sup>	ppm
.0010	13.186
.0051	13.415
.0101	13.572
.0151	13.667
.0200	13.741
.0302	13.833
.0400	13.883
.0501	13.925
.0650	13.961
.0801	13.980
.1003	13.983
.1298	13.998

**APPENDIX 2. Supplementary Crystallographic Data**

Supplementary Data. Final Hydrogen Positional ( $\times 10^3$ )  
and Thermal ( $\times 10^2$ ) Parameters for [Na.C211.NCS]

Atom	x	y	z	U11
H(1)	439(1)	173(1)	395(1)	13(2)
H(2)	523(1)	174(1)	454(1)	13(2)
H(3)	621(2)	239(2)	352(2)	13(2)
H(4)	540(2)	301(2)	375(2)	13(2)
H(5)	540(1)	293(1)	167(1)	13(2)
H(6)	539(1)	356(1)	242(1)	13(2)
H(7)	688(1)	301(1)	275(1)	13(2)
H(8)	689(1)	345(1)	189(1)	13(2)
H(9)	796(2)	131(1)	169(1)	13(2)
H(10)	827(2)	226(1)	189(1)	13(2)
H(11)	780(1)	212(1)	333(2)	13(2)
H(12)	849(1)	137(1)	315(2)	13(2)
H(13)	698(1)	139(1)	429(1)	13(2)
H(14)	746(1)	49(1)	419(1)	13(2)
H(15)	620(1)	-13(1)	387(1)	13(2)
H(16)	596(1)	42(1)	465(1)	13(2)
H(17)	400(1)	54(1)	366(1)	13(2)
H(18)	460(1)	-29(1)	377(1)	13(2)
H(19)	348(1)	17(1)	283(1)	13(2)
H(20)	391(1)	108(1)	298(1)	13(2)
H(21)	381(1)	25(1)	111(1)	13(2)
H(22)	375(1)	119(1)	146(1)	13(2)
H(23)	460(2)	109(2)	29(2)	13(2)
H(24)	527(2)	43(2)	69(2)	13(2)
H(25)	649(1)	115(1)	44(1)	13(2)
H(26)	610(1)	201(1)	8(1)	13(2)
H(27)	742(2)	199(2)	74(2)	13(2)
H(28)	672(2)	275(2)	86(2)	13(2)
H(1')	635(2)	210(2)	421(2)	11(2)
H(2')	546(2)	172(2)	462(2)	11(2)
H(3')	508(2)	293(2)	371(2)	11(2)
H(4')	467(2)	208(2)	335(2)	11(2)
H(7')	680(2)	325(2)	172(2)	11(2)
H(8')	600(2)	318(2)	109(2)	11(2)
H(9')	764(2)	136(2)	108(2)	11(2)
H(10')	781(2)	235(2)	101(2)	11(2)
H(11')	782(2)	241(2)	263(2)	11(2)
H(12')	860(2)	177(2)	237(2)	11(2)
H(13')	749(3)	195(2)	364(2)	11(2)
H(14')	825(3)	123(2)	366(2)	11(2)
H(17')	578(2)	-29(2)	377(2)	11(2)
H(18')	537(2)	19(2)	452(2)	11(2)
H(21')	369(2)	103(2)	244(2)	11(2)
H(22')	351(2)	6(2)	220(2)	11(2)
H(25')	491(2)	107(3)	34(2)	11(2)
H(26')	481(2)	202(3)	66(2)	11(2)



Supplementary Data. Final Hydrogen Positional ( $\times 10^4$ ) and  
Thermal ( $\times 10^3$ ) Parameters for [Na.C21C<sub>5</sub>.NCS]

Atom	x	y	z	U11
H(1)	10886(3)	2085(2)	2029(3)	68(2)
H(2)	9948(3)	1268(2)	1908(3)	68(2)
H(3)	9110(4)	2972(2)	1634(3)	68(2)
H(4)	9001(4)	2253(2)	737(3)	68(2)
H(5)	6888(3)	2542(2)	1300(3)	68(2)
H(6)	7421(3)	2307(2)	2501(3)	68(2)
H(7)	6960(4)	1173(2)	773(3)	68(2)
H(8)	7779(4)	900(2)	1870(3)	68(2)
H(9)	5501(3)	456(2)	1765(3)	68(2)
H(10)	5060(3)	1427(2)	1721(3)	68(2)
H(11)	5950(3)	252(2)	4446(3)	68(2)
H(12)	5346(3)	-178(2)	3356(3)	68(2)
H(13)	7484(3)	-256(2)	2760(3)	68(2)
H(14)	7514(3)	-707(2)	3899(3)	68(2)
H(15)	10152(3)	-180(2)	3956(3)	68(2)
H(16)	9360(3)	199(2)	2815(3)	68(2)
H(17)	11399(3)	1030(2)	3598(3)	68(2)
H(18)	10583(3)	1186(2)	4614(3)	68(2)
H(19)	10908(3)	2504(2)	4515(3)	68(2)
H(20)	11140(3)	2864(2)	3358(3)	68(2)
H(21)	9005(4)	3481(2)	3269(3)	68(2)
H(22)	9972(4)	3848(2)	4241(3)	68(2)
H(23)	7291(4)	3657(2)	5562(4)	68(2)
H(24)	7845(4)	4270(2)	4694(4)	68(2)
H(25)	6432(4)	3671(2)	3354(4)	68(2)
H(26)	5550(4)	3926(2)	4300(4)	68(2)
H(27)	3925(3)	2702(2)	3696(3)	68(2)
H(28)	4885(3)	2593(2)	2760(3)	68(2)
H(29)	3830(3)	1292(2)	3148(3)	68(2)
H(30)	4573(3)	1329(2)	4327(3)	68(2)

Supplementary Data. Final Positional ( $\times 10^4$ ) and Thermal ( $\times 10^3$ ) Parameters for [Na.C211.NCS]

	X	Y	Z	U11	U22	U33	U23	U13	U12
Na(1)	6035(2)	929(2)	2263(2)	56(2)	52(2)	57(2)	0(2)	5(2)	-10(2)
S(1)	7463(2)	-1287(2)	400(2)	85(2)	84(2)	78(2)	-17(2)	4(2)	2(2)
O(1)	7199(8)	1050(8)	3177(9)	72(4)					
O(2)	4560(9)	440(7)	2055(8)	65(4)					
O(3)	5498(13)	1553(11)	1003(12)	109(6)					
O(4)	5217(7)	2369(6)	2706(6)	48(3)					
N(1)	6682(7)	-285(7)	1583(7)	120(9)	87(8)	141(11)	-55(7)	1(8)	15(7)
N(2)	5337(10)	844(9)	3626(7)	55(4)					
N(3)	7026(14)	2137(10)	1837(12)	92(6)					
C(1)	7010(7)	-692(6)	1089(7)	61(7)	41(6)	82(8)	-2(6)	-12(6)	0(6)
C(2)	5047(11)	1682(10)	3985(10)	133(6)					
C(3)	5558(20)	2455(28)	3523(27)	84(10)					
C(4)	5601(8)	3014(7)	2222(8)	100(9)	76(7)	126(11)	31(9)	44(9)	41(7)
C(5)	6658(13)	2973(12)	2203(14)	96(7)					
C(6)	7826(26)	1821(15)	2007(15)	75(8)					
C(7)	7898(14)	1606(13)	3014(26)	76(6)					
C(8)	6991(9)	872(8)	3977(8)	97(10)	111(10)	83(9)	3(8)	-39(8)	13(9)
C(9)	6118(15)	433(14)	4075(12)	80(6)					
C(10)	4567(8)	256(7)	3507(8)	78(9)	70(7)	108(10)	8(7)	26(8)	-7(7)
C(11)	4012(14)	522(11)	2475(12)	68(5)					
C(12)	4151(9)	713(8)	1356(9)	85(10)	116(11)	124(12)	5(9)	-34(9)	-28(8)
C(13)	4898(28)	927(28)	790(28)	120(9)					
C(14)	6221(10)	1700(11)	573(7)	125(13)	207(27)	57(8)	18(10)	15(9)	-14(11)
C(15)	6843(23)	2157(29)	980(20)	141(12)					
O(1')	7483(14)	1286(12)	2648(11)	67(5)					
O(2')	4691(13)	258(10)	2695(13)	69(6)					
O(3')	4847(28)	1243(15)	1391(15)	108(8)					
O(4')	5902(26)	2446(12)	2876(13)	87(7)					
N(2')	6040(29)	949(15)	3746(13)	73(7)					
N(3')	6528(29)	2064(15)	1371(29)	73(7)					
C(2')	5779(25)	1805(29)	4110(20)	106(11)					
C(3')	5231(20)	2370(20)	3503(27)	42(10)					
C(5')	6256(20)	2934(28)	1572(29)	80(10)					
C(6')	7530(29)	1904(27)	1330(28)	66(8)					
C(7')	7948(28)	1882(27)	2343(29)	45(8)					
C(8')	7622(37)	1364(23)	3510(22)	94(10)					
C(10')	5459(22)	208(20)	3939(29)	87(10)					
C(12')	3962(25)	519(21)	2209(22)	90(10)					
C(14')	5124(24)	1480(38)	744(24)	96(13)					

Primes denote the minor contributors to the disordered ligand

Supplementary Data. Final Positional and Thermal Parameters for [Na.C21C<sub>5</sub>.NCS]

Atom	x	y	z	U(11)	U(22)	U(33)	U(23)	U(13)	U(12)
Na(1)	76782(11)	17255(7)	44974(10)	394(7)	417(7)	513(8)	-3(6)	67(5)	8(5)
S(1)	76287(10)	3864(6)	82118(8)	617(6)	598(6)	701(7)	110(5)	149(5)	29(5)
O(1)	8397(2)	419(1)	3944(2)	34(1)	42(1)	58(1)	-4(1)	10(1)	-1(1)
O(2)	8565(3)	3106(1)	4667(2)	74(2)	50(1)	90(2)	-9(1)	27(2)	-11(1)
O(3)	5869(2)	2693(1)	4202(2)	48(1)	49(1)	59(2)	7(1)	10(1)	8(1)
N(1)	7515(4)	1298(2)	6295(3)	114(3)	94(3)	56(2)	9(2)	15(2)	34(2)
N(2)	9884(2)	1871(2)	3320(2)	34(1)	48(2)	51(2)	5(1)	9(1)	-4(1)
N(3)	5821(2)	1050(2)	3189(2)	31(1)	53(2)	52(2)	-3(1)	4(1)	-3(1)
C(1)	7557(3)	914(2)	7100(3)	44(2)	58(2)	64(3)	-22(2)	2(2)	10(2)
C(2)	10009(3)	1855(2)	2153(3)	49(2)	67(2)	61(2)	7(2)	26(2)	-1(2)
C(3)	8933(4)	2372(2)	1494(3)	78(3)	71(3)	42(2)	9(2)	21(2)	0(2)
C(4)	7497(3)	2178(2)	1747(3)	59(2)	64(2)	34(2)	5(2)	1(2)	7(2)
C(5)	7069(4)	1268(2)	1545(3)	61(2)	74(3)	38(2)	-7(2)	1(2)	2(2)
C(6)	5751(3)	1029(2)	2002(3)	51(2)	70(2)	59(2)	-11(2)	-12(2)	-3(2)
C(7)	6034(3)	205(2)	3679(3)	43(2)	46(2)	77(3)	-3(2)	8(2)	-15(2)
C(8)	7401(3)	-167(2)	3521(3)	56(2)	37(2)	74(3)	-4(2)	7(2)	-6(2)
C(9)	9708(3)	301(2)	3586(3)	43(2)	51(2)	66(2)	9(2)	17(2)	14(2)
C(10)	10506(3)	1101(2)	3839(3)	30(2)	62(2)	70(2)	12(2)	8(2)	7(2)
C(11)	10471(3)	2651(2)	3811(3)	41(2)	62(2)	79(3)	6(2)	6(2)	-11(2)
C(12)	9487(4)	3347(2)	3960(3)	58(2)	54(2)	80(3)	-7(2)	8(2)	-19(2)
C(13)	7515(4)	3701(2)	4823(4)	86(3)	47(2)	88(3)	-17(2)	37(3)	-7(2)
C(14)	6261(4)	3554(2)	4094(4)	84(3)	46(2)	88(3)	5(2)	28(3)	15(2)
C(15)	4743(3)	2434(2)	3493(3)	41(2)	77(3)	67(2)	8(2)	11(2)	21(2)
C(16)	4637(3)	1481(2)	3579(3)	31(2)	79(3)	74(3)	-4(2)	6(2)	-1(2)

Na and S coordinates x 10<sup>5</sup>, for the other atoms x 10<sup>4</sup>.

Na and S thermal parameters x 10<sup>4</sup>, others x 10<sup>3</sup>.